NOTICE

The quality of this microform is heavily dependent upon the quality of the original thesis submitted for microfilming. Every effort has been made to ensure the highest quality of reproduction possible.

If pages are missing, contact the university which granted the degree.

Some pages may have indistinct print especially if the original pages were typed with a poor typewriter ribbon or if the university sent us an inferior photocopy.

Reproduction in full or in part of this microform is governed by the Canadian Copyright Act, R.S.C. 1970, c. C-30, and subsequent amendments.

AVIS

La qualité de cette microforme dépend grandement de la qualité de la thèse soumise au microfilmage. Nous avons tout fait pour assurer une qualité supérieure de reproduction.

S'il manque des pages, veuillez communiquer avec l'université qui a conféré le grade.

La qualité d'impression de certaines pages peut laisser à désirer, surtout si les pages originales ont été dactylographiées à l'aide d'un ruban usé ou si l'université nous a fait parvenir une photocopie de qualité inférieure.

La reproduction, même partielle, de cette microforme est soumise à la Loi canadienne sur le droit d'auteur, SRC 1970, c. C-30, et ses amendements subséquents.

UNIVERSITY OF ALBERTA

COMPLEX WORMHOLES AND THE CONTOUR OF INTEGRATION IN QUANTUM COSMOLOGY

BY

JASON MARK TWAMLEY

A THESIS SUBMITTED
TO THE FACULTY OF GRADUATE STUDIES AND RESEARCH
IN PARTIAL FULFILLMENT OF THE REQUIREMENTS FOR THE
DEGREE
OF

DOCTOR OF PHILOSOPHY
IN
THEORETICAL PHYSICS

DEPARTMENT OF PHYSICS

EDMONTON, ALBERTA
SPRING 1991

ISBN 0-315-66717-6

ABSTRACT

Using a Friedmann-Robinson-Walker minisuperspace model with a minimally coupled homogenous scalar field we search for, and discover, wormhole-type solutions, which connect two asymptotically flat Euclidean spaces, when (a) $V = \frac{\lambda}{4}\phi^4$ and (b) $V = \frac{m^2}{2}\phi^2 + \frac{\lambda}{4}\phi^4$. For these potentials, stationary configurations satisfying the boundary conditions of asymptotic flatness necessitate that the scalar field be imaginary. All solutions found can be labeled by an asymptotic constant; however, in distinction from all previously found wormhole solutions, they do not possess a conserved charge. In the case of potential (a) all solutions found have negative actions whereas for potential (b), there exist regions of the (m, λ) parameter space for which the solutions have negative, zero, and positive action. The existence of such solutions may seriously undermine current arguments concerning the resolution of the "Large Wormhole Problem" of Fischler and Susskind. Those wormholes with negative action would, presumably, not be included into the path-integral for the vacuum to vacuum quantum amplitude. The criterion used to choose those wormholes that should contribute to the path-integral differs from one previously conjectured by Halliwell and Hartle.

We also consider a "small universe" model cosmology, consisting of closed spatial sections of constant negative three-curvature. Investigation of the allowable three-topologies provide a typical repetition scale between multiple images of a single object. Assuming minimal topological complexity for the three-topology, typical repetition scales concurrent with those seen by Broadhurst, Ellis, Koo and Szalay in a deep sky pencil beam galaxy survey are found, and a possible mechanism for microwave isotropy is discussed.

PREFACE

The University of Alberta Faculty of Graduate Studies and Research currently accepts two styles of thesis: the 'traditional format' and the 'paper format'. I have prepared this thesis in the paper format.

The first chapter contains introductory information concerning quantum cosmology and background material pertinent to Chapters 2 and 3. The material in Chapter 2 is based on a paper *"Wormholes without a conserved charge"*, by J. Twamley and D. N. Page (to be submitted). The research presented in Chapter 3 was performed in collaboration with D. N. Page. D. N. Page also derived most of the equations in section 4.4, which were checked and written in a presentable form by J. Twamley. Chapter 4 is based on a paper presented by J. Twamley at the Banff Summer Institute on Gravitation entitled *"It's all done with mirrors: Large scale structure in a hyperbolic small universe model"*, in the Proceedings of the Banff Summer Institute in Gravitation, eds. R. Mann and P. Wesson, to appear (World Scientific, Singapore, 1991). Also included is a concluding chapter summarizing the results of the thesis. Two technical appendices concerning numerical techniques needed in Chapters 2 and 3 follow the conclusion, and a *curriculum vitae* is given.

ACKNOWLEDGEMENTS

I am pleased to acknowledge Professor Don N. Page for his inspiring guidance throughout this doctoral program and for our many revealing discussions and collaborations. In connection with work presented here in Chapter 4, I also acknowledge collaborator Dr. Geoff Hayward for many interesting discussions, together with Sascha Davidson, Prof. Richard Meyerhoff and Prof. George Peschke. I especially thank Dr. Jorma Louko and Dr. Alex Lyons for stimulating conversations regarding work presented in Chapters 2 and 3. I finally thank my parents, John Twamley and Ella Mary Maloney. I thank them for twenty seven years of love, caring, encouragement and stimulation, without which this thesis would not have begun, let alone ended.

TABLE OF CONTENTS

LIST OF TABLES

LIST OF FIGURES

CHAPTER ONE

INTRODUCTION

1.1 Quantum cosmology

Quantum cosmology is the application of quantum theory to the dynamics of the whole Universe. It attempts to combine the two most successful descriptions of nature, general relativity and quantum theory, into a complete quantum description of the cosmos. It aspires to answer some of the most fundamental questions concerning the origin and evolution of the Universe, the existence of a classical world, and the existence of a universal arrow of time. Such questions have previously been considered beyond the realm of physics to even formulate, let alone fathom.

The basic premise of quantum cosmology is to treat the nature of matter, and of spacetime itself, as fundamentally quantum. Classical behaviour on macroscopic scales is believed to arise from both the dynamical structure *and* the initial conditions present within a complete theory of quantum cosmology. It is also expected that quantum cosmology will provide an essential description of the universe when a length scale L (such as the curvature length scale $|R_{\mu\nu\rho\sigma}|^{-1/2}$) becomes as small as, or smaller than, the Planck length $L_{pl} = (\hbar G/c^3)^{1/2} \sim 1.616 \times 10^{-33}$cm. Near such singularities, classical mechanics ceases to be a valid approximation of the underlying quantum theory and recourse to the full theory of quantum gravity, *à la* quantum cosmology, must be employed.

Research into the field of quantum cosmology was pioneered by DeWitt [1],

Misner [2] and Wheeler [3] in the 1960s. Combining Einstein's theory of general relativity as expressed as an action integral by Arnowitt, Deser and Misner (ADM) [4], with the techniques of quantising constrained Hamiltonian systems devised by Dirac [5], early researchers were able to analyse the dynamics of model cosmologies via a Schrödinger-like equation known as the Wheeler-DeWitt equation [6]. During the 1970's however, interest in quantum cosmology waned. With the introduction, in the early 1980's, of the Euclidean Path-Integral methods, together with proposals for boundary conditions for the universe by Hartle, Hawking and Vilenkin [7,8,9], interest in the field was re-kindled and has waxed until today [10].

In the major part of this thesis we search for, and discover, wormhole-like solutions to the complexified (in the $\sqrt{-1}$ sense) Euclidean Einstein field equations. Very little is known concerning the behaviour of complex solutions of the Einstein's field equations, and the discovery of these solutions not only adds to our present understanding but also significantly increases the small menagerie of specific wormhole solutions of the Einstein's field equations. More pressing motivations for this work arise from two currently topical areas in quantum cosmology. The first concerns recent research on the rigorous implementation of the Euclidean path-integral formalism for quantum cosmology, while the other studies the low-energy effects of including Euclidean wormhole configurations into the Euclidean path-integral for quantum cosmology. Essentially, the solutions discovered in this thesis are the first wormhole solutions not to possess a conserved charge and thus demonstrate that a conserved charge is unnecessary for a wormhole solution. They also show that previous arguments attempting to resolve the "Large Wormhole Problem" of Susskind and Fischler [11], cannot be used in settings where such non-charge-conserving wormholes are present. It is also found that, in some cases, the actions of the wormholes discovered can be negative. Inclusion of such config-

urations in the path-integral could prove disastrous. The contour of integration in the Euclidean path-integral presumably should be chosen so as not to include such wormholes. The criterion for such a choice differs from that hypothesized in reference [12].

In the following sections of this introductory chapter we briefly describe the Euclidean path-integral formalism as applied to quantum cosmology, the problem of the contour of integration, and the postulated effects of wormholes in the Euclidean path-integral. The descriptions provide essential background material for the in-depth motivations given in the beginnings of Chapters 2 and 3.

In Chapter 2 we adopt a Friedmann-Robertson-Walker (FRW) cosmological model minimally coupled to a scalar field with a quartic self-interaction. Rotating the scalar field to imaginary values, the Euclidean Einstein field equations are numerically integrated, yielding two separate wormhole configurations whose throats are held open by virtue of the non-linear aspect of the dynamics rather than by a conserved charge. In both cases we find the overall action to be negative.

In Chapter 3 we again adopt a FRW cosmological model with the scalar field minimally coupled and with a potential $V(\phi) = \frac{m^2}{2}\phi^2 + \frac{\lambda}{4}\phi^4$. Rotating the scalar field to the imaginary axis, an intricate structure of wormhole "spectra" is revealed through numerical and analytical analysis. Wormholes with negative, zero, and positive actions are found.

In Chapter 4 we divert ourselves from quantum cosmology per se, and present a cosmological model of a "small universe" possessing closed and compact spatial sections of constant negative curvature. We analyse the distribution of ghost images (ghost images are images of objects whose light has not taken the shortest path before being observed) and compare the findings of the model

with the extraordinary observational results of Broadhurst, Ellis, Koo, and Szalay [13], who have reported the discovery of long-range phase coherence in the galaxy distribution of a deep sky pencil beam survey.

1.2 Euclidean Path-Integrals in Quantum Cosmology

To consider the theory of quantum cosmology in its entirety is extremely difficult. In practice, the quantum cosmologist is restricted to one of three gross approximations: the microsuperspace, the minisuperspace, and the midisuperspace approximations. In the microsuperspace approximation, the four-geometry $\mathcal{M}$, and matter fields $\mathcal{S}$ in $\mathcal{M}$, are completely specified by a finite set of numbers. In the minisuperspace approximation, $\mathcal{M}$ and $\mathcal{S}$ are described by a finite set of functions of a small number of variables, whereas in the midisuperspace approximation [14], one must specify an infinite number of functions. In this thesis we will restrict ourselves to the minisuperspace approximation. The validity of such an approximation is suspect as we are, in effect, setting both the values of the ignored degrees of freedom and their conjugate momenta simultaneously to zero (see [15] for an analysis on the effects of enlarging the minisuperspace). However, it is hoped that certain gross features exhibited by these toy models will be reflected in the full theory.

The central idea of quantum cosmology is to describe the whole universe by a wave function Ψ. Just as quantum mechanics gives the probability of finding a particle in a certain state at a given time, quantum cosmology gives the probability of finding a certain three-geometry ${}^3g$, given by a three-surface Σ with a specified three-geometry h_{ij}, with matter fields Φ residing on Σ, representing a configuration of the Universe. In the latter case, however, the wave function does not depend on

time and is only a function of the geometry ${}^3g$ and matter configurations Φ. The concept of time can only be extracted when the theory exhibits classical behaviour.

Historically, early researchers used Hamiltonian or Dirac quantisation to obtain a Schrödinger-like operator which annihilates $\Psi[h, \Phi, \Sigma]$, giving the Wheeler-DeWitt equation. We begin with the ADM form for the Lorentzian action of a closed cosmology which we minimally couple to a scalar field with a potential $V(\phi)$. Choosing $16\pi G = 1$ for simplicity,

$$S = \int_{\mathcal{M}} {}^4R(-{}^4g)^{1/2} d^4x - 2\int_{\partial\mathcal{M}} K {}^4g^{1/2} d^3x + \int_{\mathcal{M}} \left[-\frac{1}{2}(\nabla\phi)^2 - V(\phi)\right] {}^4g^{1/2} d^4x \ . \tag{1.1}$$

Introducing a 3+1 split of the four-geometry

$$ds^2 = -(N dt)^2 + g_{ij}\left(dx^i + N^i dt\right)\left(dx^j + N^j dt\right) \ , \tag{1.2}$$

and introducing the second fundamental form

$$K_{ij} = \frac{1}{2N}\left(\frac{\partial g_{ij}}{\partial t} - N_{i|j} - N_{j|i}\right) \ , \tag{1.3}$$

the action becomes

$$I = \int L dt = \int dt\, d^3x \sqrt{g} N \left[(K_{ij}K^{ij} - K^2 + {}^3R) + \tfrac{1}{N^2}\left(\tfrac{1}{2}\dot{\phi}^2 - N^i\dot{\phi}\phi_{,i} + \tfrac{1}{2}N^iN^j\phi_{,i}\phi_{,j}\right) - \tfrac{1}{2}g^{ij}\phi_{,i}\phi_{,j} - V(\phi)\right] \ . \tag{1.4}$$

The primary constraints, *à la* Dirac, are

$$\pi \equiv \frac{\delta L}{\delta \dot{N}} = 0, \quad \pi^i \equiv \frac{\delta L}{\delta \dot{N}^i} = 0 \ . \tag{1.5}$$

Identifying the momenta conjugate to g_{ij} and ϕ as π^{ij} and π_ϕ, respectively, we can write the Hamiltonian as

$$H = \int d^3x \left(\pi\dot{N} + \pi^i\dot{N}_i + N\mathcal{H} + N_i\mathcal{H}^i\right) \ , \tag{1.6}$$

where

$$\mathcal{H} \equiv G_{ijkl}\pi^{ij}\pi^{kl} + \frac{1}{2}g^{-1/2}\pi_\phi^2 - g^{-1/2}\,{}^3R + \frac{1}{2}g^{1/2}\left(g^{ij}\phi_{,i}\phi_{,j} + 2V\right) = g^{1/2}\left(2G_0^0 - T_0^0\right) \ , \tag{1.7}$$

$$\mathcal{H}^i = -2\pi^{ik}_{\ \ ,k} - g^{il}\left(2g_{il,k} - g_{ik,l}\right)\pi^{jk} + g^{ij}\phi_{,j}\pi_\phi = g^{1/2}\left(2G^{0i} - T^{0i}\right) \ , \tag{1.8}$$

and

$$G_{ijkl} \equiv \frac{1}{2}g^{-1/2}\left(g_{ik}g_{jl} + g_{il}g_{jk} - g_{ij}g_{kl}\right) \tag{1.9}$$

is the DeWitt supermetric.

Varying the action with respect to π^{ij} and π_ϕ gives their relation to $\dot{g}_{ij}$ and $\dot{\phi}$. Varying with respect to N_i and N gives the secondary constraints, $\mathcal{H}^i = 0$ and $\mathcal{H} = 0$, which are respectively known as the supermomentum constraint equations and the Hamiltonian constraint equation [1]. We follow the method of Dirac quantisation by promoting the classical constraints to quantum annihilation operators, which act on the wavefunction, by $p \to \hat{p} = -i\frac{\partial}{\partial q}$. The primary constraints become $\hat{\pi}\Psi = -i\frac{\partial\Psi}{\partial N} = 0$ and $\hat{\pi}^i\Psi = -i\frac{\partial\Psi}{\partial N^i} = 0$, indicating that Ψ is independent of N and N^i. The secondary constraint $\hat{\mathcal{H}}^i\Psi = 0$ can be shown to imply that Ψ is unchanged under any series of infinitesimal diffeomorphisms of the three-space [2,16]. Thus, the pertinent argument of Ψ is the actual three-geometry ${}^3g$ of the surface Σ. The other secondary constraint, $\hat{\mathcal{H}} = 0$, gives the Wheeler-DeWitt equation [1,3]

$$\hat{\mathcal{H}}\Psi = \left[-G_{ijkl}\frac{\delta}{\delta g_{ij}}\frac{\delta}{\delta g_{kl}} - \frac{1}{2}g^{-1/2}\frac{\delta^2}{\delta\phi^2} - g^{1/2}\,{}^3R + g^{1/2}g^{ij}\phi_{,i}\phi_{,j} + g^{1/2}V(\phi)\right]\Psi = 0 \ . \tag{1.10}$$

As G_{ijkl} depends on g_{ij}, there is a non-trivial operator-ordering ambiguity in $\hat{\mathcal{H}}\Psi = 0$. Two natural choices of factor ordering are [1,17],

$$\hat{\mathcal{H}}\Psi = \left(-\frac{1}{2}\nabla^2 + U\right)\Psi = 0 \ , \tag{1.11}$$

or

$$\hat{\mathcal{H}}\Psi = \left(-\frac{1}{2}\nabla^2 + \frac{n-2}{8(n-1)}R + U\right)\Psi = 0 \ , \tag{1.12}$$

where

$$U \equiv \int d^3x g^{1/2} N(x) \left[-{}^3R + \frac{1}{2}g^{ij}\phi_{,i}\phi_{,j} + V\right] \ , \tag{1.13}$$

∇^2 is the Laplacian in the auxiliary metric

$$ds^2 = G_{AB}dX^A dX^B = \int d^3x \, N^{-1}(x) \left[\frac{1}{2}G^{ijkl}(x)\delta g_{ij}\delta g_{kl} + g^{1/2}\delta\phi\delta\phi\right] \ , \tag{1.14}$$

and n is the dimension of ds^2, where we have set $N^i = 0$ for simplicity. [Note: typically (1.12) is used in the context of a minisuperspace model where n is finite. However, it is not clear that (1.12) is well defined in the full superspace as one must regularize the the quantities appearing in (1.12).]

However, in the late seventies, it was recognised that this formalism possessed a number of serious deficiencies. The first concerns the Hamiltonian approach and the need for a 3+1 split of the four-geometry $\mathcal{M}$, of which Σ is a three-section. This splitting essentially restricts the overall four-geometry $\mathcal{M}$, in which the three-geometry (h, Σ), the argument of Ψ, is embedded, to have the product topology $X \times \mathbb{R}$, where X is the topology of Σ. A deficiency in the Lorentzian path-integral approach concerns the difficulty in choosing a physically natural class of Lorentzian four-geometries to include in the path-integral which yields a particular amplitude, i.e., the ground state. Perhaps the most damning shortcoming of Lorentzian techniques is that they forbid a change in the topology of the three-geometry Σ. Since the conception of quantum cosmology in the early 1960's, the phenomenon of a topological change in the structure of space-time has been much sought for by many researchers [18,19]. However, it has been shown [20], that the imposition of a Lorentzian four-metric on any compact (with or without boundary) four-manifold essentially implies that the Euler number of the

four-manifold vanishes. This condition, however, does not forbid the existence of handles in the four-geometry. Imposing the desirable conditions of stable causality and global hyperbolicity essentially renders the topology to be $X \times \mathsf{R}$. [Definitions: A spacetime $(\mathcal{M}, g_{ab})$ is stably causal iff there exists a differentiable function f on $\mathcal{M}$ such that $\nabla^a f$ is a past-directed timelike vector field. A spacetime $(\mathcal{M}, g_{ab})$ which possess a Cauchy surface is said to be globally hyperbolic. [21]]

With these deficiencies in mind, and in analogy with the situation in quantum field theory in flat spacetime, Hawking proposed rotating time to be imaginary and adopting Feynman's path-integral approach to quantisation [18]. He thus avoided the above deficiencies. One now utilises Euclidean metrics, for which topology change is allowed. With the path-integral approach, these different topologies can, in principle, all be included in the calculation of Ψ. (However, in practice, except for a small number of examples, e.g. Regge Calculus [22], a 3+1 skeletonisation of space-time is made to evaluate the path-integral.) The path-integral approach also lends itself to standard imaginary time techniques of quantum field theory which can calculate the partition function for thermodynamic ensembles together with the ground and excited states of the system [18]. This, along with the "ease" of visualising *Euclidean* four-geometries, partially led to the "No-Boundary" proposal of Hartle and Hawking for the ground state of the universe.

However, the analogy between quantum cosmology and quantum field theory in flat spacetime suffers from a very serious problem, namely the unboundedness of the gravitational action from below. Because of the freedom to add an arbitrary constant to the Lagrangian without effecting the dynamics in ordinary quantum theory, calculation of decay rates, ground state energies, etc. via the path-integral is possible for systems with energy spectrums bounded from below.

For gravity, however, the action cannot be arbitrarily re-adjusted and moreover, the action, under conformal deformations of the four-geometry, may become arbitrarily negative. To see this set $g_{ij} \rightarrow \hat{g_{ij}} = \Omega^2 g_{ij}$. The Euclidean action transforms as

$$I_E[\hat{g}] = -\frac{1}{16\pi G}\int_{\mathcal{M}} \left(\Omega^2 R + 6(\nabla\Omega)^2 - 2\Lambda\Omega^4\right)\sqrt{g}d^4x - \frac{1}{8\pi G}\int_{\partial\mathcal{M}} \Omega^2\left(K - K^0\right)\sqrt{h}\,d^3x \ , \tag{1.15}$$

where I_E is the Euclidean action, Λ the cosmological constant, h_{ab} the induced metric on the boundary, K the actual extrinsic curvature of the boundary $\partial\mathcal{M}$, while K^0 is the extrinsic curvature of the boundary if the interior was flat. The $(\nabla\Omega)^2$ term can make the action arbitrarily negative. Since the path-integral is of the form

$$Z(\mathcal{C}) = \int_{\mathcal{C}} \mathcal{D}\mathcal{G}\, e^{-I_E[\mathcal{G}]} \ , \tag{1.16}$$

where $\mathcal{C}$ is some collection of Euclidean space-times, $\mathcal{G}$'s, $\mathcal{D}\mathcal{G}$ is the measure, and $I_E[\mathcal{G}]$ is the Euclidean action over $\mathcal{G}$, we see that the path-integral will badly diverge.

1.3 The Contour of Integration in the Euclidean Path-Integral

From the remarks above, the Euclidean path-integral for quantum cosmology can be written as

$$\Psi[h,\Phi,\Sigma] = \sum_{\mathcal{M}}\int_{\mathcal{C}} \mathcal{D}\mathcal{G}\mathcal{D}\chi\, \exp\left(-I_E\left[\mathcal{G},\chi,\mathcal{M}\right]\right) \ . \tag{1.17}$$

I_E is the Euclidean action for the metric $\mathcal{G}$ and matter field configuration χ on a four-manifold $\mathcal{M}$. The integral is over an as yet unspecified class $\mathcal{C}$ of metrics and matter fields on $\mathcal{M}$, and the sum is over four-manifolds with a boundary Σ on

which the arguments of the wavefunction are specified. The functional integrals are over four-metrics $\mathcal{G}$ and matter fields χ on $\mathcal{M}$ that give the required arguments of the wavefunction, i.e. (h, Φ), on the boundary Σ.

To make the construction (1.17) rigorous, three essential ingredients must be specified: the class of manifolds to be summed over, the measure associated with the functional integrals, and the contour of integration within the space of metrics on $\mathcal{M}$. In quantum cosmology we are primarily interested in four-manifolds $\mathcal{M}$ where Σ is closed and compact. If one implements the Hartle-Hawking no-boundary proposal for the ground state of the universe, $\Sigma = \partial\mathcal{M}$, and Σ is the *only* boundary of $\mathcal{M}$. Σ may be connected or disconnected. However, for technical reasons, Σ is almost always taken to be connected (see however [23]). Specification and enumeration of those $\mathcal{M}$ to be included in (1.17) has been considered by Hartle [24]. One can also consider compact four-manifolds without boundary. The resulting path-integral would be expected to yield the vacuum partition function. It is this amplitude that the complete wormhole solutions, found in Chapters 2 and 3, will contribute to. Various forms for the measure have been advanced [25]. Recent work [26,27] has suggested that the complex analytic structure of the measure may influence the choice of integration contour. However, the central point of interest to us is the contour of integration.

Except for very simple models, the naive Wick rotation $t \rightarrow -i\tau$, as suggested by Hawking, fails to give a convergent path-integral. One is thus forced to rotate the contour of integration and integrate over complex metrics. For the case of asymptotically flat spacetimes there exists a prescription by Gibbons, Hawking and Perry (GHP) [28], which, by means of a complex rotation of the conformal degrees of freedom, avoids the manifest divergence of (1.17) when $\nabla\Omega$ is made arbitrarily large in (1.15). However, even if the problem associated with

the conformal instability is solved, the path-integral may not converge since there still exists ultra-violet divergences in the theory as it is nonrenormalizable. As stated by Hartle and Schleich [22,29], the bad behaviour of the path-integral in the case of asymptotically flat spacetimes is essentially due to the inclusion of non-physical gauge degrees of freedom into the functional integrals. For linearised and perturbative gravity, these redundant variables can be explicitly isolated and, using the GHP prescription, their integration contours rotated to the imaginary by hand. The resulting path-integral, now in terms of the physical degrees of freedom, is manifestly convergent. In short, the GHP prescription decomposes the four-metrics $\mathcal{G}$ in the functional integral into conformal equivalence classes represented by a metric $\hat{g}_{\mu\nu}$ satisfying ${}^4R(\hat{g}) = 0$, and a conformal factor defined by $g_{\mu\nu} = \Omega^2 \hat{g}_{\mu\nu}$. Setting $\Omega = 1 + Y$, one integrates over imaginary Y, with Y vanishing asymptotically. Returning to (1.15), one finds that the Y integration over imaginary values does not have a divergence due to the action being unbounded below (as it would for real Y), whereas the integration over the conformal equivalence class would also not give actions unbounded below by virtue of the positive action theorem of Schoen and Yau [30]. However, as pointed out by Hawking [18], not all asymptotically flat spacetimes can be decomposed into the above description (particularly those spacetimes far from Einstein vacuum solutions). Also the GHP conformal rotation may adversely effect the positivity of a conformally non-invariant matter action and thus the path-integral over the matter fields would fail to converge unless the contours for these integrations were rotated as well. Thus, even for the case of asymptotically flat spacetimes, the Gibbons-Hawking-Perry prescription is not the complete *elixir veritas*.

In quantum cosmology we are moreover interested in closed cosmologies. There, the literal application of the GHP prescription has only succeeded in very

few models [31]. The central obstacle is the absence of a positive action theorem for closed cosmologies. Without such a theorem, the convergence of the integration over the metric class specified by ${}^4R(\hat{q}) = 0$ is not guaranteed. In the presence of a cosmological constant Λ, the condition ${}^4R = 4\Lambda$ has been proposed but again, one has no guarantee that the integration over this class will converge. Furthermore, not all four-metrics can be continuously connected to either of these conditions. Likewise, there is no known method, as in linearised gravity, to isolate the physical degrees of freedom.

For these reasons it seems worthwhile to examine simple models where all the convergent contours of integration can be explicitly found. By identifying those contours which yield physically appealing quantum amplitudes, one may find characteristics of the chosen contours which are common to the models and which may possibly apply to the full theory of quantum cosmology. A program to study the complex contours in simple models has been carried out by Hartle, Halliwell, Louko and others [22,12,26,32].

To see how one generally proceeds in such an analysis, we adopt a minisuperspace model with a 3+1 split. Denoting the configurational coordinates (h_{ab}, χ) by q^α, their conjugate momenta by π^α, setting $N^i = 0$ for simplicity, and calling the arguments of the wavefunction (h, Φ), $q^\alpha_{\rm final}$, the reparametrisation invariance of the action,

$$\delta_\epsilon q^\alpha = \epsilon(t)\,\{q^\alpha, \mathcal{H}\}\,, \quad \delta_\epsilon \pi_\alpha = \epsilon(t)\,\{\pi_\alpha, \mathcal{H}\}\,, \tag{1.18}$$

$$\delta_\epsilon N = \dot{\epsilon}(t), \qquad \epsilon(0) = \epsilon(1) = 0\ , \tag{1.19}$$

may be completely broken by the gauge fixing condition

$$\zeta \equiv \dot{N} - \mu(\pi_\alpha, q^\alpha, N) = 0\ , \tag{1.20}$$

where μ is an arbitrary function of π_α, q^α, N. The path-integral now has the form

$$\Psi[q^\alpha_{\rm final}] = \int \mathcal{D}\pi_\alpha \mathcal{D}q^\alpha \mathcal{D}N \delta[\zeta]\Delta_\zeta e^{-I_E[\pi,q,N]} \ , \tag{1.21}$$

where Δ_ζ is the Faddeev-Popov measure associated with the gauge fixing condition ζ. In the $\dot{N} = 0$ gauge, (1.21) becomes

$$\Psi\,[q^\alpha_{\rm final}] = \int dN \mathcal{D}\pi \mathcal{D}q e^{-I_E[\pi,q,N]} \ , \tag{1.22}$$

where the functional integral over N has reduced to an ordinary integral over N. In some cases, the convergent contours for the dN integral can be factored completely from the $\mathcal{D}\pi\mathcal{D}q$ contours and the final result can be studied by steepest descents. More often this factoring cannot be done. While no rigorous method of evaluating (1.22) is known, a prescription for approximating (1.22) is presented in [27]. In the semiclassical limit, we expect the path-integral to be well approximated by a stationary-point evaluation of (1.22),

$$\Psi[q^\alpha_{\rm final}] \approx \sum_i C_i \exp\left[-I^c_{E\,i}(q^\alpha_{\rm final})\right] \ , \tag{1.23}$$

where C_i is the prefactor and $I^c_{E\,i}$ are the stationary solutions to the complex Einstein field equations with the prescribed boundary conditions $q^\alpha_{\rm final}$. For a given boundary configuration $q^\alpha_{\rm final}$, there may exist several stationary solutions (here labeled by i). Some may occur for real, imaginary and complex, values of N and can represent a Euclidean, Lorentzian and genuinely complex spacetime (by complex spacetime we imply a complex four-metric on a real four-manifold, i.e., $g_{\mu\nu}(z^\alpha)$ is a complex tensor field of the real variables z^α). The resulting contour of integration may be deformed into sections of steepest descent curves connecting these stationary solutions. The choice of contour will determine which of the C_i are non-zero and thus will enter the semiclassical expansion for Ψ. Different

contours can represent separate proposals for the ground state of the universe (i.e. Hartle-Hawking vs. Vilenkin's tunnelling proposal).

A list of five criteria, aimed at selecting those contours which yield the most physically appealing quantum state for the universe, have been advanced by Halliwell and Hartle [12]. These are: (i) The integral defining Ψ should converge. (ii) The resulting Ψ should satisfy the constraints implementing diffeomorphism invariance i.e. the Wheeler-DeWitt and χ equations. With an invariant choice of measure and either an infinite or closed complex contour of integration for N, it has been shown that this criterion is fulfilled. (iii) The wavefunction should imply classical spacetime when the universe is large. This is predicted when (a) alternative histories for the spacetime geometry do not interfere on scales far above the Planck length, and (b) the histories are highly correlated according to classical laws. Typically, in the semiclassical limit, these conditions imply that the action can be written as $I_E^c = I_r^c - iI_i^c$, where I_i varies much more rapidly than I_r^c. (iv) In the limit where spacetime is classical, a consistent quantum field theory for the matter fields Φ on the classical backgrounds must be recovered. (v) From current wormhole arguments, the contour should be consistent with the vanishing of the low-energy effective Λ. They then conjectured that in the same way that four-spheres with $Re(\sqrt{g}) > 0$ possess negative action, wormholes with $Re(\sqrt{g}) > 0$ possess positive action.

It is this conjecture which is called into question by the results of Chapters 2 and 3.

The status of this research program is as yet unclear. In the models studied, choosing a particular boundary proposal and implementing the above criteria may fail to give a suitable contour or may yield a non-unique result.

1.4 Wormholes in the Euclidean Path-Integral

In this section we briefly describe current arguments concerning the effects of including wormholes into the Euclidean path-integral for quantum cosmology.

A number of authors have argued that the inclusion of wormhole configurations may cause the low-energy effective coupling constants to float unpredictably [33,34]. Coleman has argued that this effect may explain why the cosmological constant is zero [34]. Fischler and Susskind have shown that the couplings of large, smooth, spherical four-geometries by small wormholes leads to wormholes becoming dense in spacetime on all possible scales (The "Large Wormhole Problem") [11]. To avoid this disastrous consequence, Coleman and Lee have suggested that for wormholes possessing a conserved charge, the summation over small wormholes creates a charge non-conserving interaction which drains the charge from large wormholes, thus de-stabilizing them [35]. Such an effect has been demonstrated by Iwazaki [36]. The "Large Wormhole Problem" is discussed in more detail in the introduction to Chapter 2. Here we describe the derivation of the probability distribution function for the coupling constants (2.1.1) [37].

Beginning with (1.17) for the ground state wavefunction for a singly connected boundary with no matter fields (for simplicity), we sum over all connected four-manifolds $\mathcal{M}$, for which $\Sigma = \partial\mathcal{M}$. Although one is assuming the no-boundary proposal for Ψ_0, it is asserted that the results found are insensitive to the particular boundary conditions used. It is also assumed, though questionable, that the Euclidean path-integral method, as applied to quantum cosmology, is correct, and an appropriate mechanism for dealing with the conformal divergence of gravity is available. (For a critical examination of the assumptions made in these arguments see reference [38]). One then splits the integration over $\mathcal{M}$ into (a) a

sum over smooth large connected four-manifolds ($\mathcal{M}_c$) that have $\Sigma = \partial\mathcal{M}$, (b) a sum over smooth large disconnected four-manifolds with no boundary ($\mathcal{M}_d$), (c) a sum over small wormhole configurations connecting these two. One then considers the effective Lagrangian obtained by integrating out the configurations on scales smaller than ρ, where ρ is larger than the wormhole scale. The effect of a wormhole connecting x and x' can be mimicked by the insertion of the bi-local operator $\sum_{ij} C^{ij}(x,x')\theta_i\theta_j$, where $C^{ij} \sim \exp(-I_{WH})$ and where θ_i is a complete set of local scalar densities. The Euclidean path-integral expectation value of an observable $\mathcal{W}$ in a singly connected universe, smooth on scales less than ρ, with coupling constants λ, and no wormholes, is

$$< \mathcal{W} >_\lambda = \frac{\int_{\mathcal{M}_c} d\mathcal{G}\, e^{-I(\mathcal{G},\lambda)}\mathcal{W}}{\int_{\mathcal{M}_c} d\mathcal{G}\, e^{-I(\mathcal{G},\lambda)}} \quad . \tag{1.24}$$

Including one wormhole we get

$$< \mathcal{W} >_\lambda \sim \int_{\mathcal{M}_c} d\mathcal{G}\, e^{-I(\mathcal{G},\lambda)}\mathcal{W} \times \frac{1}{2}C^{ij}\int dx dx' \theta_i(x)\theta_j(x') \quad . \tag{1.25}$$

The sum over any number of wormholes attached to one large smooth universe is

$$< \mathcal{W} >_\lambda \sim \int_{\mathcal{M}_c} d\mathcal{G}\, \mathcal{W} e^{-I(\mathcal{G},\lambda)} \exp\left(\frac{1}{2}C^{ij}\int dx dx' \theta_i(x)\theta_j(x')\right) \quad . \tag{1.26}$$

To make this a local theory we use $e^{1/2C^{ij}V_iV_j} \sim \int \prod_k d\alpha_k e^{-1/2D^{ij}\alpha_i\alpha_j - \alpha_i V_i}$ where $D_{ij} = C_{ij}^{-1}$. Noting that $I(\mathcal{G},\lambda) = \lambda_i \int dx\, \theta_i(x)$, we have

$$< \mathcal{W} > \sim \int \prod_k d\alpha_k e^{-1/2D^{ij}\alpha_i\alpha_j} \int d\mathcal{G}\, \mathcal{W} e^{-I[\mathcal{G},\lambda+\alpha]} \sim \int d\alpha\, \rho_1(\alpha) < \mathcal{W} >_{\lambda+\alpha} \tag{1.27}$$

where $\rho_1(\alpha) = e^{-1/2D^{ij}\alpha_i\alpha_j}\mathcal{O}_1(\alpha)$ and $\mathcal{O}_1(\alpha) = \int d\mathcal{G}\, e^{-I[\mathcal{G},\lambda+\alpha]}$ is the Euclidean vacuum partition function for a large smooth universe without wormholes. The expectation (1.27), is now a sum over coupling constants!

Considering the sum (b), each addition of a large smooth four-geometry introduces a factor $\int d\mathcal{G}'\, e^{-I[\mathcal{G}',\lambda+\alpha]}$ into the α-integral. The sum once again exponentiates,

$$< \mathcal{W} > \sim \int d\alpha\, e^{-1/2 D^{ij}\alpha_i\alpha_j} \exp\left(\int d\mathcal{G}'\, e^{-I[\mathcal{G}',\lambda+\alpha]}\right) \int d\mathcal{G} e^{-I[\mathcal{G},\lambda+\alpha]} \mathcal{W}$$
$$\int d\alpha\, \rho_2(\alpha) < \mathcal{W} >_{\lambda+\alpha} \ , \tag{1.28}$$

where

$$\rho_2(\alpha) = e^{-1/2\alpha_i D^{ij}\alpha_j} \mathcal{O}_1(\alpha) e^{\mathcal{O}_2(\alpha)} \ , \tag{1.29}$$

and

$$\mathcal{O}_2(\alpha) = \int_{\mathcal{M}_d} d\mathcal{G}\, e^{-I[\mathcal{G},\lambda+\alpha]} \ . \tag{1.30}$$

Thus from (1.27) and (1.28), we see that one effectively has a statistical distribution for the coupling constants α_k.

To approximate (1.27) while assuming the low-energy effective action is the Einstein-Hilbert action, we take the leading-order contribution of $\mathcal{O}_1$ to arise from saddle points for which the real part of the action to be that of half a four-sphere. The dominant contribution to $\mathcal{O}_2$ arises from saddle points for which the real part of the action is that of a whole four-sphere, i.e.

$$\mathcal{O}_1 \sim e^{-\frac{3}{16G^2\Lambda}}, \qquad \mathcal{O}_2 \sim e^{-\frac{3}{8G^2\Lambda}} \ . \tag{1.31}$$

Summing over the coupling constant $\alpha_1 = \Lambda$, the most probable value predicted by these distributions is $\Lambda = 0$. However, summing over the coupling constant $1/16\pi G$ appears also to yield $G \to 0$. Equation (1.27) is identical to that discovered by Baum and Hawking while equation (1.28) was suggested by Coleman. Although they both lead to a desirable prediction for Λ, the inclusion of coupling constants other than Λ in (1.28) results in the "Large Wormhole Problem". This is explained below.

BIBLIOGRAPHY

[1] B. S. DeWitt, *Phys. Rev.* **160** (1967) 1113.

[2] C. W. Misner, *Rev. Mod. Phys.* **29** (1957) 497.

[3] J. A. Wheeler, *"Superspace and the Nature of Quantum Geometrodynamics"*, Batelle Rencontres, eds. C. DeWitt and J. A. Wheeler (Benjamin, New York, 1968).

[4] R. Arnowitt, S. Deser, and C. W. Misner, *Gravitation: An Introduction to Current Research*, ed. L. Witten (Wiley, New York, 1962).

[5] P. A. M. Dirac, *Lectures in Quantum Mechanics*, (Academic, New York, 1965); P. A. M. Dirac, *Can. J. Math.* **2** (1950) 129; A. Hanson, T. Regge, and C. Teitelboim, *Constrained Hamiltonian Systems*, (Accademia Nazionale dei Lincei, Roma, 1976).

[6] M. A. H. MacCallum, in *General Relativity: An Einstein Centenary Survey*, eds. S. W. Hawking and W. Israel (Cambridge University Press, Cambridge, 1979); M. P. Ryan, Jr. *Hamiltonian Cosmology*, Lecture notes in physics Vol **13** (Springer-Verlag, Berlin).

[7] S. W. Hawking, in *Astrophysical Cosmology*, eds. H. A. Brück, G. V. Coyne, and M. S. Longair (Pontifica Academia Scientarium, Vatican City, 1982); S. W. Hawking, *Nucl. Phys.* **B239** (1984) 257.

[8] J. B. Hartle and S. W. Hawking, *Phys. Rev.* **D28** (1983) 2960.

[9] A. Vilenkin, *Phys. Rev.* **D30** (1984) 509; *ibid.*, *Phys. Rev.* **D33** (1986) 3560; *ibid.*, *Phys. Rev.* **D37** (1988) 888.

[10] For an extensive bibliography see, J. J. Halliwell, *Int. J. Mod. Phys.* **A5** (1990) 2473.

[11] W. Fischler and L. Susskind, *Phys. Lett.* **217B** (1989) 48.

[12] J. J. Halliwell and J. B. Hartle, *Phys. Rev.* **D41** (1990) 1815.

[13] T. J. Broadhurst, R. S. Ellis, D. C. Koo, and A. S. Szalay, *Nature*, (1990) 726.

[14] K. V. Kuchař, *Phys. Rev.* D4 (1971) 955.

[15] K. V. Kuchař and M. P. Jr. Ryan, *Phys. Rev.* D40 (1989) 3982; B. L. Hu and S. Sinha, *"Minisuperspace as the infrared limit of quantum gravity"*, presented at GR12.

[16] P. W. Higgs, *Phys. Rev. Lett.* **1** (1959) 373.

[17] C. W. Misner, in *Magic without Magic*, ed. J. R. Klauder (Freeman, San Francisco, 1972); K. V. Kuchař in *Relativity, Astrophysics and Cosmology*, ed. W. Israel (Reidel, Dordrecht,1973); M. Henneaux, M. Pilati and C. Teitelboim, *Phys. Lett.* **110B** (1982) 123; T Christodoulakis and J. Zanelli, *Phys. Rev.* D**29** (1984) 2733; *ibid*, *Phys. Lett.* **102A** (1984) 227; S. W. Hawking and D N Page, *Nucl. Phys.* B**264** (1986) 185.

[18] S. W. Hawking, in *General Relativity: An Einstein Centenary Survey*, eds. S. W. Hawking and W. Israel (Cambridge University Press, Cambridge, 1979);

[19] R. P. Geroch, *J. Math. Phys.* **8** (1967) 8; F .J. Tipler, *Ann. Phys.* (N. Y.) **108** (1977) 1; *ibid.*, *Phys. Rev. Lett.* **37** (1976) 879; M. S. Morris and K .S. Thorne, *Am. J. Phys.* **56** (1988) 395.; C. W. Misner and J. A. Wheeler, *Ann.*

Phys. (N. Y.) **2** (1957) 2; T. Regge, *Nuovo Cim.* **19** (1961) 558; C. J. Isham, *Class. Quantum Grav.* **6** (1989) 1508.

[20] M. Visser, *Phys. Rev.* **D41** (1990) 1116; R D. Sorkin, *Phys. Rev.* **D33** (1986) 978.

[21] S. W. Hawking and G. F. R. Ellis, *The large scale structure of space-time*, (Cambridge University Press, Cambridge, England, 1973).

[22] J. B. Hartle , *J. Math. Phys.* **30** (1989) 452.

[23] S. P. Braham, *Phys. Rev.* **D41** (1990) 3671.

[24] J. B. Hartle , *Class. Quantum Grav.* **2** (1985) 707.

[25] H. Leutwyler, *Phys. Rev.* **134** (1964) 1155; E. Faddeev and V. Popov, *Sov. Phys. Usp.* **16** (1974) 777; H. Hamber, in *Critical Phenomena, Random Systems and Gauge theories, Proceedings of the Les Houches Summer School*, Les Houches, France, 1984, eds. K. Osterwalder and R. Stora.

[26] J. J. Halliwell and J. Louko, *Phys. Rev.* **D39** (1989) 2206; *ibid.*, *Phys. Rev.* **D40** (1989) 1868.

[27] J. J. Halliwell and J. Louko, *Phys. Rev.* **D42** (1990) 3997.

[28] G. W. Gibbons, S. W. Hawking, and M. Perry, *Nucl. Phys.* **B138** (1978) 141.

[29] K. Schleich, *Phys. Rev.* **D36** (1987) 2342; J. B. Hartle and K. Schleich, in *Quantum Field Theory and Quantum Statistics*, eds. T. A. Batalin, C. J. Isham, and G. A. Vilkovisky (Hilger, Bristol, 1987).

[30] R. Schoen and S. T. Yau, *Phys. Rev. Lett.* **61** (1988) 263.

[31] K. Schleich, *Phys. Rev.* D**39** (1989) 2192; J. Louko and P. Tuckey, (in preparation).

[32] S. Chakraborty, *Phys. Rev.* D**42** (1990) 2924; J. J. Halliwell and R. Myers, *Phys. Rev.* D**40** (1989) 4011.

[33] S. B. Giddings and A. Strominger, *Nucl. Phys.* B**307** (1988) 854; S. Coleman, *Nucl. Phys.* B**307** (1988) 867; T. Banks, *Nucl. Phys.* B**309** (1988) 493; S. W. Hawking, *Nucl. Phys.* B**335** (1990) 155.

[34] S. Coleman, *Nucl. Phys.* B**310** (1988) 643.

[35] S. Coleman and K. Lee, *Phys. Lett.* **221**B (1989) 242; S. Coleman and K. Lee, *Nucl. Phys.* B**341** (1990) 101.

[36] A. Iwazaki, *Phys. Lett.* **229**B (1989) 211.

[37] From *"Lectures on Baby Universes"*, by L. Susskind, (TASI, 1989).

[38] W. G. Unruh, *Phys. Rev.* D**40** (1989) 1053.

CHAPTER TWO

WORMHOLES WITHOUT A CONSERVED CHARGE

2.1 Introduction

Recent work has shown that the inclusion of topologically non-trivial four-geometries in the Euclidean path-integral formulation of quantum gravity may have severe effects on the low-energy effective coupling constants [2]. Essentially, the inclusion of Planckian wormholes which either connect large disconnected four-geometries, or connect separate regions of the same large four-geometry, may cause the effective low-energy coupling constants to 'float' unpredictably. We now adopt the rules of wormhole calculus (though questionable) and assume a) the Euclidean path-integral method is a viable formulation for quantum gravity, and b) wormholes connect large four-geometries together which are smooth on the scale of the wormhole. Having done this, one can evaluate a probability distribution function for the coupling constants through a semi-classical approximation of the partition function. In the approximation that the large four-geometries are large four-spheres, this probability distribution function takes the form [3]

$$P(\alpha) \sim e^{-\frac{1}{2}D_{ij}\alpha_i\alpha_j} e^{-I_{cl}} e^{e^{-I_{cl}(g,\lambda+\alpha)}} , \qquad (2.1.1)$$

where the α's are the low-energy corrections to the coupling constants and $I_{cl}(g, \lambda+\alpha)$ is the action of a four-sphere with the altered couplings. We see that the effective low-energy coupling 'constants' are now functions of the α's. The most probable configuration is that which maximizes the argument of the double exponential in (2.1.1). Keeping the first three coupling constants Λ, κ, γ (γ is the

coefficient of the R^2 term), semi-classical evaluation of action of a four-sphere [3] gives the argument of the second exponential to be

$$\frac{1}{[\Lambda(\rho)+\alpha_1]\,[\kappa^2(\rho)+\alpha_2]} + [\gamma(\rho)+\alpha_3] \quad . \tag{2.1.2}$$

Maximizing (2.1.2) with respect to the α's gives us $\Lambda_{effective} \rightarrow 0$. This process is most efficient with small wormholes. However, to study the behaviour of κ (the gravitational constant) and γ one must introduce infra-red cutoffs [4,5]. Naively, one would expect γ_{eff} and all higher order effective coupling constants to be forced to their maximum allowable values. However, Preskill [5] has advocated that the determination of the unique minimum of $1/\kappa_{eff}$ will fix all other couplings through renormalization effects. Either way, the processes effecting shifts in all coupling other than Λ are most efficient if large wormholes are dense in spacetime on all possible scales. This is the infamous large-wormhole problem.

A number of authors [5,6,7] have suggested mechanisms attempting to resolve the large-wormhole problem. The presence of a conserved charge plays a key role in the operation of these mechanisms[1]. However, as pointed out by Polchinski, [7] the large-wormhole problem will occur for any classical wormhole solution. In this chapter we present new classical wormhole solutions to the Euclidean Einstein field equations which connect two asymptotically flat regions. In distinction from all other previously known solutions, these wormholes do not possess any conserved charge. It is not clear that the mechanisms which have been suggested with reference to charged wormholes [6] will still apply to these new solutions. The large-wormhole problem may reappear.

[1]Preskill [5] did not utilize this charge but instead advocated that small wormholes will crowd out large wormholes. However, Polchinski showed [7] that this can only lead to a finite suppression of large wormholes and consequently cannot beat the infinite enhancement caused by (2.1.2).

2.2 Description of Model

For simplicity we will adopt the $k = +1$ Euclidean Robertson-Walker O(3)-invariant metric ansatz, appropriately scaled for later convenience,

$$ds_4^2 = \frac{2G}{3\pi}\left[N^2(t)dt^2 + a^2(t)d\Omega_3^2\right] \quad , \tag{2.2.1}$$

where $d\Omega_3^2$ is the standard O(3)-invariant metric on the unit S^3, and $\hbar = c = 1$. The scalar field will be taken to be

$$\Phi = \left(\frac{3}{4\pi G}\right)^{1/2}\phi(t) \quad , \tag{2.2.2}$$

with a self-interaction potential

$$\tilde{V}(\Phi) = \left(\frac{9}{8G^2}\right)V(\phi) \quad . \tag{2.2.3}$$

The Euclidean Einstein-Hilbert action, with the York-Gibbons-Hawking boundary term [8] at the S^3 boundaries at $t_\pm$, is

$$\begin{aligned} I_E &= \int_M d^4x\sqrt{g}\left[-\frac{1}{16\pi G}R + \frac{1}{2}(\nabla\Phi)^2 + \tilde{V}(\Phi)\right] - \int_{\partial M} d^3x\sqrt{h}\frac{1}{8\pi G}(K - K_0) \\ &= \frac{1}{2}\int_{t_-}^{t_+} N dt\left(-a\dot{a}^2 + a^3\dot{\phi}^2 - a + 2a^3V\right) + \frac{1}{2}a^2(t_+) + \frac{1}{2}a^2(t_-) \\ &= \frac{1}{2}\int_{t_-}^{t_+} N dt\left(G_{AB}\dot{X}^A\dot{X}^B + 2U\right) + \frac{1}{2}a_+^2 + \frac{1}{2}a_-^2 \quad , \end{aligned} \tag{2.2.4}$$

where K is the trace of the actual extrinsic curvature of the boundaries in the metric (2.2.1), K_0 is that of the corresponding flat metric inside the same boundary, an overdot denotes $N^{-1}d/dt$,

$$ds^2 = G_{AB}dX^AdX^B = -ada^2 + a^3d\phi^2 = e^{3\alpha}(-d\alpha^2 + d\phi^2) \tag{2.2.5}$$

is the metric on the (a, ϕ) minisuperspace, $\alpha \equiv \ln a$, and

$$U = -\frac{1}{2}a + a^3V(\phi) \tag{2.2.6}$$

is the minisuperspace potential.

The classical Euclidean equations of motion are

$$2\mathcal{H} = G_{AB}\dot{X}^A\dot{X}^B - 2U = a\left(-\dot{a}^2 + a^2\dot{\phi}^2 + 1 - 2a^2V\right) = 0 \ , \tag{2.2.7}$$

$$\ddot{\phi} + 3\frac{\dot{a}}{a}\dot{\phi} - \frac{dV}{d\phi} = 0 \ , \tag{2.2.8}$$

$$\ddot{a} + 2a\dot{\phi}^2 + 2aV = 0 \ , \tag{2.2.9}$$

giving the trajectories of a particle of mass-squared $-2U$ in the metric (2.2.5), or spacelike geodesics in the conformally-related metric

$$d\tilde{s}^2 = 2U ds^2 = \left(a^2 - 2a^4V\right)\left(da^2 - a^2d\phi^2\right) = e^{4\alpha}\left(1 - 2e^{2\alpha}V\right)\left(d\alpha^2 - d\phi^2\right) \ . \tag{2.2.10}$$

We are looking for wormhole solutions connecting two asymptotically flat regions, so $\dot{a} \to \pm 1$ as $t \to \pm\infty$, and $\phi \to \phi_\pm$ with $V(\phi_\pm) = 0$ and $dV(\phi_\pm)/d\phi = 0$. We will primarily be interested in solutions with finite action (2.2.4) as $t_\pm \to \pm\infty$, though wormholes with infinite action may also be relevant in certain circumstances [9,10].

It is well known that no real wormhole solutions exist for pure gravity [11,12]. It is essentially necessary for the Ricci tensor, and hence for the matter stress-tensor, to have at least one negative eigenvalue [13]. This does not occur for a real scalar field with a non-negative potential $V(\phi)$. In our O(3)-symmetric model, this is illustrated by the fact that equation (2.2.9) does not allow a wormhole throat with $\ddot{a} > 0$ if $\dot{\phi}^2 \geq 0$ and $V \geq 0$. This restriction can be circumvented by going to imaginary $\phi = i\varphi$, which makes $\dot{\phi}^2 = -\dot{\varphi}^2 < 0$. For a massless imaginary scalar field ($V = 0$), wormhole solutions have been found [14]. These have a conserved charge, the value of π_ϕ, which is the momentum conjugate to ϕ.

Solutions exist for any value of π_ϕ and have a linear throat size proportional to $\pi_\phi^{1/2}$.

We are interested in discovering solutions with no conserved charge and so consider non-constant $V(\phi)$. The simplest potential one might consider is $V = \frac{1}{2}m^2\phi^2 = -\frac{1}{2}m^2\varphi^2$ for a massive scalar field. Unfortunately, Jungman and Wald [15] show that no wormholes are possible for a real scalar field with $\phi dV/d\phi \geq 0$, and their argument also applies virtually unchanged for an imaginary scalar field with $\varphi dV/d\varphi \leq 0$, which includes the massive field case with $m^2 > 0$.

To avoid this limitation and yet use a potential which is non-negative for real ϕ, we shall consider the simplest nontrivial example, which is

$$\tilde{V} = \frac{1}{4}\tilde{\lambda}\Phi^4 \ , \tag{2.2.11}$$

or

$$V = \frac{1}{4}\lambda\phi^4 = \frac{1}{4}\lambda\varphi^4 \tag{2.2.12}$$

with $\lambda = \tilde{\lambda}/2\pi^2$. It is convenient to use the conformal radial coordinate

$$\eta = \int \frac{N dt}{a} = \int N dt\, e^{-\alpha} \ , \tag{2.2.13}$$

with a prime denoting $d/d\eta = aN^{-1}d/dt$, so the action and equations of motion become

$$I_E = -\frac{1}{2}\int_{\eta_-}^{\eta_+} d\eta \left(a'^2 + a^2\varphi'^2 + a^2 - \frac{1}{2}\lambda a^4\varphi^4\right) + \frac{1}{2}a_+^2 + \frac{1}{2}a_-^2 \ , \tag{2.2.14}$$

$$\alpha'^2 + \varphi'^2 \ = 1 - 2e^{2\alpha}V(\varphi) = \ 1 - \frac{1}{2}\lambda e^{2\alpha}\varphi^4 \ , \tag{2.2.15}$$

$$\alpha'' \ = 2(\varphi'^2 - e^{2\alpha}V(\varphi)) = \ 2\varphi'^2 - \frac{1}{2}\lambda e^{2\alpha}\varphi^4 \ , \tag{2.2.16}$$

$$\varphi'' \;= -2\alpha'\varphi' - e^{2\alpha}\frac{dV(\varphi)}{d\varphi} = \; -2\alpha'\varphi' - \lambda e^{2\alpha}\varphi^3 \;\; . \tag{2.2.17}$$

Another coordinate system which allows a more descriptive portrayal of the dynamics are the polar coordinates

$$r = \frac{a^2}{2} \;\; , \;\; \theta = 2\varphi \;\; . \tag{2.2.18}$$

Rescaling the lapse to be $N = \nu/a$ and denoting $\frac{d}{\nu dt}$ by a hat, the action and equations of motion become

$$I_E = -\frac{1}{2}\int_{t_-}^{t_+} dt\,\nu\left(\hat{r}^2 + r^2\hat{\theta}^2 + 1 - r\frac{\lambda}{16}\theta^4\right) + r_+ + r_- \;\; . \tag{2.2.19}$$

$$\hat{r}^2 + r^2\hat{\theta}^2 \;= 1 - 4rV = \; 1 - \frac{r\lambda\theta^4}{16} \;\; , \tag{2.2.20}$$

$$\hat{\hat{r}} - r\hat{\theta}^2 \;= -2V = \; -\frac{\lambda\theta^4}{32} \;\; , \tag{2.2.21}$$

$$r\hat{\hat{\theta}} + 2\hat{r}\hat{\theta} \;= -2r\frac{dV}{d\theta} = \; -\frac{r\lambda\theta^3}{16} \;\; . \tag{2.2.22}$$

The solutions are spatial geodesics of

$$d\tilde{s}^2 = e^{4\alpha}\left(1 - 2e^{2\alpha}V(\varphi)\right)\left(d\alpha^2 + d\varphi^2\right) = e^{4\alpha}\left(1 - \frac{1}{2}\lambda e^{2\alpha}\varphi^4\right)\left(d\alpha^2 + d\varphi^2\right) \tag{2.2.23}$$

and

$$d\tilde{s}^2 = (1 - 4rV(\theta))\left(dr^2 + r^2 d\theta^2\right) = \left(1 - \frac{\lambda r\theta^4}{16}\right)\left(dr^2 + r^2 d\theta^2\right) \tag{2.2.24}$$

in the above two sets of coordinates. Constructing the Hamiltonian and utilizing Hamilton's equations one can eliminate the time parameter dependence and obtain a second order ordinary differential equation relating the geometry and matter.

For the case where one has a cartesian minisuperspace metric which is conformally flat with conformal factor $F(\alpha,\varphi)$ (i.e. (2.2.23)) the dynamics obeys

$$\frac{d^2\varphi}{d\alpha^2} = \frac{1}{2}\left[1+\left(\frac{d\varphi}{d\alpha}\right)^2\right]\left(\frac{\partial}{\partial\varphi} - \frac{d\varphi}{d\alpha}\frac{\partial}{\partial\alpha}\right)(\ln F) \quad . \tag{2.2.25}$$

For a polar parametrized minisuperspace metric which is conformally flat with conformal factor $P(r,\theta)$ (i.e. (2.2.24)) the dynamics obeys

$$\frac{d^2r}{d\theta^2} = r + \frac{2}{r}\left(\frac{dr}{d\theta}\right)^2 + \frac{1}{P}\left[r^2+\left(\frac{dr}{d\theta}\right)^2\right]\left(-2V + \frac{2}{r}\frac{dr}{d\theta}\frac{dV}{d\theta}\right) \quad . \tag{2.2.26}$$

For the present model we have

$$F(\alpha,\varphi) = -e^{4\alpha} + \frac{\lambda}{2}e^{6\alpha}\varphi^4 \quad , \tag{2.2.27}$$

$$P(r,\theta) = 1 - \frac{\lambda}{16}r\theta^4 \quad , \tag{2.2.28}$$

which, when inserted into (2.2.25) and (2.2.26), yield

$$\frac{d^2\varphi}{d\alpha^2} = -\left(1-\frac{1}{2}\lambda e^{2\alpha}\varphi^4\right)^{-1}\left[1+\left(\frac{d\varphi}{d\alpha}\right)^2\right]\left[\left(2-\frac{3}{2}\lambda e^{2\alpha}\varphi^4\right)\frac{d\varphi}{d\alpha} + \lambda e^{2\alpha}\varphi^3\right] \quad , \tag{2.2.29}$$

$$\frac{d^2r}{d\theta^2} = r + \frac{2}{r}\left(\frac{dr}{d\theta}\right)^2 - \left(1-\frac{\lambda r\theta^4}{16}\right)^{-1}\left[r^2+\left(\frac{dr}{d\theta}\right)^2\right]\left[\theta - \frac{4}{r}\left(\frac{dr}{d\theta}\right)\right]\frac{\lambda\theta^3}{32} \quad . \tag{2.2.30}$$

For large α (2.2.29) has the asymptotic form

$$\frac{d^2z}{d\alpha^2} - z + \lambda z^3 = \mathcal{O}(e^{-2\alpha})\mathcal{O}\left[z^3, z^2\frac{dz}{d\alpha}, z\left(\frac{dz}{d\alpha}\right)^2, \left(\frac{dz}{d\alpha}\right)^3\right] \quad , \tag{2.2.31}$$

with $z \equiv e^{\alpha}\varphi \equiv a\varphi$, so when we can neglect the right hand side we get an asymptotically conserved quantity

$$E = \frac{1}{2}\left(\frac{dz}{d\alpha}\right)^2 - \frac{1}{2}z^2 + \frac{1}{4}\lambda z^4 \quad , \tag{2.2.32}$$

which is the energy of a unit-mass particle in the potential $-\frac{1}{2}z^2 + \frac{1}{4}\lambda z^4$, if the time is taken to be α.

If we eliminate the arbitrary constant associated with the zero of η, equations (2.2.15)-(2.2.17) or equation (2.2.29) has a two-parameter set of solutions. In one asymptotic region, the two parameters may be taken to be E and an associated phase angle of the oscillations of z, the integration constant α_0 obtained in solving (2.2.32) for

$$\alpha \approx \int \frac{dz}{\sqrt{2E + z^2 - \frac{1}{2}\lambda z^4}} = \epsilon^{-1/2} \mathrm{cn}^{-1} \left[\sqrt{\frac{\lambda}{1+\epsilon}} z \,|\, k^2 = \frac{1}{2}\left(1 + \frac{1}{\epsilon}\right) \right] + \alpha_0 \ , \quad (2.2.33)$$

$$\epsilon = (1 + 4\lambda E)^{1/2} \ . \quad (2.2.34)$$

Alternatively, the two parameters may be taken to be the minimum value of a and the value of φ (or $\dot{\varphi}$) there.

Although all of the solutions are asymptotically flat, when $E \neq 0$ the scalar field $\varphi = z/a$ undergoes oscillations of amplitude decreasing only as a^{-1}, which is too slow for the action (2.2.14) to remain finite as $\eta_\pm \to \pm\infty$. For a complete finite-action wormhole solution, we need $E_+ = E_- = 0$ in both asymptotic regions. These two conditions on the two-parameter set of generic solutions may be expected to lead to a discrete set of finite-action solutions.

An alternative, more intuitive approach to finding asymptotically flat Euclidean wormhole solutions can be found through the examination of the asymptotic behaviour of ϕ for various potentials $V(\phi)$. From the equations of motion (2.2.7)-(2.2.9) we see that the asymptotic behaviour of the solutions corresponding to the decaying ϕ mode for a potential

$$V(\phi) \sim \frac{\lambda}{2p}\phi^{2p} \ , \quad (2.2.35)$$

where $p > 3/2$ and $\lambda > 0$, is that of $V = 0$, i.e. like the Giddings-Strominger wormhole [14]. For real ϕ Jungman and Wald's argument disallows wormhole solutions. For imaginary $\phi = i\varphi$ the same argument shows that no wormholes are allowed when p is odd (as we mentioned above for the massive case with $m^2 > 0$). The simplest case for which wormholes might exist is thus $p = 2$. For $V = 0$ equations (2.2.15)-(2.2.17) (with $\lambda = 0$) can be solved exactly to give

$$\varphi_{gs} = \tan^{-1} e^{-2\eta} + \varphi_+ \ , \tag{2.2.36}$$

$$a_{gs} = (2c \cosh 2\eta)^{1/2} \ , \tag{2.2.37}$$

which is the well-known Giddings-Strominger solution expressed as a massless scalar field [14] with $-2c$ being the asymptotic charge $a^2(d\varphi/d\eta)$. For this solution φ_{gs} tends asymptotically to two different values $\varphi_\pm$ where $|\varphi_+ - \varphi_-| = \pi/2$. The action is zero by virtue of scale invariance and the fact that it extremizes the Euclidean action. The asymptotic behaviour is approximately

$$\varphi_{gs} - \varphi_+ \sim e^{-2\eta} \ , \ a_{gs} \sim \sqrt{c} e^{\eta} \ . \tag{2.2.38}$$

Returning to the case $V = \frac{\lambda}{4}\varphi^4$, equation (2.2.15) yields

$$a^2 \frac{d\varphi}{d\eta} = -2c - \int a^4 F(\varphi) d\eta \ , \tag{2.2.39}$$

where $F = dV/d\varphi$. For $V = 0$ the solution is identically the Giddings-Strominger wormhole. For $V = \frac{\lambda}{4}\phi^4$, with $\phi \to 0$ as $\eta \to +\infty$, the solution tends asymptotically to the Giddings-Strominger wormhole. Thus to a first approximation, the asymptotic behaviour of $\varphi(\eta)$ and $a(\eta)$ for large $+\eta$, may be obtained from (2.2.39) by approximating φ and a on the right hand side by φ_{gs} and a_{gs} with $\varphi_+ = 0$. This gives,

$$a_{gs}^2 \frac{d\varphi}{d\eta} \approx -2c - \int a_{gs}^4 F(\varphi \approx \varphi_{gs}) d\eta \ . \tag{2.2.40}$$

Inserting (2.2.36) and (2.2.37) we obtain

$$\frac{d\varphi}{d\eta} \approx \frac{1}{\cosh 2\eta}\left[-1 + \frac{c\lambda}{4}e^{-2\eta}\right] + \mathcal{O}(e^{-8\eta}) \ , \tag{2.2.41}$$

which upon integration gives

$$\varphi \approx \tan^{-1} e^{-2\eta} - \frac{\lambda}{8}ce^{-4\eta} + \mathcal{O}(e^{-8\eta}) \ , \tag{2.2.42}$$

or more generally ($V = \frac{\lambda}{2p}\phi^{2p}$)

$$\varphi \approx \tan^{-1} e^{-2\eta} - \frac{c\lambda(-1)^p e^{4\eta(1-p)}}{8(1-p)(2p-3)} + \mathcal{O}(e^{-4p\eta}) \ . \tag{2.2.43}$$

Using equation (2.2.16) and integrating twice with the boundary conditions $\alpha' = \dot{a} = 1$ at $\eta = +\infty$, and choosing a suitable integration constant to obtain (2.2.37) when $\lambda = 0$, we get

$$\alpha \approx \frac{1}{2}\ln(2c\cosh 2\eta) - \frac{\lambda}{8}ce^{-6\eta} + \mathcal{O}(e^{-10\eta}) \ , \tag{2.2.44}$$

$$a \approx (2c\cosh 2\eta)^{1/2}\left[1 - \frac{\lambda}{8}ce^{-6\eta}\right] + \mathcal{O}(e^{-9\eta}) \ , \tag{2.2.45}$$

or, for the more general potential (2.2.35),

$$a \approx (2c\cosh 2\eta)^{1/2}\left[1 - \frac{3\lambda c(-1)^p e^{-2\eta(2p-1)}}{4p(2p-1)(2p-3)}\right] + \mathcal{O}(e^{-(4p+1)\eta}) \ . \tag{2.2.46}$$

By iterating (2.2.39) and (2.2.16) one can obtain a more accurate asymptotic solution.

If $E = 0$ in one asymptotic region, say $E_- = 0$ at $\eta = -\infty$, then in that region one can find a late time asymptotic solution for φ as a function of a by assuming the asymptotic form for φ and a to be

$$a(t) \approx t + \sum_{i=1}^{\infty} \frac{b_i}{t^{2i+1}} \ , \tag{2.2.47}$$

$$\varphi(t) \approx \sum_{i=1}^{\infty} \frac{c_i}{t^{2i}} \ . \tag{2.2.48}$$

This form yields dominant behaviour at $t = \infty$ when inserted into the equations of motion (2.2.7-2.2.9). Inserting these expansions into any two of the equations of motion, one can solve iterativly for the unknowns b_i, c_i. Inverting the functional dependence $a(t)$ to give $t(a)$ and substituting back into $\varphi(t)$ we obtain

$$\varphi = c_- a^{-2} - \frac{1}{8}\lambda c_-^3 a^{-4} + \left(\frac{2}{3}c_-^3 + \frac{1}{64}\lambda^2 c_-^5\right) a^{-6} + \left(-\frac{19}{48}\lambda c_-^5 - \frac{1}{512}\lambda^3 c_-^7\right) a^{-8}$$
$$+ \left(\frac{6}{5}c_-^5 + \frac{171}{1280}\lambda^2 c_-^7 + \frac{1}{4096}\lambda^4 c_-^9\right) a^{-10} + \mathcal{O}(a^{-12}) \ , \tag{2.2.49}$$

where c_- can be taken to be the second free parameter, which in the expansion (2.2.48) corresponds to c_1 (see Appendix A for a symbolic computer program which confirms this calculation). We integrated equations (2.2.15)-(2.2.17) (one of the latter two of which is redundant) by a fourth-order Runge-Kutta ODE solver from one asymptotic region (large a_-) where $E_- = 0$ and φ had the asymptotic form (2.2.49), through the throat, and out to the other asymptotic region (large a_+), where E_+ was evaluated. The function $E_+(c_-)$ showed two zeroes for positive c_-, corresponding to two discrete wormholes (see Figure (2.1)). Using Brent's root-finding algorithm, we found the two solutions occurred at

$$\text{(i) } c_- = c_1 \approx 0.486421\,\lambda^{-1} \approx 9.6015\,\tilde{\lambda}^{-1} \ , \tag{2.2.50}$$

$$\text{(ii) } c_- = c_2 \approx 6.0055\,\lambda^{-1} = 118.5438\,\tilde{\lambda}^{-1} \ . \tag{2.2.51}$$

The symmetry $\varphi \leftrightarrow -\varphi$ implies that there are two other wormholes with the same geometry but opposite values of φ, given by $c_- = -c_1$ and $c_- = -c_2$.

If we choose the gauge $N = 1$ and set $t = 0$ and $\eta = 0$ at the throat, then for both wormholes a is an even function of t and η. Solution (i) has $\varphi(t)$ and

$\varphi(\eta)$ also even, but Solution (ii) has φ an odd function of t or η (see Figs. (2.2) and (2.3)).

The values of a at the throat are

$$\text{(i) } a = a_1 \approx 1.04307\,\lambda^{-1/2} \approx 4.63434\tilde{\lambda}^{-1/2} \ , \tag{2.2.52}$$

$$\text{(ii) } a = a_2 \approx 0.75575\,\lambda^{-1/2} \approx 3.3577\tilde{\lambda}^{-1/2} \ . \tag{2.2.53}$$

For Solution (i), $\ddot{a} = -a_1^{-1} < 0$ at $t = 0$, and the minimum value of a occurs at $t = \pm t_0 \approx \pm 0.650888\,\lambda^{-1/2}$, where

$$a(\pm t_0) = a_{min1} \approx 0.94981131\,\lambda^{-1/2} \approx 4.2199\tilde{\lambda}^{-1/2} \ . \tag{2.2.54}$$

For Solution (ii), $\ddot{a} = 2a_2^{-1} > 0$ at $t = 0$, and a_2 is the global minimum of a. Remembering that a is a dimensionful quantity in the metric (2.2.1), the dimensionful three-volumes of the minimal surfaces in the two cases are thus

$$\text{(i) } 2\pi^2 L_1^3 = 2\pi^2 \left(\frac{2G}{3\pi}\right)^{3/2} a_{min1}^3 \approx 145.0022\tilde{\lambda}^{-3/2}G^{3/2} \ , \tag{2.2.55}$$

$$\text{(ii) } 2\pi^2 L_2^3 = 2\pi^2 \left(\frac{2G}{3\pi}\right)^{3/2} a_2^3 \approx 73.0499\tilde{\lambda}^{-3/2}G^{3/2} \ , \tag{2.2.56}$$

and the linear sizes of the three-surfaces of circumference $2\pi L$ are

$$\text{(i) } L_1 \approx 12.2141\tilde{\lambda}^{-1/2}G^{1/2} \ , \tag{2.2.57}$$

$$\text{(ii) } L_2 \approx 9.7187\tilde{\lambda}^{-1/2}G^{1/2} \ , \tag{2.2.58}$$

where we have expressed these quantities in terms of the coupling constant $\tilde{\lambda}$ in the origina potential (2.2.11). Note that $G^{1/2} = \mathrm{M_P^{-1}} = \mathrm{L_P} \approx 1.616 \times 10^{-33}\mathrm{cm}$ is the Planck length.

The Euclidean action for the complete wormhole solution may be split up into a gravitational part, a kinetic matter part and a potential matter part, i.e.

$I_E = I_G + I_K + I_V$. By considering the constant or scaling conformal transformation of the metric, $g_{\mu\nu} \rightarrow \tilde{g}_{\mu\nu} = \Omega^2 g_{\mu\nu}$ where $\Omega = 1 + \epsilon$, setting the first variation of the action to zero gives

$$I_G + I_K = -2I_V \ , \tag{2.2.59}$$

or $I_E = -I_V$. Referring to (2.2.14) we see that $I_V \geq 0$ and thus the total Euclidean action must be negative. By performing the transformation $\varphi \rightarrow \tilde{\varphi} = \kappa\varphi$ and setting the first variation of the action to zero, we see that $I_K = -2I_V$ and thus from (2.2.59), $I_G = 0$ identically. When we take $t_\pm \rightarrow \pm\infty$ or $\eta_\pm \rightarrow \pm\infty$ to obtain the complete wormhole solutions, the numerical results of the Euclidean action I_E (2.2.4) or (2.2.14) are

$$\text{(i) } I_1 \approx -0.479314\,\lambda^{-1} \approx -9.46128\,\tilde{\lambda}^{-1} \ , \tag{2.2.60}$$

$$\text{(ii) } I_2 \approx -2.26035\,\lambda^{-1} \approx -44.6175\,\tilde{\lambda}^{-1} \ . \tag{2.2.61}$$

It is of interest to note that there exits finite action, spherically symmetric solutions in *flat space* with imaginary ϕ obeying the boundary conditions $\varphi \rightarrow 0$, $|\dot{a}| \rightarrow 1$ as $t \rightarrow \pm\infty$ and $\dot{\varphi} = 0$ at $t = 0$. The relevant equation for φ in flat space is

$$\frac{d^2\varphi}{dr^2} + \frac{3}{r}\frac{d\varphi}{dr} + \lambda\varphi^3 = 0 \ , \tag{2.2.62}$$

where the solution for φ, obeying the above boundary conditions is,

$$\varphi = \frac{\sqrt{8/\lambda}\, r_0}{1 + r^2/r_0^2} \ , \tag{2.2.63}$$

which is the imaginary field analogue of the Fubini instanton [17]. The total action for this solution is $I_E = -\frac{4}{3}\lambda^{-1}$. Thus, one might consider comparing the action for each of the two wormhole solutions with the action for two copies of flat space i.e. $-\frac{8}{3}\lambda^{-1} \approx -2.666\,\lambda^{-1}$. Since the actions (2.2.60) and (2.2.61) are negative, it appears that these wormholes are enhanced rather than suppressed. The action

for a single wormhole is bounded below, however. The possible consequences of a negative action for these wormholes is discussed in chapter 3.

Because the scalar field Φ has a nontrivial potential $\tilde{V}(\Phi) = \frac{1}{4}\tilde{\lambda}\Phi^4$, the conjugate momentum

$$\pi_\Phi = \frac{\partial L}{\partial(\partial\Phi/\partial t)} = \int \Phi_{,\mu} d^3\Sigma^\mu = -\sqrt{\frac{8G}{9}} a^3 \dot{\varphi} \ , \tag{2.2.64}$$

(defined using the Lorentzian action

$$I_L = \int L\, dt = i I_E \ , \tag{2.2.65}$$

and the choice of gauge

$$N = i\left(\frac{3\pi}{2G}\right)^{1/2} \tag{2.2.66}$$

so that t becomes the proper Lorentzian time) is not conserved but rather obeys the equation

$$\dot{\pi}_\Phi \equiv N^{-1}\frac{d\pi_\Phi}{dt} = -\frac{1}{3}\sqrt{8G}\lambda a^3 \varphi^3 \ . \tag{2.2.67}$$

However, the right hand side tends to zero sufficiently rapidly in the asymptotic regions of the wormhole solutions that π_Φ tends toward the constant values

$$\text{(i) } \pi_\Phi(t=-\infty) = -\pi_\Phi(t=+\infty) = \pi_1 = -\frac{2}{3}\sqrt{8G}c_1 \approx -18.1049\, G^{1/2}\tilde{\lambda}^{-1} \ , \tag{2.2.68}$$

$$\text{(ii) } \pi_\Phi(t=-\infty) = \pi_\Phi(t=+\infty) = \pi_2 = -\frac{2}{3}\sqrt{8G}c_2 \approx -223.5339\, G^{1/2}\tilde{\lambda}^{-1} \ , \tag{2.2.69}$$

in each asymptotic region of the two wormhole solutions. These may be viewed as the asymptotic charges of the wormhole. Note that the asymptotic charges are opposite for Solution (i), so that the wormhole effectively adds asymptotic charge to *both* flat regions it connects (or drains charge if one takes the sign-reversed solution $c_- = -c_1$). Solution (ii) connects two flat regions where the asymptotic

charges are equal. Here the wormhole appears as normal, acting as a sink for asymptotic charge on one side and as a source on the other side, but again the charge π_Φ is *not* conserved within the throat.

A more pictorial description of the two wormhole solutions can be obtained by going to the polar coordinate representation (2.2.24) where the dynamics obey the second order ODE (2.2.26). Using the polar coordinates (2.2.18) the two solutions are plotted in Figs. (2.4) and (2.5). The dynamics is that of a particle with unit mass moving in a potential $U = (r\frac{\lambda}{16}\theta^4 - 1)/2$. The scalar curvature of the auxiliary two dimensional minisuperspace (2.2.24) is given by

$$R = \frac{\lambda\theta^2\left(\lambda r\theta^4 + 4\theta^2 + 48\right)}{64r\left(1 - \dfrac{\lambda r\theta^4}{16}\right)^3} \quad . \tag{2.2.70}$$

This diverges for $\theta = \pm 2/(\lambda r)^{1/4}$, that is, when $P(r,\theta)$, the conformal factor in the minisuperspace metric (2.2.24) as defined in equation (2.2.26), is zero. The loci of various values of $P(r,\theta)$, (including zero) are shown in Figs. (2.4) and (2.5). In this auxiliary minisuperspace, all the dynamics occurs within the region $P \geq 0$ while the typical trajectory will avoid the infinite barrier $P(r,\theta) = 0$ (see for example the behaviour of the type (ii) wormhole solution). However, on the surface $P = 0$ we see from (2.2.20) that $\dot{r} = \dot{\theta} = \dot{a} = \dot{\varphi} = 0$ indicating a complete time reversal of the dynamics. However, in equation (2.2.26) we have eliminated the time dependence and so the behaviour of $\dfrac{d^2r}{d\theta^2}$ is regular at $P = 0$. For this to be so we must have

$$\left.\frac{dr}{d\theta}\right|_{P=0} = \frac{r\theta}{4} \quad . \tag{2.2.71}$$

This is demonstrated in the type (i) wormhole behaviour. Figure (2.5) shows the detail near the origin and displays the multiple covering of the plane by these coordinates. This is due to θ not being restricted to the interval $[-\pi, +\pi]$.

Solution (ii) also possesses at least one Lorentzian section. This occurs at the time symmetric surface at the throat's center where $\varphi = 0$ and the extrinsic curvature vanishes. The Lorentzian section represents the Lorentzian evolution of a O(3)-symmetric three-geometry from a singularity to a maximum size (that of the time symmetric three-geometry of the Euclidean wormhole) and recollapse to a singularity. In this evolution the Lorentzian extrinsic curvature is zero uniquely at the point of maximum expansion (see Fig. (2.6) for details of this Lorentzian evolution). We note that there may exist other Lorentzian sections which may be obtained through complex transformations. We have not, however, succeeded in discovering such transforms.

For a fixed λ there exists a maximum size for a classical wormhole solution with finite action. Thus naively it appears that the unbridled fury of the large wormhole problem is somewhat abated and only the two finite action solutions are dense in spacetime. It could well prove, however, that the relaxing of the dilute gas approximation will allow the solutions with infinite action (if evaluated out to infinity) to be patched together, thus allowing wormholes of arbitrary size.

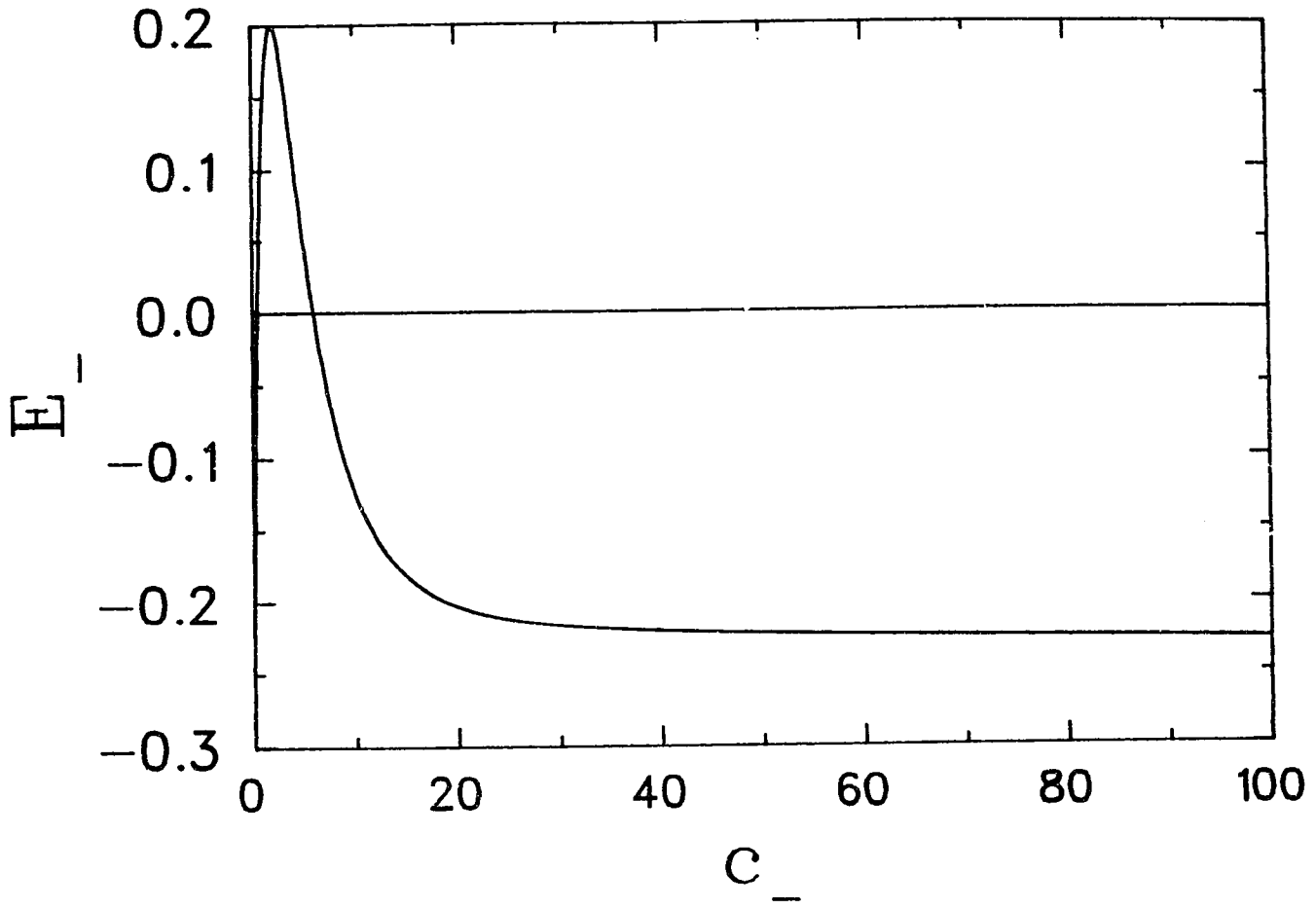

Figure 2.1: Behaviour of $E_+(c_-)$. The zeros correspond to type (i) $c_- = c_1 \approx 0.486421\,\lambda^{-1}$ and type (ii) $c_- = c_2 \approx 6.0055\,\lambda^{-1}$ wormhole solutions.

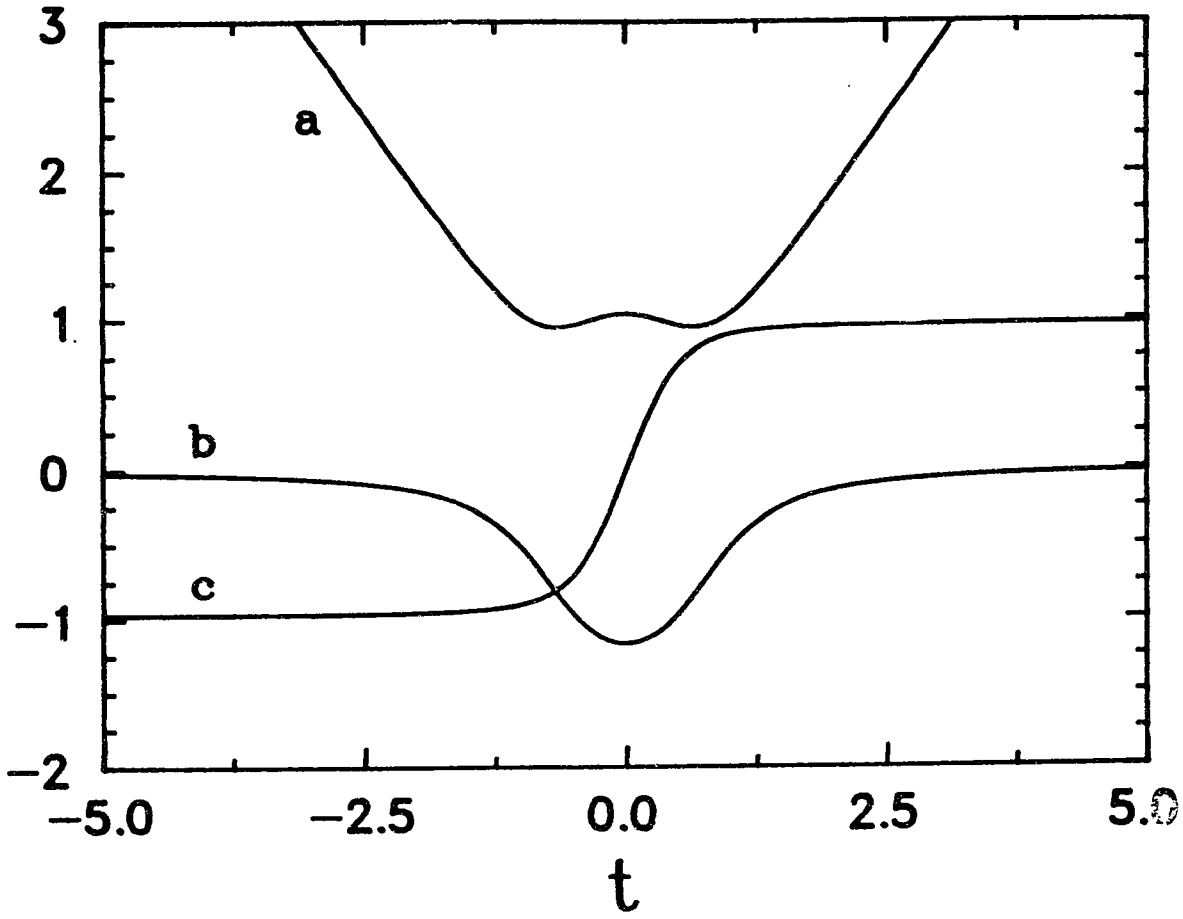

Figure 2.2: Behaviour of wormhole solution (i) in the throat region where the abscissa is t in the gauge $N = \lambda^{-1/2}$ with the origin of t at the point of symmetry of $a(t)$. This solution corresponds to $c_- \approx 0.486421\,\lambda^{-1}$. The separate graphs refer to (a) scale factor $\lambda^{1/2}a(t)$, (b) behaviour of φ (which does not scale with λ) and (c) $\lambda a^3\dot{\varphi}$.

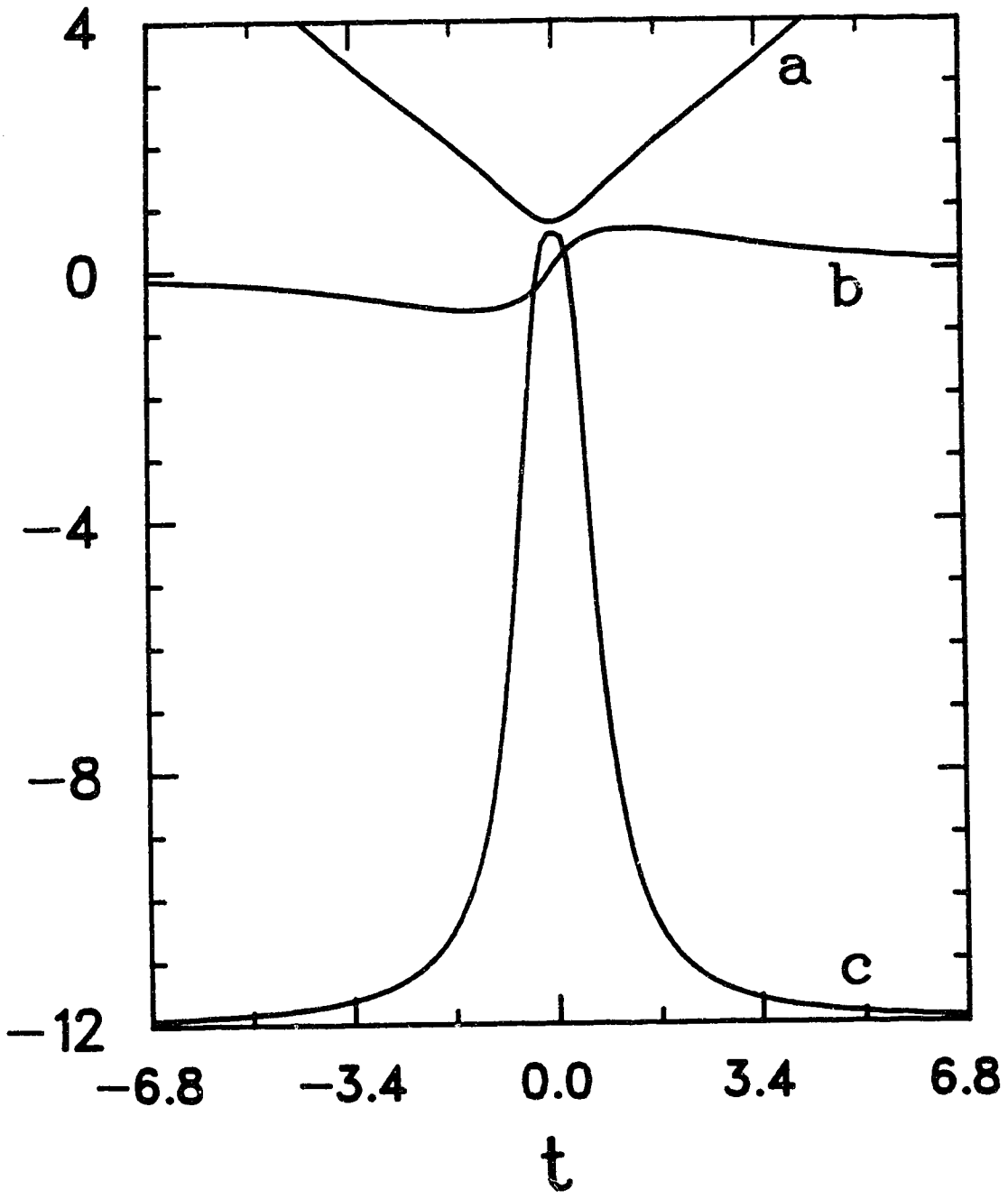

Figure 2.3: Behaviour of wormhole solution (ii) in the throat region. This solution corresponds to $c_- \approx 6.0055\,\lambda^{-1}$. The separate graphs refer to: (a) $\lambda^{1/2}a(t)$, (b) φ, and (c) $\lambda a^3\dot{\varphi}$. Note: we have compressed t by a factor of 5 for curve (c) so that the large t behaviour is apparent.

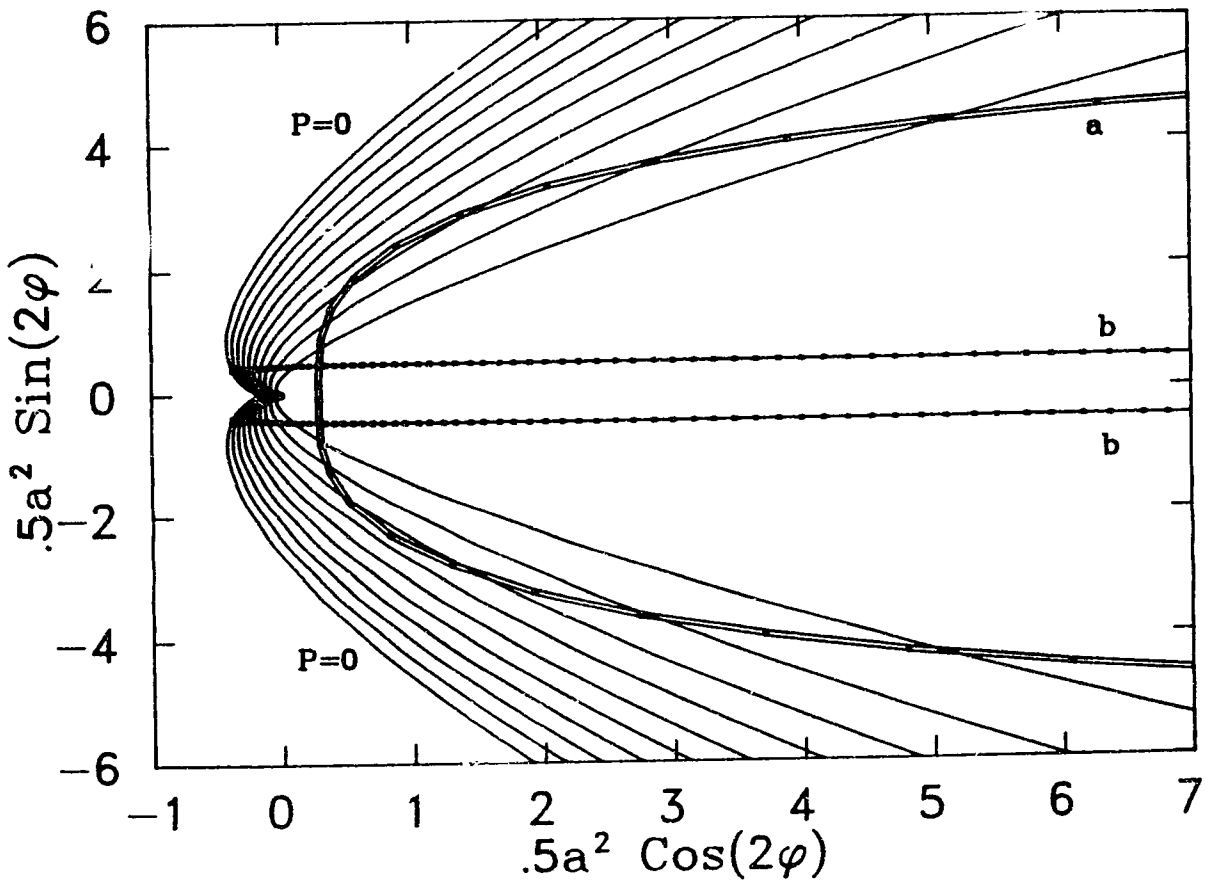

Figure 2.4: Behaviour of types (i) and (ii) wormhole solutions in the polar coordinates (2.2.18). Graph (a) shows type (ii) wormhole which is is antisymmetric and passes through $\theta = 0$. Graphs (b) show type (i) wormhole which is symmetric in θ. Because of the $\theta \rightarrow -\theta$ symmetry two solutions of this type are shown. Also shown are lines of constant conformal factor $P = (1 - r\theta^4/16)$ ranging from $P = 0$ to $P = .9$ in steps of .1.

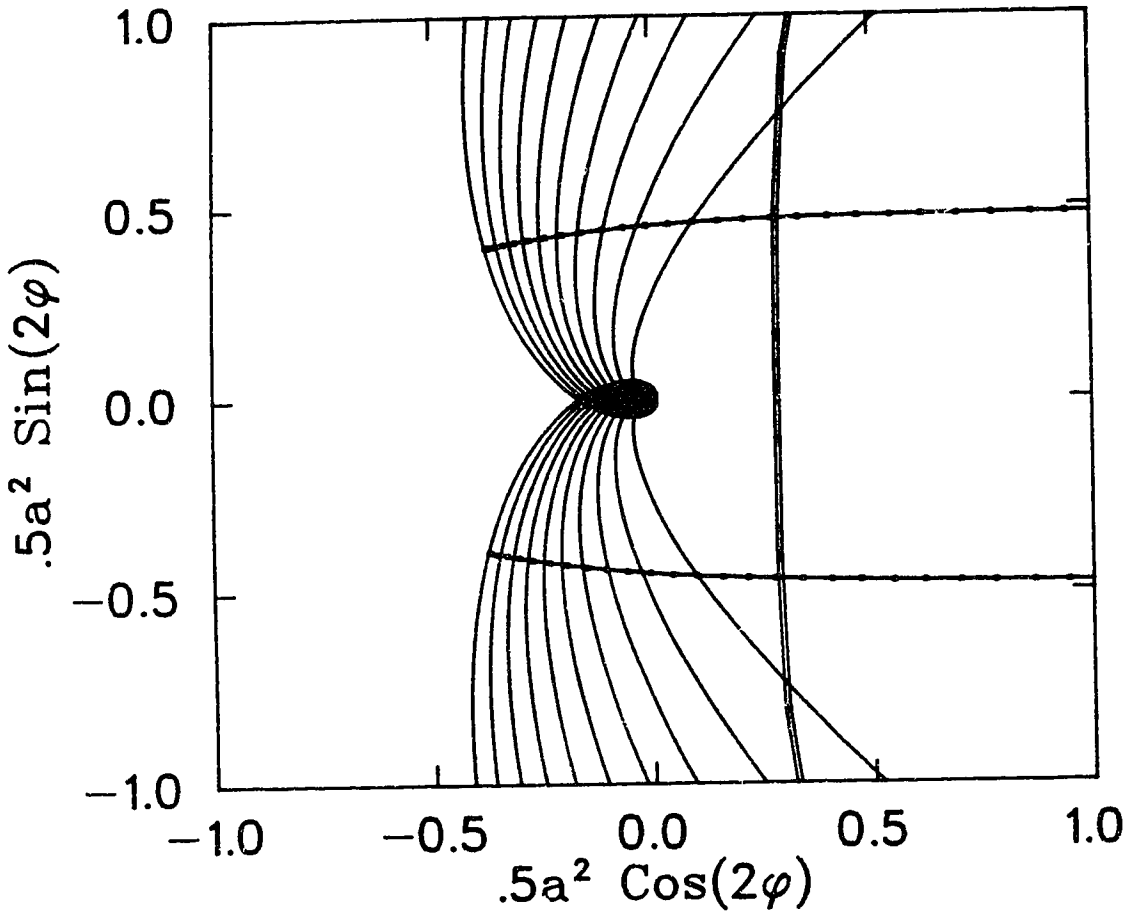

Figure 2.5: Detail near the origin of types (i) and (ii) wormholes in polar coordinates. Also shown are loci of constant conformal factor $P = (1 - r\theta^4/16)$ (see Fig. (2.4) for values). Note the spiraling behaviour of these contours due to the multiple covering of the coordinate system (2.2.18).

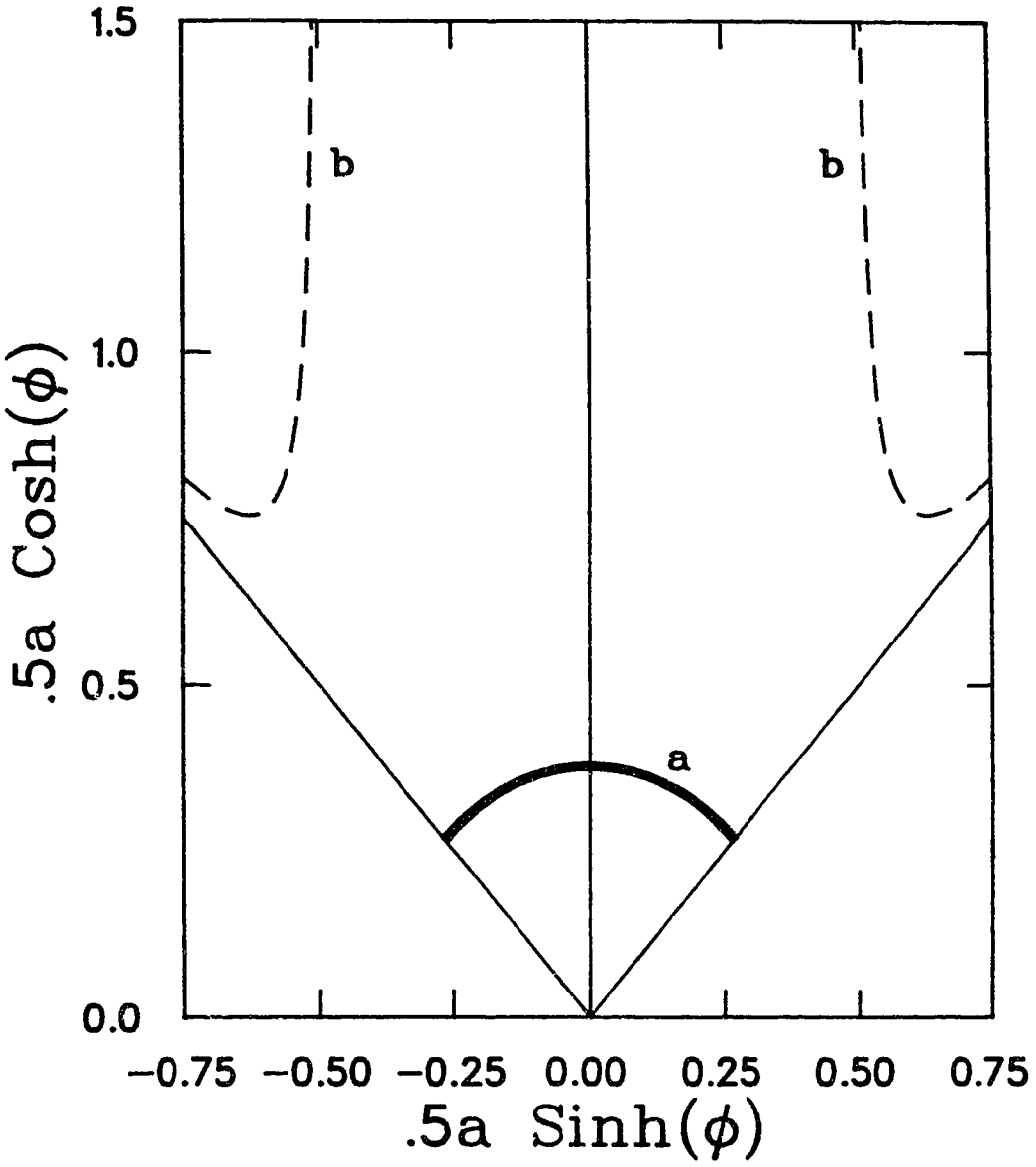

Figure 2.6: Behaviour of Lorentzian section of type (ii) wormhole. The section is taken at the time-symmetric three-geometry where $\varphi = 0$ and Lorentzian momenta conjugate to the Lorentzian matter field $\phi = -i\varphi$ is real. The Lorentzian evolution is plotted in coordinates $x = .5a \sinh \phi$, $y = .5a \cosh \phi$. Graph (a) is the evolution of the Lorentzian geometry. Graphs (b) represent $F = (a^4 - \frac{\lambda}{2}a^6\phi^4) = 0$ i.e. where the conformal factor for the auxiliary minisuperspace (which has a Lorentzian signature) vanishes (see (2.2.24)). We note that on the y-axis $\phi = 0$ and thus the Euclidean and Lorentzian sections join at the intersection of (a) and the y-axis in this plot.

BIBLIOGRAPHY

[1] J. Twamley and D. N. Page, "Wormholes without a conserved charge", submitted to *Phys. Lett.* **B**.

[2] S. B. Giddings and A. Strominger, *Nucl. Phys.* **B307** (1988) 854; S Coleman, *Nucl. Phys.* **B307** (1988) 867; T Banks, *Nucl. Phys.* **B309** (1988) 493; S Coleman, *Nucl. Phys.* **B310** (1988) 643; S W. Hawking, *Nucl. Phys.* **B335** (1990) 155.

[3] W. Fischler and L. Susskind, *Phys. Lett.* **217B** (1989) 48.

[4] L. F. Abbott and M. B. Wise, *Nucl. Phys.* **B325** (1989) 687.

[5] J. Preskill, *Nucl. Phys.* **B323** (1989) 141.

[6] S. Coleman and K. Lee, *Phys. Lett.* **221B** (1989) 242; A Iwazaki, *Phys. Lett.* **229B** (1989) 211; S Coleman and K. Lee, *Nucl. Phys.* **B341** (1990) 101; B Grinstein, *Nucl. Phys.* **B321** (1989) 439.

[7] J. Polchinski, *Nucl. Phys.* **B325** (1989) 619.

[8] J. W. York, *Phys. Rev. Lett.* **28** (1972) 1082; G W. Gibbons and S. W. Hawking, *Phys. Rev.* **D15** (1977) 2752.

[9] S. Coleman and K. Lee, *Nucl. Phys.* **B329** (1990) 387.

[10] L. F. Abbott and M. B. Wise, *Nucl. Phys.* **B325** (1989) 687.

[11] G. W. Gibbons and C. Pope, *Commun. Math. Phys.* **66** (1979) 267.

[12] R. Schoen and S. T. Yau, *Commun. Math. Phys.* **79** (1982) 281.

[13] J. Cheeger and D. Grommol, *J. Diff. Geom.* **4** (1971) 119.

[14] S. Giddings and A. Strominger, *Nucl. Phys.* **B306** (1988) 890; K Lee, *Phys. Rev. Lett.* **61** (1988) 263; C P. Burgess and A. Kshirsagar, *Nucl. Phys.* **B324** (1989) 157; J D. Brown, C. P. Burgess, A. Kshirsagar, B. F. Whiting and J. W. York, *Nucl. Phys.* B**328** (1989) 213.

[15] G. Jungman and R. M. Wald, *Phys. Rev.* D**40** (1989) 2615.

[16] D. N. Page, in *Proceedings of the Banff Summer Institute in Gravitation*, eds. R. Mann and P. Wesson, to appear (World Scientific, Singapore, 1991).

[17] S. Fubini, *Nuovo Cim.* **34A** (1976) 521.

CHAPTER THREE

WORMHOLES IN A $\frac{1}{2}m^2\phi^2 + \frac{1}{4}\lambda\phi^4$ POTENTIAL

3.1 Introduction

In a previous paper [1], (hereafter known as paper I), we presented an explicit solution of the Euclidean Einstein field equations which connects two asymptotically flat Euclidean four spaces. This was the first such solution not to possess a conserved charge. In this paper we present a second solution using a different potential, which again connects two asymptotically flat four spaces and does not possess a conserved charge. In distinction from the model discussed in paper I, the solution presented here displays a much richer spectrum of eigensolutions and related dynamics and arises, in a sense, from a more "natural" potential $V(\phi) = m^2\phi^2/2 + \lambda\phi^4/4$, where we set ϕ to be imaginary ($\varphi = -i\phi$ real).

The discovery of these solutions dispels the conjecture [5], that a wormhole throat of non-zero size is only possible if the wormhole possesses a conserved charge. The conservation of the current associated with the charge resists the collapse of the throat. With the exception of the solution in I, all previously found wormhole solutions possessed a conserved charge related to a cyclic coordinate appearing in the lagrangian.

The presence of a conserved charge associated with the wormhole has played an integral part in current arguments addressing the "Large Wormhole Problem" [3,4,2]. Preliminary results of recent work concerning the inclusion of Euclidean wormhole configurations into the path integral formalism of quantum gravity indicate that wormholes may cause the fundamental coupling constants to float

unpredictably [4]. However, when one attempts to evaluate the probability distribution function for these "constants" semiclassically, together with the prediction that $G\Lambda \to 0$, one finds that wormholes are predicted to be dense on all possible length scales[2]! To circumvent this, Coleman has hypothesised that large wormholes, having a large conserved charge, are de-stabilised by smaller wormholes[5]. The small wormholes bleed off the charge of the larger one, and thus the large wormhole problem has been resolved. This may be the case for theories wherein the wormhole solutions possess a conserved charge, but not so for the wormholes dealt with below and in paper I. In these theories the large wormhole problem re-appears to the extent that the wormholes predicted to exist will be dense in spacetime.

Referring to the results of paper I, we see that even though the charge $a^3\dot{\varphi}$, where a is the scale factor and φ is the imaginary scalar field, was not conserved throughout the wormhole, one can still label the separate wormhole solutions by the asymptotic values that this charge takes in the flat regions connected by the wormhole. However for the wormhole described below, this is not so. The separate solutions can indeed be labeled by the asymptotic value of a particular quantity. This quantity is not that of paper I but is instead the asymptotic constant $a^{3/2}e^{ma}\varphi$, where $\varphi = -i\phi$.

Another property of the solutions described below, not shared by any other known wormhole solution with an imaginary scalar field (i.e. Giddings-Strominger[6], $V = \lambda\varphi^4$[1]) is this: For any non-negative integer N_{MAX}, it is possible to choose ranges for the parameters λ and m such that there will exist at least N_{MAX} pairs of wormhole configurations with each pair possessing N zero crossings of the imaginary scalar field φ, where N ranges from 0 to N_{MAX}. Other characteristics, including the minimum throat size, are elucidated below. How-

ever, of more import is the consideration of the actions of the wormholes of paper I and those described below (hereafter known as paper II). The $\lambda\varphi^4$ wormholes of paper I both have negative actions whereas those of paper II have negative, zero and positive actions depending on N and the quotient $\mu = m/\sqrt{\lambda}$.

a) Contour of Integration

One of the motivations for this work arises from recent research on the "Problem of the Contour of Integration" in the path integral approach to quantum gravity[7,12]. This problem occurs when one attempts to construct a sum over histories formulation for the transition amplitude between two three surfaces Σ, Σ' with matter fields S, S' defined on them, in an effort to create a Feynman-like quantisation scheme for gravity. One essentially sums over all four-geometries $\mathcal{M}$, and matter fields $\mathcal{S}$, that interpolate between (Σ, S) and (Σ', S'), weighted by $\exp(-I_E)$, where I_E is the total Euclidean action of the interpolating geometry $\mathcal{M}$ and matter fields $\mathcal{S}$. However, this path integral is ill-defined, as the Euclidean gravitational action is unbounded below for geometries possessing conformal variations. Thus, it becomes necessary to rotate the contour of integration in the path integral to become complex. One thus sums over complex intermediate geometries and matter fields.

For the case where the four-space is asymptotically flat, a prescription for the rotation of the contour has been advanced by Gibbons, Hawking and Perry[8]. This leads to convergent meaningful results in a number of examples[9]. If the four geometry is closed, as in the case of quantum cosmology, no prescription exists. A program to search quite generally for convergent contours has been carried out by J. J. Halliwell, J. Hartle and J. Louko[7,12]. In this program, the emphasis is on finding a suitable complex contour which is capable of describing the wavefunction

of the Universe, i.e., they implement a number of proposed cosmological boundary conditions for the beginning of the universe at Σ (the no-boundary proposal of Hartle and Hawking [10] and the tunnelling proposal of Vilenkin [11]). Having examined a number of minisuperspace models without matter content, Halliwell and Hartle proposed a list of criteria which the contour should obey[12]. These are (1) The integral defining the wavefunction should converge. (2) The wavefunction should satisfy the constraints implementing diffeomorphism invariance. (3) Classical spacetime, when the universe is large, should be predicted. (4) The correct quantum field theory should be predicted. (5) To the extent that wormholes make the cosmological constant dependent on initial conditions, the wavefunction should predict its vanishing. Of interest to us is criterion (5).

Preliminary analysis by Halliwell and Hartle [12], of semi-classical solutions of the complex Einstein field equations satisfying the no-boundary boundary conditions, indicated that for every solution possessing $Re(\sqrt{g}) > 0$ with action I_1, there existed a complementary solution with $Re(\sqrt{g}) < 0$ having an action I_2, whose real part satisfied $Re(I_2) = -Re(I_1)$. [Later analysis by Halliwell and Louko has shown that in more complicated models, the topology of the space of geometries of the particular minisuperspace in question may conspire to restrict one to either the positive or negative sector of $Re(\sqrt{g}) > 0$ within the model.] It was then conjectured in reference [12], that whereas $Re(\sqrt{g}) > 0$ implies negative action for four-spheres, $Re(\sqrt{g}) > 0$ implies positive action for wormholes. Similarly, wormhole configurations possessing $Re(\sqrt{g}) < 0$ would have negative action. Thus, wormholes with $Re(\sqrt{g}) > 0$ would be suppressed and such configurations would then be included into the contour of integration. Wormholes with $Re(\sqrt{g}) < 0$ and therefore $Re(I_E) < 0$, would not be suppressed and, just as the imaginary analogue of Fubini instantons [13] with negative action do not

dominate the path integral for flat space in $\lambda\phi^4$ theory, so too should the dominant contribution to the contour not arise from such saddle points with negative action.

From the results of papers I and II we see this conjecture not to be valid when the matter action is considered. Inclusion of imaginary matter configurations have a significant effect on the sign of the action. For the case at hand, taking the potential $V = \lambda\phi^4/4$, or $V = m^2\phi^2/2 + \lambda\phi^4/4$, the transition amplitude between two asymptotically flat Euclidean spaces for particular ranges of m and λ, would include wormhole configurations where ϕ is purely imaginary and where the action can become negative. Wormhole production would then proceed at an exponential rate[14]. The wormholes found in papers I and II all have $Re(\sqrt{g}) > 0$ while I_E can become negative. These wormholes would presumably not be included in the contour of integration. However, for some ranges of m and λ, wormholes II possess zero and positive actions. These would seem more likely to be included into the path integral. Thus, when the matter action is included and one allows fully complex matter configurations, $Re(\sqrt{g})$ ceases to be a good indicator concerning the treatment of a particular stationary point of the action as the dominant contributor to the path integral if one wishes the suppression of large wormholes.

The negative actions in wormholes I and II are *not* due to the unboundedness of the conformal mode of the gravitational action, but rather due to the kinetic term of the scalar field lagrangian having the "wrong sign". We note that in both models $I_G \geq 0$. In the other known wormhole solution possessing an imaginary scalar field, i.e. the Giddings-Strominger solution[6], the action is identically zero by virtue of scale invariance and the equations of motion. This "wrong sign" for the kinetic energy of the scalar field is necessary for the construction of a wormhole solution in the minisuperspace ansätze we consider. It appears quite

likely that utilisation of imaginary matter fields will generically lead to negative actions except in special cases of high symmetry in the lagrangian.

To summarise, large wormholes are *not* suppressed by the criterion $Re(\sqrt{g}) > 0$. Furthermore, if one requires that large wormholes be suppressed, then the criterion $Re(\sqrt{g}) > 0$, taken alone, *fails* to include the appropriate saddle points of the action into the contour of integration. This differs from what was conjectured in [12]. The probable reason for the failure of this criterion is the appearance of a negative matter action due to the imaginary nature of the scalar field.

In the following sections we proceed with a derivation of a wormhole-yielding potential within the particular metric ansatz we use. We then perform some preliminary analytical analysis and obtain asymptotic solutions labelled by a parameter χ for the wormhole solutions in the large t domain. The numerical results concerning the first six wormholes are then described, giving the positions in the two dimensional parameter space (χ, μ) where a valid wormhole solution exists together with the actions and individual characteristics of the separate wormholes. We then briefly describe some analytical approximations which treat the ϕ oscillations as adiabatic and which agree very well with the numerical data.

3.2 Description of model

As in our previous paper [1], we will adopt the $k = +1$ Euclidean Robertson-Walker O(3)-invariant metric ansatz,

$$ds_4^2 = \frac{2G}{3\pi}\left[N^2(t)dt^2 + a^2(t)d\Omega_3^2\right] \quad , \tag{3.2.1}$$

appropriately scaled for future convenience, where $d\Omega_3^2$ is the standard O(3)-invariant metric on the unit S^3, and $\hbar = c = 1$. The scalar field will be taken to

be of the form

$$\Phi = \left(\frac{3}{4\pi G}\right)^{1/2} \phi(t) \ , \tag{3.2.2}$$

with a self-interaction potential

$$\tilde{V}(\Phi) = \left(\frac{9}{8G^2}\right) V(\phi) \ . \tag{3.2.3}$$

Using these definitions the Euclidean Einstein-Hilbert action, with the Gibbons-Hawking boundary term [15] at the S^3 boundaries $t_\pm$, is

$$\begin{aligned} I_E &= \int_M d^4x\sqrt{g}\left[-\frac{1}{16\pi G}R + \frac{1}{2}(\nabla\Phi)^2 + \tilde{V}(\Phi)\right] - \int_{\partial M} d^3x\sqrt{h}\frac{1}{8\pi G}(K - K_0) \\ &= \frac{1}{2}\int_{t_-}^{t_+} N dt \left(-a\dot{a}^2 + a^3\dot{\phi}^2 - a + 2a^3V\right) + \frac{1}{2}a^2(t_+) + \frac{1}{2}a^2(t_-) \\ &= \frac{1}{2}\int_{t_-}^{t_+} N dt \left(G_{AB}\dot{X}^A\dot{X}^B + 2U\right) + \frac{1}{2}a_+^2 + \frac{1}{2}a_-^2 \ , \end{aligned} \tag{3.2.4}$$

where K is the trace of the actual extrinsic curvature of the boundaries in the metric (3.2.1), K_0 is that of the corresponding flat metric inside the same boundary while an overdot denotes $N^{-1}d/dt$.

The metric on the (a, ϕ) minisuperspace (DeWitt reduced supermetric) is

$$ds^2 = G_{AB}dX^A dX^B = -ada^2 + a^3 d\phi^2 = e^{3\alpha}(-d\alpha^2 + d\phi^2) \tag{3.2.5}$$

where $\alpha \equiv \ln\, a$, while the minisuperspace potential is

$$U = -\frac{1}{2}a + a^3V(\phi) \ . \tag{3.2.6}$$

The classical equations of motion are

$$2\mathcal{H} = G_{AB}\dot{X}^A\dot{X}^B - 2U = a\left(-\dot{a}^2 + a^2\dot{\phi}^2 + 1 - 2a^2V\right) = 0 \ , \tag{3.2.7}$$

$$\ddot{\phi} + 3\frac{\dot{a}}{a}\dot{\phi} - \frac{dV}{d\phi} = 0 \ , \tag{3.2.8}$$

$$\ddot{a} + 2a\dot{\phi}^2 + 2aV = 0 \ , \tag{3.2.9}$$

describing the dynamics of a particle of mass-squared $-2U$ in the metric (3.2.5), or a spacelike geodesic in the conformally related metric

$$d\tilde{s}^2 = 2U ds^2 = \left(a^2 - 2a^4 V\right)\left(da^2 - a^2 d\phi^2\right) = e^{4\alpha}\left(1 - 2e^{2\alpha}V\right)\left(d\alpha^2 - d\phi^2\right) \ . \tag{3.2.10}$$

We are interested in wormhole solutions connecting two asymptotically flat regions, so $\dot{a} \to \pm 1$ as $t \to \pm\infty$, and $\phi \to \phi_\pm$ with $V(\phi_\pm) = 0$ and $dV(\phi_\pm)/d\phi = 0$. In [1] (hereafter known as paper one), we showed the existence of two such wormhole configurations where Φ is made imaginary and a self-interaction potential of the form $\tilde{V} = \frac{1}{4}\tilde{\lambda}\Phi^4 = \frac{1}{4}\lambda\phi^4$ was used. In both of these configurations ϕ crossed zero at most once, the total action was negative, and only two separate configurations existed for any given value of λ.

In this paper we will elucidate the behaviour of similar asymptotically Euclidean wormhole solutions using a less simplistic, more realistic self-interaction potential. We will also impose the natural restrictions that

$$V(\Phi) \in \mathbb{R} \quad \forall \Phi \in \mathbb{R} \ , \tag{3.2.11}$$

$$V(\Phi) \geq 0 \quad \forall \Phi \in \mathbb{R} \ . \tag{3.2.12}$$

We now investigate the possible form of the potential $V(\Phi)$.

a) Form of the potential $V(\phi)$

It is well known that no real wormhole solutions exist for pure gravity [16,17]. It is essentially necessary for the Ricci tensor, and hence for the matter stress-tensor, to have at least one negative eigenvalue [18]. With the metric (3.2.1)

and with restrictions (3.2.11,3.2.12) and treating Φ as a real field, no wormhole configurations are possible in this model, as (3.2.9) does not allow a wormhole throat if $V(\phi) \geq 0$. More generally, it has been shown by Wald and Jungman [19] that for real Φ, asymptotically flat Euclidean wormholes with Φ tending to 0 sufficiently rapidly in both asymptotic regions, are not possible if $\Phi\, dV(\Phi)/d\Phi \geq 0$. Their argument also rules out similar wormholes for imaginary Φ if $\Phi\, dV(\Phi)/d\Phi \leq 0$. However, imaginary scalar field wormholes have been discovered. By going to imaginary $\phi = i\varphi$, which makes $\dot{\phi}^2 = -\dot{\varphi}^2 \leq 0$, configurations possessing negative eigenvalues for the stress-energy tensor can arise. For a massless scalar field ($V = 0$), wormhole solutions have been found [6]. (The asymptotic values of Φ differ at the two ends, circumventing the Wald-Jungman theorem while leaving the metric itself asymptotically flat.) These possess a conserved charge, the value of π_ϕ, which is the momentum conjugate to ϕ. Solutions exist for any value of π_ϕ and have a linear throat size proportional to $\sqrt{\pi_\phi}$. The total action for these solutions is zero by virtue of scale invariance. For a quartic interaction potential $V(\phi) = \frac{\lambda}{4}\phi^4$, wormhole solutions have also been found [1]. These solutions do *not* possess a conserved charge but can be characterized by the asymptotic value of π_ϕ in the asymptotically flat regions. The two solutions found correspond to (i) opposite values of π_ϕ, (ii) equal values of π_ϕ, at the two asymptotically flat regions. For a fixed value of λ, only two solutions (or four, when one considers the symmetry $\phi \to -\phi$), with specific values of π_ϕ, exist. The total action for each of these wormholes is negative.

The action and equations of motion, in terms of $\varphi = -i\phi$, are

$$I_E = -\frac{1}{2}\int_{t_-}^{t_+} N dt \left(a\dot{a}^2 + a^3\dot{\varphi}^2 + a - 2a^3 V(i\varphi)\right) + \frac{1}{2}\left(a_+^2 + a_-^2\right) \ , \qquad (3.2.13)$$

$$2\mathcal{H} = -a\left(\dot{a}^2 + a^2\dot{\varphi}^2 - 1 + 2a^2 V(i\varphi)\right) = 0 \ , \qquad (3.2.14)$$

$$\ddot{\varphi} + 3\dot{a}\dot{\varphi} = -\frac{dV(i\varphi)}{d\varphi} \quad , \tag{3.2.15}$$

$$\ddot{a} = 2a\left(\dot{\varphi}^2 - V(i\varphi)\right) \quad . \tag{3.2.16}$$

The limits $t_\pm \to \infty$ are taken in (3.2.13) to evaluate the action of a complete wormhole. If we assume that $V(i\varphi_\pm) = 0$, $\frac{dV(i\varphi_\pm)}{d\varphi} = 0$, but $\frac{d^2V(i\varphi_\pm)}{d\varphi^2} < 0$, in the limit $t_\pm \to \pm\infty$, then φ approaches $\varphi_\pm$ exponentially as $t \to \pm\infty$, and the solutions have finite action. We will choose a potential such that these conditions may be satisfied to get a finite action solution; however, one need not necessarily have φ decaying exponentially for finite action. Near the throat region we wish φ to oscillate more than once for most of our solutions. Again referring to equation (3.2.15), this requires $\frac{dV(i\varphi)}{d\varphi} > 0$ for some range of φ. For asymptotic flatness we also need $V(i\varphi_\pm) = 0$, $\frac{dV(i\varphi_\pm)}{d\varphi} = 0$.

Assuming $V(\varphi)$ to be of the form

$$V(\varphi) = \lambda\left[\frac{\varphi^4 - a^2}{\varphi^4 + a^2}\right]\varphi^4 \quad , \tag{3.2.17}$$

and setting $\varphi_\pm = 0$, all of the above requirements are satisfactorily met except $V(\Phi) \not\geq 0 \forall \Phi \in \mathbf{R}$ and $\frac{d^2V(i\varphi_\pm)}{d\varphi^2} \not< 0$. Since $\varphi^4 = (-i\Phi)^4 = \Phi^4$, the form of $V(\Phi)$ is unchanged,

$$V(\Phi) = \lambda\left[\frac{\Phi^4 - a^2}{\Phi^4 + a^2}\right]\Phi^4 \quad , \tag{3.2.18}$$

and is shown in figure (3.1). Numerical analysis has shown the existence of asymptotically flat wormhole configurations[1]. However, this form of potential violates the positivity of V for real Φ and is, by construction, quite artificial. A more realistic $V(\Phi)$ is suggested by Fig. (3.1). We will assume $V(\phi)$ to be of the form

$$\tilde{V}(\Phi) \;=\; \frac{\tilde{m}^2}{2}\Phi^2 + \frac{\tilde{\lambda}}{4}\Phi^4 \quad , \tag{3.2.19}$$

[1]Taking $a^2 \approx 0.1815$, $\lambda = 1$, integrate out from the throat with the scale factor at the throat set to unity.

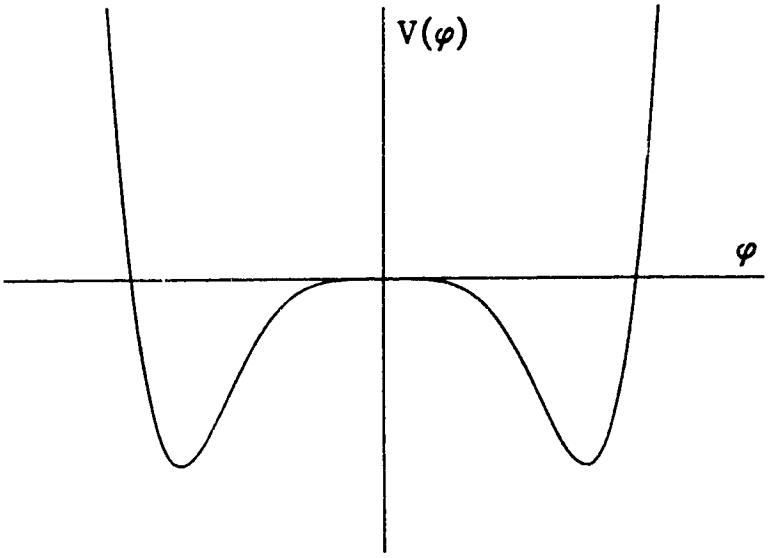

Figure 3.1: Plot of $V(\varphi)$ vs. φ where $V(\varphi) = \lambda\left[\frac{\varphi^4-a^2}{\varphi^4+a^2}\right]\varphi^4$

$$V(\phi) = \frac{m^2}{2}\phi^2 + \frac{\lambda}{4}\phi^4 \ , \tag{3.2.20}$$

$$V(i\varphi) = -\frac{m^2}{2}\varphi^2 + \frac{\lambda}{4}\varphi^4 \ , \tag{3.2.21}$$

With this potential all of the above criteria are satisfied.

3.3 Preliminary Analytical Analysis

By performing a constant conformal transformation $g_{\mu\nu} \rightarrow \tilde{g}_{\mu\nu} = \Omega^2 g_{\mu\nu}$, the classical equations of motion (3.2.7-3.2.9) are left unchanged if one also rescales the potential by $V \rightarrow \tilde{V} = \Omega^{-2}V$. Using this freedom to scale out λ from V, and denoting $\mu = m/\lambda^{1/2}$, the action and equations of motion become

$$\lambda I_E = -\frac{1}{2}\int_{t_-}^{t_+} N dt \left(a\dot{a}^2 + a^3\dot{\varphi}^2 + a + a^3\left[\mu^2\varphi^2 - \frac{\varphi^4}{2}\right]\right) + \frac{1}{2}\left(a_+^2 + a_-^2\right) \tag{3.3.1}$$

$$= -\frac{1}{2}\int_{t_-}^{t_+} N dt e^{3\alpha}\left(\dot{\alpha}^2 + \dot{\varphi}^2 + e^{-2\alpha} + \mu^2\varphi^2 - \frac{\varphi^4}{2}\right) + \frac{1}{2}\left(a_+^2 + a_-^2\right) \ , \tag{3.3.2}$$

$$\dot{\alpha}^2 + \dot{\varphi}^2 \;\; = -2V(\varphi) + e^{-2\alpha} = \;\; \mu^2\varphi^2 - \frac{\varphi^4}{2} + e^{-2\alpha} \;\; , \tag{3.3.3}$$

$$\ddot{\varphi} + 3\dot{\alpha}\,\dot{\varphi} \;\; = -\frac{dV(\varphi)}{d\varphi} = \;\; \mu^2\varphi - \varphi^3 \;\; , \tag{3.3.4}$$

$$\ddot{\alpha} = 3\dot{\varphi}^2 - e^{-2\alpha} = -\dot{\alpha}^2 + 2\dot{\varphi}^2 - 2V(\varphi) = -\dot{\alpha}^2 + 2\dot{\varphi}^2 + \mu^2\varphi^2 - \frac{\varphi^4}{2} \;\; . \tag{3.3.5}$$

For ease of visualization and future analytical approximations, we will also introduce the polar coordinates

$$r = \frac{a^2}{2}, \quad \theta = 2\varphi \;\; . \tag{3.3.6}$$

The action and equations of motion in these polar coordinates are

$$\lambda I_E = -\frac{1}{2}\int_{t_-}^{t_+} \nu dt \left(\hat{r}^2 + r^2\hat{\theta}^2 + 1 - 4rV(\theta)\right) + (r_+ + r_-) \tag{3.3.7}$$

$$= -\frac{1}{2}\int_{t_-}^{t_+} \nu dt \left(\hat{r}^2 + r^2\hat{\theta}^2 + 1 - \frac{r\theta^2}{16}\left(\theta^2 - 8\mu^2\right)\right) + (r_+ + r_-) \;\; , \tag{3.3.8}$$

$$\hat{r}^2 + r^2\hat{\theta}^2 = 1 - 4rV(\theta) = 1 - \frac{r\vartheta^2}{16}\left(\theta^2 - 8\mu^2\right) \;\; , \tag{3.3.9}$$

$$\hat{\hat{r}} - r\hat{\theta}^2 = -2V(\theta) = \frac{\theta^2}{32}\left(\theta^2 - 8\mu^2\right) \;\; , \tag{3.3.10}$$

$$r\hat{\hat{\theta}} + 2\hat{r}\hat{\theta} = -2r\frac{dV}{d\theta} = -\frac{r\theta}{8}\left(\theta^2 - 4\mu^2\right) \;\; , \tag{3.3.11}$$

where $N = \nu/a$ and a hat denotes $\dfrac{d}{\nu dt}$.

As noted above, the solutions describe the dynamics of a particle of mass-squared $-2U$ moving in the flat auxiliary minisuperspace (3.2.5). They are also that of a particle of mass-squared

$$F(\alpha,\varphi) = e^{4\alpha}\left(2e^{2\alpha}V(\varphi) - 1\right) = e^{4\alpha}\left(e^{2\alpha}\left[\mu^2\varphi^2 - \frac{\varphi^4}{2}\right] - 1\right) \;\; , \tag{3.3.12}$$

moving in the alternate flat metric $d\alpha^2 + d\varphi^2$, or of

$$P(r,\theta) = 1 - 4rV(\theta) = 1 - \frac{\theta^2}{16}\left(\theta^2 - 8\mu^2\right) r \ , \tag{3.3.13}$$

in the flat metric $dr^2 + r^2 d\theta^2$. Alternatively, the solutions are spatial geodesics of

$$d\hat{s}^2 = F(\alpha,\varphi)\left(d\alpha^2 + d\varphi^2\right) \ , \tag{3.3.14}$$

$$= P(r,\theta)\left(dr^2 + r^2 d\theta^2\right) \tag{3.3.15}$$

in (α,φ) and (r,θ) coordinate systems.

Eliminating the time parameter, one finds that the evolution is governed by a second-order ordinary differential equation, given, in the above two coordinates, by

$$\frac{d^2\varphi}{d\alpha^2} = \frac{1}{2}\left[1 + \left(\frac{d\varphi}{d\alpha}\right)^2\right]\left(\frac{\partial}{\partial\varphi} - \frac{d\varphi}{d\alpha}\frac{\partial}{\partial\alpha}\right)(\ln F) \ , \tag{3.3.16}$$

in the cartesian coordinates (α,φ), and by

$$\frac{d^2r}{d\theta^2} = r + \frac{2}{r}\left(\frac{dr}{d\theta}\right)^2 + \frac{1}{P}\left[r^2 + \left(\frac{dr}{d\theta}\right)^2\right]\left(-2V + \frac{2}{r}\frac{dr}{d\theta}\frac{dV}{d\theta}\right) \ , \tag{3.3.17}$$

in the polar coordinates (3.3.6). Inserting the explicit forms (3.3.12),(3.3.13) into (3.3.16) and (3.3.17), we get

$$\left(1 + a^2\left[\mu^2\varphi^2 - \frac{\varphi^4}{2}\right]\right)\frac{d^2\varphi}{d\alpha^2} + \left[1 + \left(\frac{d\varphi}{d\alpha}\right)^2\right]\left[\left(2 + 3a^2\left[\mu^2\varphi^2 + \frac{\varphi^4}{2}\right]\right)\frac{d\varphi}{d\alpha} - a^2\left(\mu^2\varphi - \varphi^3\right)\right] = 0 \tag{3.3.18}$$

and

$$\frac{d^2r}{d\theta^2} = r + \frac{2}{r}\left(\frac{dr}{d\theta}\right)^2 +$$

$$\left(1 - \frac{r\theta^2}{16}\left(\theta^2 - 8\mu^2\right)\right)^{-1}\left[r^2 + \left(\frac{dr}{d\theta}\right)^2\right]\left[\theta\left(\theta^2 - 8\mu^2\right) - \frac{4}{r}\left(\theta^2 - 4\mu^2\right)\left(\frac{dr}{d\theta}\right)\right]\frac{\theta}{32} \ . \tag{3.3.19}$$

Equations (3.3.18) and (3.3.19) will prove useful in deriving the asymptotic behaviour of the wormhole solutions.

It is also instructive to compute the two dimensional scalar curvature of the conformally flat metric (3.3.14)

$$ {}^2R = \frac{\theta^8 + 4(\theta^2 - 4\mu^2)\left[\theta^4(r^2 - 4\mu^2) + 16r\right] + 128r\theta^2}{2^8 P(r,\theta)^3} \quad . \tag{3.3.20} $$

This diverges when $P = 0$, which occurs on the curve

$$ r = \frac{16}{\theta^2(\theta^2 - 8\mu^2)} \quad . \tag{3.3.21} $$

However, equation (3.3.17) does not obstruct particular trajectories from crossing $P = 0$. In fact, equations (3.3.16) and (3.3.17) are insensitive to a change in signature of the metric (3.3.14) from $(+,+)$ to $(-,-)$. This makes sense, as we have eliminated the time in obtaining (3.3.16) and (3.3.17). Euclidean time dynamics is restricted to those regions of configuration space where $F(\alpha,\varphi) \geq 0$ (or $P(r,\theta) \geq 0$), while Lorentzian time dynamics is restricted to those regions where $F(\alpha,\varphi) \leq 0$ (or $P(r,\theta) \leq 0$). Trajectories in the auxiliary minisuperspace can cross the $F(\alpha,\varphi) = 0$ (or $P(r,\theta) = 0$) curve and will be regular there. However, re-inserting the time dependence, one sees that on the curve $F(\alpha,\varphi) = 0$, $\dot{\alpha} = \dot{\varphi} = 0$ and the Euclidean time dynamics of any trajectory in the (α,φ) auxiliary minisuperspace that reaches the $F(\alpha,\varphi) = 0$ curve from the $F > 0$ region will have a time-symmetric bounce in both the geometry and matter and hence return to the $F > 0$ region. Crossing $F = 0$ would correspond to analytically continuing the Euclidean time (or the lapse function N) to imaginary values, and would give a transition to a Lorentzian geometry. Regularity of $d^2r/d\theta^2$ at $P = 0$ gives

$$ \left.\frac{dr}{d\theta}\right|_{P=0} = \frac{rV}{\left(\frac{dV}{d\theta}\right)} \quad , \tag{3.3.22} $$

and the tangent at $P = 0$ is

$$\hat{T} = \left(\frac{dr}{d\theta}\right)\hat{r} + r\hat{\theta} = r\left[\frac{V}{\frac{dV}{d\theta}}\hat{r} + \hat{\theta}\right] \quad . \tag{3.3.23}$$

Since the gradient of P, in the metric $dr^2 + r^2 d\theta^2$, is given by

$$\vec{\nabla} P = -4\frac{dV}{d\theta}\left[\frac{V}{\frac{dV}{d\theta}}\hat{r} + \hat{\theta}\right] \quad , \tag{3.3.24}$$

we see, from (3.3.23), that these trajectories meet the curve $P = 0$ normally.

Up to a minus sign, the lagrangian in equation (3.3.8) is that of a unit-mass particle of zero total energy moving in the potential $-P/2$ in the flat metric $dr^2 + r^2 d\theta^2$. By (3.3.13), we get

$$\vec{a} = -\vec{\nabla}(2rV(\theta)) = -2V\vec{\nabla}r - 2r\frac{dV}{d\theta}\vec{\nabla}\theta = -2V(\theta)\hat{\mathbf{r}} - 2\frac{dV}{d\theta}\hat{\theta} \quad , \tag{3.3.25}$$

$$= \frac{1}{32}\left[\theta^2\left(8\mu^2 - \theta^2\right)\hat{\mathbf{r}} + 4\theta\left(4\mu^2 - \theta^2\right)\hat{\theta}\right] \quad , \tag{3.3.26}$$

where $\hat{\mathbf{r}}, \hat{\theta}$ are the radial and angular unit vectors. In Figure (3.2) we plot contours of constant P in the polar coordinates (r, θ). The double troughs at $\theta = \pm 2\mu$, the boundary $P = 0$ (where ${}^2R$ diverges), and the "false vacuum" at $\theta = 0$ are clearly evident. The force vector field (3.3.26) (appropriately normalized to be visible) is also plotted.

3.4 Numerical Analysis

a) Introduction

Eliminating the arbitrary constant associated with the origin of time, equations (3.3.3-3.3.5), or equations (3.3.16,3.3.17) have a two-parameter set of solutions. Since the form of $V(\theta)$ was chosen to yield an exponential solution for φ

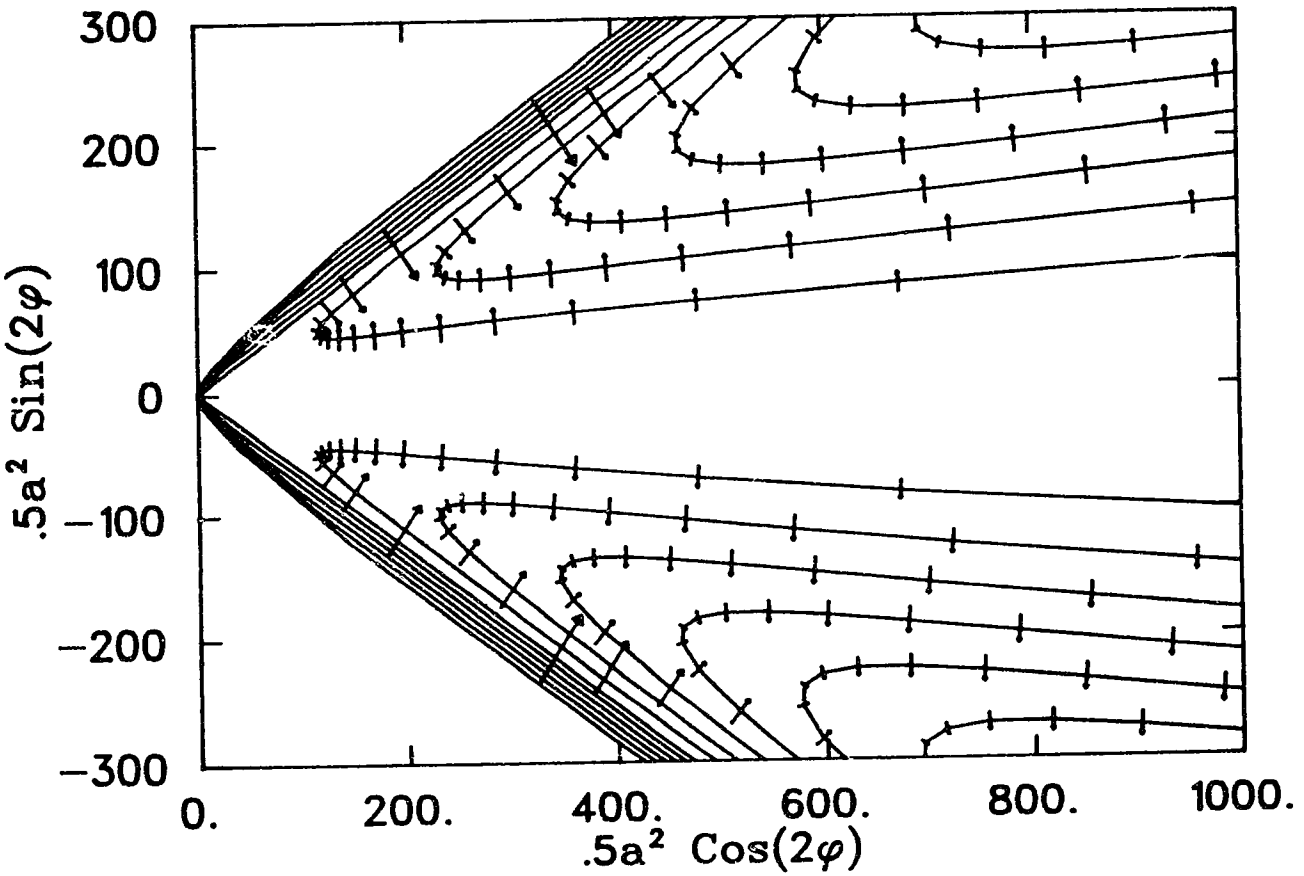

Figure 3.2: Plot of contours of constant P (3.3.13) and the force vector field (3.3.27) in the polar coordinates (r, θ). The P contours begin at zero with increments of .2, while the force vectors have been magnified by ≈ 60.

at large a, choosing the decaying mode of φ leaves us with a one parameter set of solutions. We then integrate in the $-t$ direction, through the wormhole throat and out to the other side. Imposing the boundary condition that $\varphi \to 0$ as $t \to -\infty$ yields a wormhole configuration connecting two asymptotically flat regions. Imposing a single boundary condition on a one parameter set of solutions should give a discrete "spectrum" of allowable wormhole configurations.

A more intuitive understanding can be obtained through consideration of the actual form of $V(\varphi)$. The potential V has the standard mexican-hat shape. If one begins with $\dot{\alpha} = \dot{\varphi} = 0$ at a throat where $\varphi = \varphi_0$, one needs $V(\varphi_0) > 0$ or $|\varphi_0| > \sqrt{2}\mu$. Then the scalar field φ will roll down V and will generically execute damped oscillations about either of the two true vacuums. Naively, if one increases $|\varphi_0|$, thus increasing the initial energy E_0, one expects φ to make a larger number of oscillations crossing $\varphi = 0$ before settling in either true vacuum. By continuity, there exits discrete $|\varphi_0|$ where $\varphi(t = \pm\infty) = 0$, and the field is in the "false vacuum" state.

However, because of the non-linear appearance of the friction terms in (3.2.15), the dynamics is rather more complicated. Allowing more general boundary conditions at the throat, we now partially summarize the numerical and analytical results,

(a) Wormholes only occur for $\mu \leq \mu_c \approx 0.402$.

(b) For fixed $\mu \leq \mu_c$, allowing $|\varphi|$ to range from $|\varphi_{0\,max}|$ to $|\sqrt{2}\mu|$ yields an even number of wormhole configurations where N, the number of zero-crossings of φ, changes in unit steps, increasing from zero to a maximum and decreasing back to zero.

(c) As $\mu(<\mu_c)$ decreases, the maximum N obtainable increases in unit steps.

(d) Only two type of wormholes are found, (i) those with $\dot{\alpha}=\dot{\varphi}=0$ at the throat, and (ii) those with $\dot{\alpha}=\varphi=0$ at the throat. An even N wormhole is of type (i), while an odd N wormhole is of type (ii).

These observations may be heuristically modelled as follows. Referring to paper one [1], the generic behaviour of φ in the $\frac{\lambda}{4}\varphi^4$ potential for late times was oscillatory, decreasing in amplitude as a^{-1}, too slow for a finite action. However, introducing the $-\frac{m^2}{2}\varphi^2$ term creates a small barrier which will eventually halt the oscillation of φ about zero. By making this barrier as small as we wish and arranging $\varphi(t=\pm\infty)=0$, any given N type wormhole with finite action may be obtained. The action, however, will grow with increasing N.

The friction term, $-3\dot{\alpha}\dot{\varphi}$, tends to dominate the dynamics if $|\varphi_0|>|\varphi_{0\,max}|$. For $|\varphi_0|>|\varphi_{0\,max}|$, φ will not cross zero but will settle in the nearest false vacuum. For $|\varphi_0|<|\varphi_{0\,max}|$, $\dot{\varphi}$ decreases and the friction losses are overcome by the initial energy E_0, thus enabling φ to cross zero. Decreasing $|\varphi_0|$ increases the margin of E_0 over the friction losses, thus allowing φ to cross zero more than once. Decreasing φ_0 still further will eventually reduce this margin as E_0 also decreases. Thus N decreases. Decreasing $|\varphi_0|$ to $\sqrt{2}\mu$ will not result in a wormhole as $E_0=0$ while the friction is still present. Thus N decreases to zero.

We now describe the numerical analysis in detail.

b) Preliminary Numerical Analysis

The asymptotic analysis of equations (3.3.3-3.3.5), (3.3.16,3.3.17) is quite different than that of $V(\varphi)=\frac{\lambda}{4}\varphi^4$ [1]. The dominant behaviour near small φ (large

t) may be uncovered by noting

$$\frac{d^2z}{dt^2} = z\left(\mu^2 + \frac{3}{4}\frac{\dot{a}^2}{a^2} + \frac{3}{2}\frac{\ddot{a}}{a}\right) \quad , \tag{3.4.1}$$

where $z = a^{3/2}\varphi$ and where we have discarded non-linear terms in φ. Thus, for large t, assuming $|\dot{a}| \to 1, \ddot{a} \to 0$ as $t \to \pm\infty$,

$$\varphi(t) \approx t^{-3/2}\left(Ae^{-\mu t} + Be^{+\mu t}\right) \quad . \tag{3.4.2}$$

Retaining the first two terms on the right hand side of (3.4.1) we get

$$\frac{d^2z}{dt^2} - \left[\mu^2 + \frac{3}{4t^2}\right] z = 0 \quad . \tag{3.4.3}$$

The decaying solution to (3.4.3) is

$$z = \sqrt{t}\mathrm{K}_1(\mu t) = \sqrt{\frac{\pi}{2}}e^{-\mu t}\sum_{k=0}^{\infty}\frac{\Gamma(1+k+1/2)t^{1/2}}{(2\mu t)^k k!\Gamma(1-k+1/2)} \quad , \tag{3.4.4}$$

where K_1 is the first order modified Bessel's function. Thus a first approximation gives

$$a \approx t \quad , \tag{3.4.5}$$

$$\varphi \approx A\frac{\mathrm{K}_1(\mu t)}{t} \quad . \tag{3.4.6}$$

One can re-iterate these equation to obtain further refinements. Doing this results in

$$a \approx t + A^2\pi e^{-2\mu t}\frac{3}{8t^2}\left[1 + \frac{7}{4t\mu} + \frac{75}{96t^2\mu^2} + \cdots\right] \quad , \tag{3.4.7}$$

$$\varphi \approx A\frac{\mathrm{K}_1(\mu t)}{t} \quad . \tag{3.4.8}$$

However, this method tends not to give uniformly convergent results and the estimation of the degree of approximation is difficult. Instead, we will assume the following forms for a, φ

$$a \approx t + e^{-2\tau}t^{-2}\sum_{n=0}^{\infty} b_n\tau^{-n} \quad , \quad \varphi \approx e^{-\tau}t^{-3/2}\sum_{n=0}^{\infty} c_n\tau^{-n} \quad , \tag{3.4.9}$$

where $\tau = \mu t$. Inserting these into the equations of motion and solving for the coefficients b_n, c_n gives

$$a \approx t + e^{-2\tau} t^{-2} \frac{3c^2}{4} \left[1 + \frac{3}{\tau} - \frac{11}{32\tau^2} + \mathcal{O}(\tau^{-3}) \right] \quad , \tag{3.4.10}$$

$$\varphi \approx c e^{-\tau} t^{-3/2} \left[1 + \frac{3}{8\tau} - \frac{15}{128\tau^2} + \mathcal{O}(\tau^{-3}) \right] \quad , \tag{3.4.11}$$

where $c = c_0$. A symbolic computer code (see Appendix B) was written to solve the coefficients a_n, b_n, c_n, d_n appearing in the trial expansions

$$a \approx t + e^{-2\tau} t^{-2} \sum_{n=0}^{\infty} b_n \tau^{-n} + e^{-4\tau} t^{-5} \sum_{n=0}^{\infty} c_n \tau^{-n} \quad , \tag{3.4.12}$$

$$\varphi \approx e^{-\tau} t^{-3/2} \sum_{n=0}^{\infty} d_n \tau^{-n} + e^{-3\tau} t^{-9/2} \sum_{n=0}^{\infty} e_n \tau^{-n} \quad . \tag{3.4.13}$$

Other than the expressions appearing in (3.4.12) and (3.4.13), no combinations of exponentials and powers of t, τ of lower power give consistent equations for the coefficients. With these forms for a and φ, one can include the φ^3 term in (3.3.4). The resulting solution is

$$\begin{aligned} a \approx\ & t + e^{-2\tau} t^{-2} \frac{3c^2}{4} \left[1 + \frac{3}{4\tau} - \frac{11}{32\tau^2} + \frac{103}{128\tau^3} \right. \\ & \left. - \frac{4645}{2048\tau^4} + \frac{61305}{8192\tau^5} - \frac{1855455}{65536\tau^6} + \mathcal{O}(\tau^{-8}) \right] \\ & + e^{-4\tau} t^{-5} \frac{45c^4}{128} \left[1 + \frac{456}{25\tau} - \frac{33}{40\tau^2} + \frac{7}{2\tau^3} + \mathcal{O}(\tau^{-4}) \right] \quad , \end{aligned} \tag{3.4.14}$$

$$\begin{aligned} \varphi \approx\ & \frac{\mu^{1/2} c}{t} \sqrt{\tfrac{2}{\pi}} \mathrm{K}_1(\tau) \\ & - e^{-3\tau} t^{-9/2} \frac{9c^3}{16} \left[1 + \frac{15}{8\tau} - \frac{107}{128\tau^2} + \frac{18632}{8417\tau^3} - \frac{205005}{37768\tau^4} + \mathcal{O}(\tau^{-5}) \right] \quad . \end{aligned} \tag{3.4.15}$$

Thus

$$\varphi(a) \sim c a^{-3/2} e^{-\mu a} \sim \mu \left(\frac{x}{\chi} \right)^{-3/2} e^{\chi - x} \quad , \tag{3.4.16}$$

where

$$x = \mu a \quad \text{and} \quad \chi + \frac{3}{2}\ln\chi = \ln(\quad{}^{/2}) \ . \tag{3.4.17}$$

We now obtain an expression for a test function, the zeros of which indicate the presence of asymptotically flat space. Integrating through the wormhole and beyond, φ will generically undergo decaying oscillations towards $\pm\mu$, the minimum of the potential. Assuming $\varphi \sim \varphi_0 = +\mu$ and neglecting $\dot{\varphi}$, equation (3.3.3) may be integrated to give

$$a \approx \frac{1}{\sqrt{2V_0}}\sinh(\sqrt{2V_0}t) \ , \tag{3.4.18}$$

$$\dot{a} \approx \sqrt{2V_0}\coth(\sqrt{2V_0}t) \stackrel{t\to\infty}{\to} \sqrt{2V_0} \ , \tag{3.4.19}$$

where $V_0 = \mu^4/4$.

For small perturbations in φ about μ, $\varphi = \varphi + x$, say, equation (3.3.4) becomes

$$\ddot{\varphi} + 3\dot{a}\dot{\varphi} + \frac{dV}{d\varphi} \approx \ddot{x} + \frac{3}{\sqrt{2}}\mu^2\dot{x} + 2\mu^2 x = 0 \ . \tag{3.4.20}$$

Taking $x = Ae^{i\hat{\omega}t} + c.c.$, we obtain

$$\hat{\omega} \ = \ \pm\omega + i\gamma = \pm\sqrt{2}\mu\sqrt{1 - \frac{3\mu^2}{16}} + \frac{3i\mu^2}{2\sqrt{2}} \ , \tag{3.4.21}$$

$$\approx \ \pm\omega_0 + i\gamma \ , \tag{3.4.22}$$

where $\omega_0 = \sqrt{2}\mu$ and $|\hat{\omega}| \approx \sqrt{\omega_0^2 + \gamma^2}$. If we define $S = Ae^{i\hat{\omega}t}$, then

$$x = S + S^* , \quad \dot{x} = i\hat{\omega}S - i\hat{\omega}^*S^* \ , \tag{3.4.23}$$

which can be solved for $S(x, \dot{x})$ and $S^*(x, \dot{x})$. Computing the norm $SS^* = |A|^2e^{-2\gamma t}$ yields

$$|A|^2 \approx e^{2\gamma t}\left[\frac{\omega_0^2x^2 + 2\gamma x\dot{x} + \dot{x}^2}{4(\omega_0^2 + \gamma^2)}\right] \ . \tag{3.4.24}$$

From equation (3.4.19) we can eliminate $t = \alpha/\sqrt{2V_0}$, and using the definitions of ω_0 and γ we finally obtain

$$|A|^2 = \mathcal{E} = e^{3\alpha}\left[2\mu^2(\varphi-\mu)^2 + \frac{3\mu^2}{\sqrt{2}}(\varphi-\mu)\dot{\varphi} + \dot{\varphi}^2\right] \quad . \tag{3.4.25}$$

(Note: if, instead, φ tends towards $-\mu$, we replace μ with $-\mu$ in (3.4.25)). Defining $\mathcal{E}_\infty = \lim_{t\to-\infty}\mathcal{E}$, this $\mathcal{E}_\infty$ will be larger if the trajectory spends more time near $\varphi = 0$ before rolling down into the trough. To obtain the desired test function, we calculate

$$\mathcal{F} = \lim_{t\to\pm\infty}\frac{\mathrm{sign}(\varphi)}{\mathcal{E}} \quad . \tag{3.4.26}$$

Before discussing the results of the numerical analysis, let us first consider the total action of an asymptotically flat Euclidean wormhole,

$$I_E = \int\sqrt{g}\,d^4x\left[-\frac{R}{16\pi G} - \frac{3}{8\pi G}(\nabla\varphi)^2 + \frac{9}{8G^2}\left(-\frac{1}{2}\mu^2\varphi^2 + \frac{1}{4}\varphi^4\right)\right] \quad , \tag{3.4.27}$$

$$= I_G + I_K + I_V \quad , \tag{3.4.28}$$

$$= -\frac{1}{2}\int_{-\infty}^{+\infty} N dt\, a^3\left(\ddot{\alpha} + 2\dot{\alpha}^2 + e^{-2\alpha} + \dot{\varphi}^2 + \mu^2\varphi^2 - \frac{1}{2}\varphi^4\right) \quad . \tag{3.4.29}$$

For the wormhole to be a solution of the Einstein field equations, the action must be stationary with respect to small perturbations in the metric and matter field. Making the scaling or constant conformal transformation, $g_{\mu\nu} \to \Omega^2 g_{\mu\nu}$, the action becomes

$$I \to I_G\Omega^2 + I_K\Omega^2 + I_V\Omega^4 \quad . \tag{3.4.30}$$

Assuming $\Omega = 1 + \epsilon$, the first variation of the action is

$$\delta I = (2I_G + 2I_K + 4I_V)\epsilon \quad . \tag{3.4.31}$$

Setting this to zero yields

$$I_G + I_K = -2I_V \quad , \tag{3.4.32}$$

which gives

$$I = -I_V \ . \tag{3.4.33}$$

Integrating I_K by parts, using the equations of motion and boundary conditions at infinity, one can show

$$I_K = -I_V - \frac{1}{4}\int_{-\infty}^{+\infty} N dt\, a^3 \varphi^4 \ , \tag{3.4.34}$$

that is $I_K < -I_V$, irrespective of the sign of I_V. Inserting this into (3.4.32) we obtain

$$I_G = -I_V + \frac{1}{4}\int_{-\infty}^{+\infty} N dt\, a^3 \varphi^4 \ . \tag{3.4.35}$$

This agrees with paper one [1], since for $V = \frac{1}{4}\lambda\varphi^4$,

$$I_V = \frac{1}{4}\int_{-\infty}^{+\infty} N dt a^3 \varphi^4 \tag{3.4.36}$$

and thus $I_G = 0$. With the purely quartic potential $I_V > 0$ and by (3.4.34), $I_K = -2I_V$. (This can also be obtained through an infinitesimal variation of the action with respect to φ.) The sign of the present potential term, and hence the total action, cannot be determined as the potential is the difference of two positive quantities. However, from the expression

$$I_V = -\frac{1}{2}\int_{-\infty}^{+\infty} N dt\, a^3 \left(\mu^2\varphi^2 - \frac{1}{2}\varphi^4\right) \ , \tag{3.4.37}$$

and realising that for small φ the $\mu\varphi^2$ term dominates, it would appear that wormholes with a smaller value of φ throughout the evolution, and especially near the throat, will have a more positive action. One could, for instance, take the maximum value of φ as an indicator. Note however, the $\liminf |\varphi| = \sqrt{2}\mu$. This general argument is born out in the numerical analysis.

In chapter two, we compared the total wormhole action with twice the action of a flat space, imaginary field, solution with the same potential. To find a

similar flat space solution for the present potential one must solve

$$-\frac{d^2\varphi}{dr^2}-\frac{3}{r}\frac{d\varphi}{dr}=g(\varphi)=-\mu^2\varphi+\varphi^3\ . \tag{3.4.38}$$

This is a generalized Lane-Emden equation, and the existence of spherically symmetric solutions obeying the boundary conditions $d\varphi/dr(r=0)=0,\quad \varphi(r=\infty)=0$ has been shown for $g(\varphi)>0$ [20]. However, for $g(\varphi)$ as given in (3.4.38), numerical analysis strongly suggests that no solutions satisfying these particular boundary conditions exist. Thus, we conjecture, for real Φ, non-trivial solutions exist, while for [illegible] Φ, no solutions exist.

c) Numerical results

To integrate the equations of motion, a fourth order Runge-Kutta algorithm was used. The pertinent portions of this code are described in Appendix B. Initial numerical experiments integrated outwards from the throat ($t=0$) with the boundary conditions

$$\dot{\alpha}=\dot{\varphi}=0,\quad \text{or}\quad \dot{\alpha}=\varphi=0\ , \tag{3.4.39}$$

at $t=0$, with $a(t=0)$ chosen such that $\varphi \overset{t\to\infty}{\to} 0$. The general characteristics of these solutions, as described in subsection a), were obtained during these initial experiments. To allow the possibility of throat configurations more general than those specified by (3.4.39), we impose the boundary conditions at large $+t$ through the use the of the asymptotic solutions (3.4.14) and (3.4.15). Examining the zeros of $\mathcal{F}(\chi)$ (3.3.12,3.4.17) for a fixed μ, yields all the possible wormholes occurring at this value of μ. Brent's algorithm was used to pin-point the roots of $\mathcal{F}(\chi)$ [21]. The zeros of $\mathcal{F}(\chi,\mu)$ corresponding to the first six wormholes are shown in figure

(3.3). These numerical results were obtained by a rather lengthy computer code which is briefly described in Appendix B.

As mentioned in item (b) in subsection a), the set (χ, μ) for which $\mathcal{F}(\chi, \mu) = 0$, for a particular N, is doubled valued in μ (with χ fixed), and single valued in χ (with μ fixed). Only two types of wormhole configurations were found. Even N curves represent wormholes with $\dot{\alpha} = \dot{\varphi} = 0$ at the throat, while odd N curves represent wormholes with $\dot{\alpha} = \varphi = 0$ at the throat (see figure (3.4) for information concerning the scale factor and matter fields for wormholes with $\mu = 0.2$).

From figure (3.4), we note that large χ corresponds to smaller $|\varphi^2|$ throughout the evolution. [Note: in figure (3.4) χ increases from graph (A) to (B) to (C) to (D) as can be seen from figure (3.3). Also note that $\liminf |\varphi_{\max}| = \sqrt{2}\mu$ which for $\mu = .2$ gives $\liminf \varphi \approx 0.283$. This limiting configuration is approached closest by graph (D) in figure (3.4).] If K wormholes occur at a particular μ, then the $K/2$ wormholes with larger χ represent those wormholes referred to in our previous heuristic model with low initial energy (E_0), increasing friction and N decreasing to zero in unit steps. The $K/2$ wormholes with lower χ are those wormholes possessing an increasing margin of E_0 over friction as max $|\varphi|$ decreases.

From figure (3.3), for an N-type wormhole to exist, $\mu \leq \mu_{MAX_N}$. For $N = 0$, $\mu_{MAX_0} \approx 0.402$. However, as can be seen in figure (3.5), an empirical estimate of

$$\mu_{MAX_N} \sim \frac{.402}{(N+1)^2} \tag{3.4.40}$$

models the results quite well. Also plotted in figure (3.5) is the curve $\chi = \frac{1}{2\mu}$, or $\omega = \chi\mu = 0.5$. Thus, when $\omega \approx 1/2$, for fixed μ, N is maximized, whereas for fixed N, μ is maximized, that is

$$\frac{d}{d\omega}(\mu N)\Big|_{\omega=1/2} \approx 0 \ . \tag{3.4.41}$$

The large χ asymptotic behaviour of these curves is well modeled by the formula

$$\chi \sim \frac{1}{(M+1)\mu^2} \ , \tag{3.4.42}$$

as can be seen in figure (3.6) where (3.4.42) is plotted for $M = 0,..,3$.

Information concerning the minimum scale factor, the matter action and the gravitational action along each N-type wormhole curve in the (χ, μ) parameter space was also gathered by this program.

Information concerning the minimum scale factor, and hence, the volume of the minimal hypersurface $2\pi^2 a_{MIN}^3$, is presented in figures (3.7,3.8). As a function of μ, a_{MIN} is double valued, while as a function of χ it is single valued. For fixed μ, a_{MIN} monotonically increases as N ranges from zero to a maximum and back to zero again. Thus, a_{MIN} may be used to label the "spectrum" of wormholes for a fixed μ.

Of more interest, however, is the behaviour of the action. In figures (3.9,3.10) we plot the matter action, gravitational action and total action suitably scaled in order to enhance the behaviour at small values of the action. As we predicted in section a), $I_G \geq 0$, whereas $I_E = I_G + I_M = -I_V$ changes sign when

$$I_V = -\frac{1}{2}\int_{-\infty}^{+\infty} N dt\, a^3 \left(\mu^2\varphi^2 - \frac{1}{2}\varphi^4\right) = 0 \ . \tag{3.4.43}$$

For $N = 0,..,5$, the approximate parameters (χ_{0_N}, μ_{0_N}) where $I_E = -I_V = 0$ is shown in figure (3.11). For a specific N, when $\chi < \chi_{0_N}$, the total action is negative. Note that $\chi_{0_N} > \frac{1}{2\mu_{0_N}}$. Thus there exist certain small ranges of μ where the number of negative action wormholes (N_{I-}) exceeds the number of positive action wormholes (N_{I+}). However, for most of the range of μ, $N_{I+} = N_{I-}$.

For a more concrete visualization of the various wormhole configurations,

we plot the solutions for $\mu = 0.2$ in the cartesian coordinates (α, φ) and polar coordinates (r, θ) in figures (3.12) and (3.13). See table (3.1) at the end of this chapter for the roots of $\mathcal{F}(\chi, \mu = 0.2)$. Also plotted in figure (3.12) is a non-

Label	N	χ
A	0	0.382392
B	1	2.226829
C	1	3.597605
D	0	11.881919

Table 3.1: Table of roots of $\mathcal{F}(\chi, \mu = 0.2)$ giving four wormhole solutions.

wormhole solution where φ falls into one trough. Clearly visible are the two types of wormholes, with a_{MIN} monotonically increasing and $\overline{\varphi^2}$ decreasing with each new wormhole solution. Also featured in figure (3.13) are the constant contour lines of P (3.3.13) beginning with $P = 0$. From figure (3.12) it is clear that type (i) wormholes possess three turning points in the scale factor a or α - one at $P = 0$ ($\dot{\alpha} = \dot{\varphi} = 0$) and two where the tangent of the trajectory is vertical (see also figure (3.4)). Type (ii) wormholes have only one turning point in α, that is, where $\varphi = 0$ at $a = a_{MIN}$.

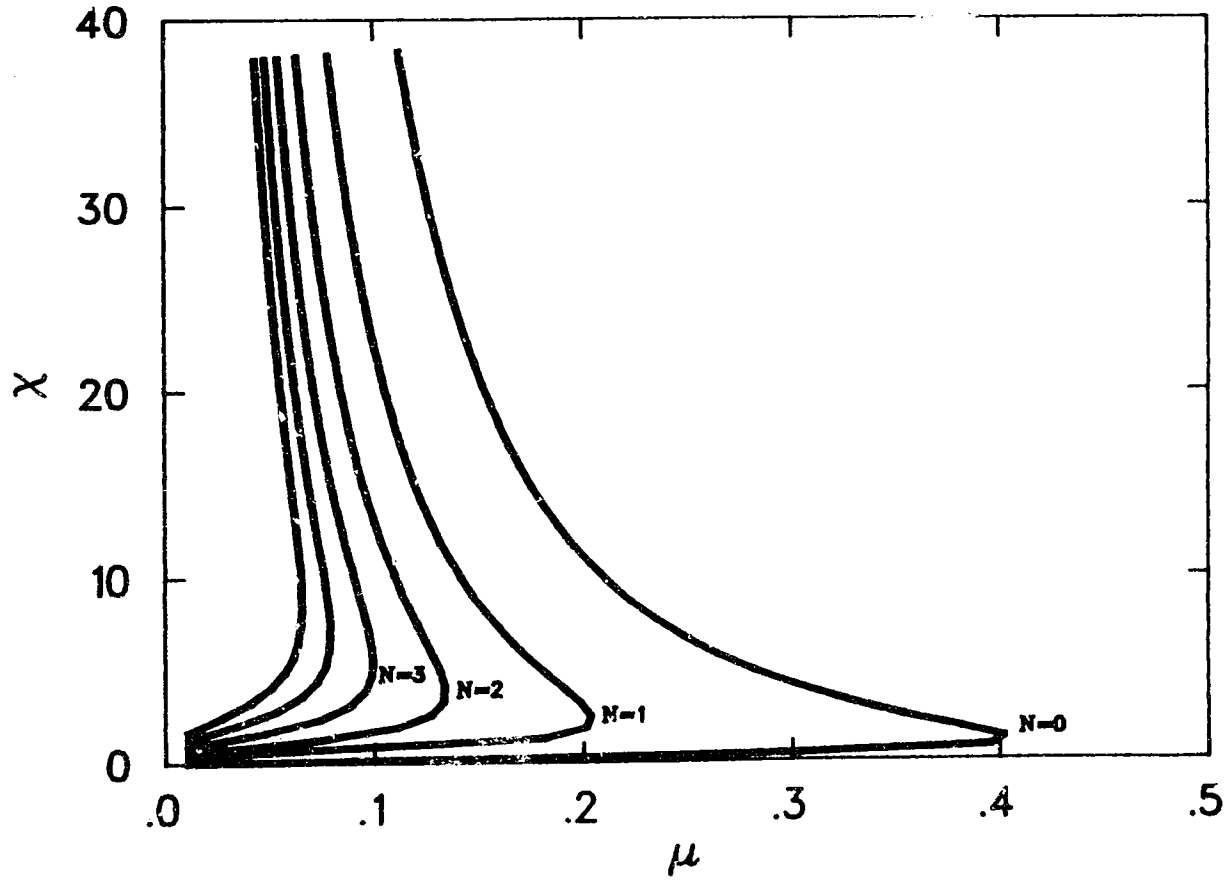

Figure 3.3: Loci of $N = 0,..,5$ wormhole solutions in the (χ,μ) parameter space (3.4.17).

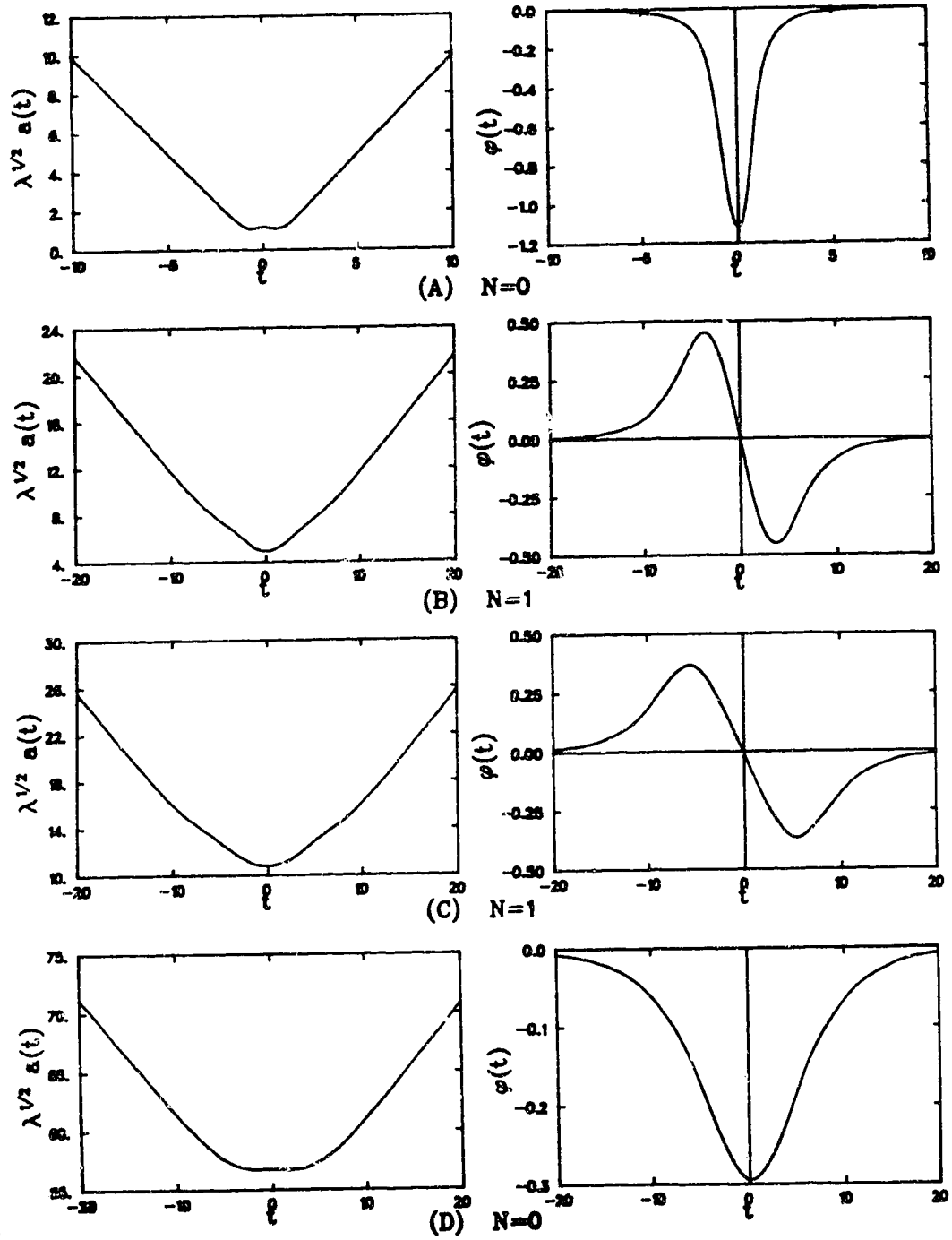

Figure 3.4: Behaviour of $a(t)$, $\varphi(t)$ for the four wormhole solutions occurring at $\mu = 0.2$. See table (3.1) for labeling.

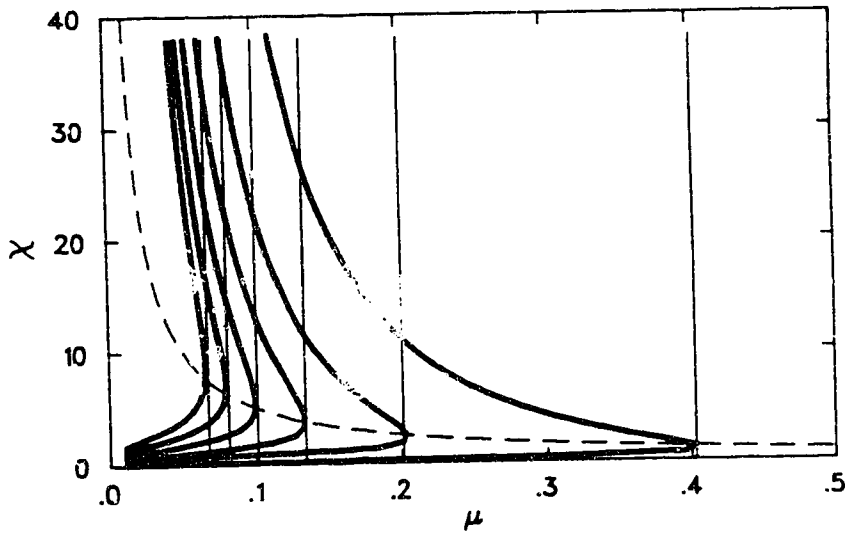

Figure 3.5: Empirical fitting to the numerical results in figure (3.3). The vertical lines occur at $.402/(N+1)$ where $N = 0,..,5$. The dashed line is given by $\frac{1}{2\mu}$.

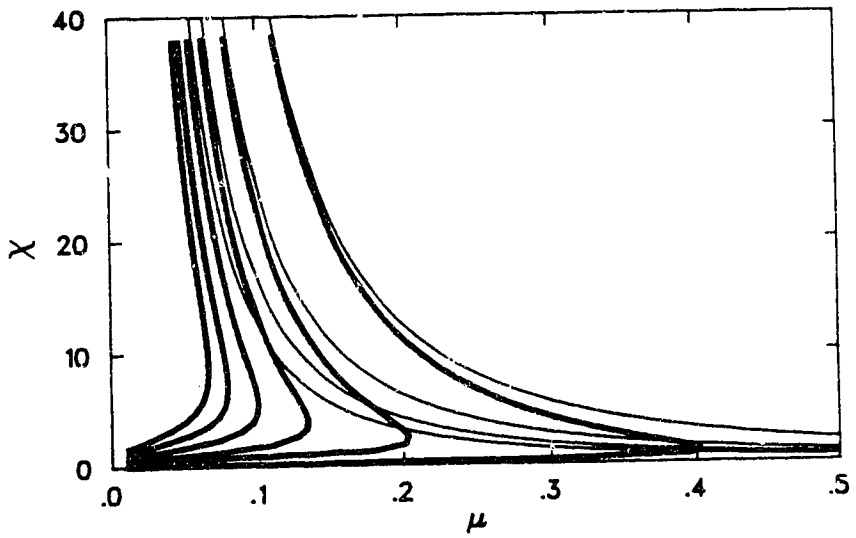

Figure 3.6: Empirical fitting to the numerical results in figure (3.3). The thin curves are given by $\frac{1}{(M+1)\mu^2}$ where $M = 0,..,3$. In both this figure and (3.5) the numerical results from figure (3.3) are represented as bold lines.

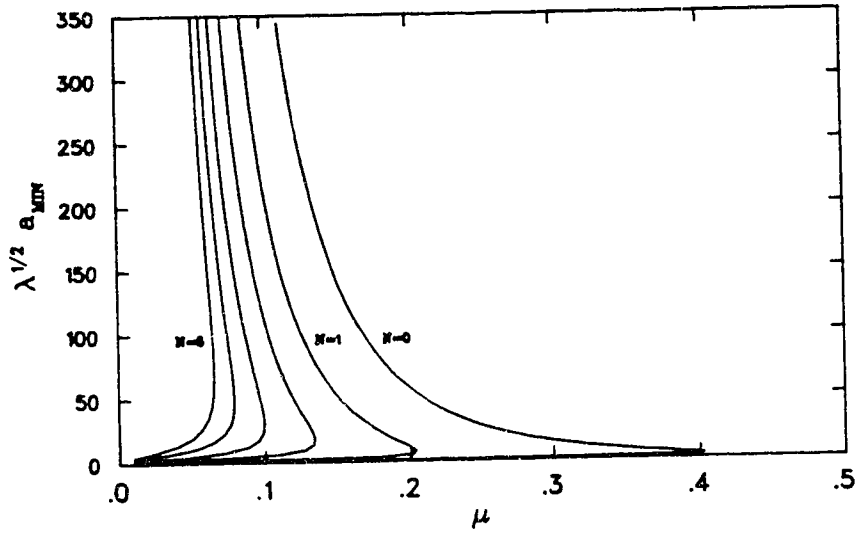

Figure 3.7: Dependence of the minimal scale factor $\lambda^{1/2}a_{MIN}$, on μ, for the $N = 0,..,5$ wormholes.

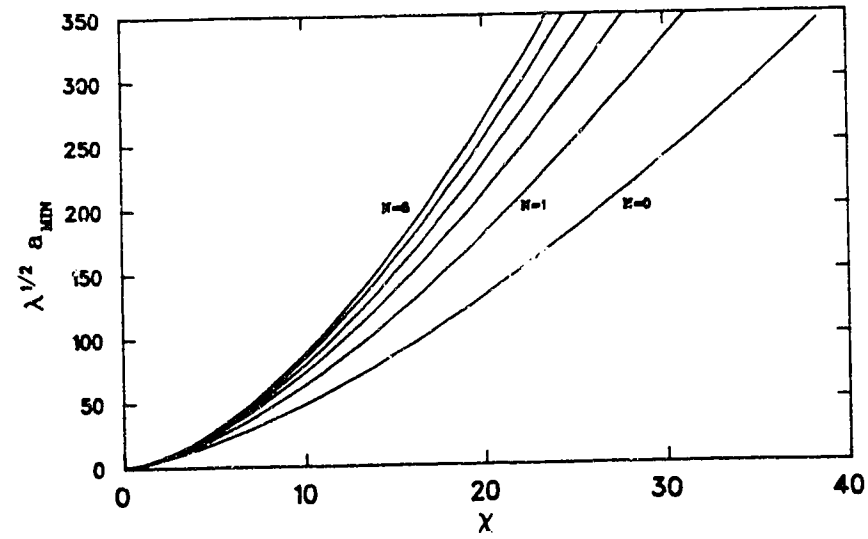

Figure 3.8: Dependence of the minimal scale factor $\lambda^{1/2}a_{MIN}$, on χ, for the $N = 0,..,5$ wormholes.

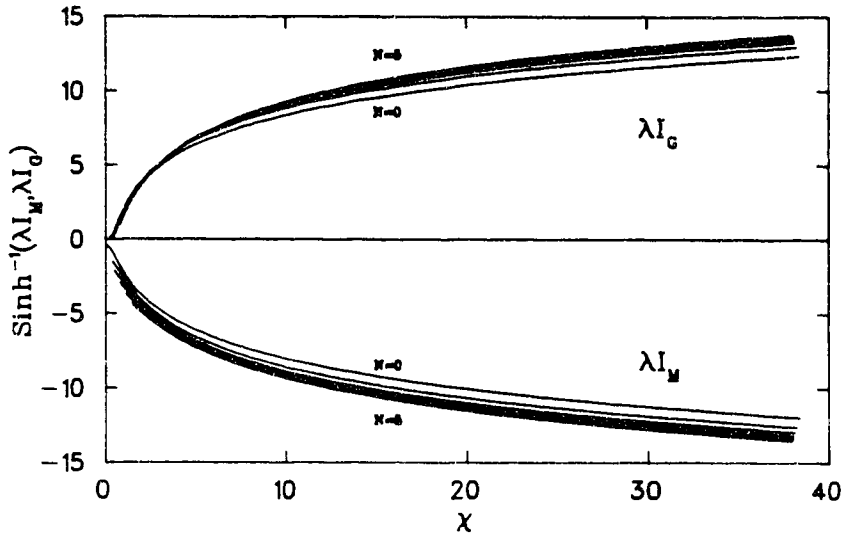

Figure 3.9: Dependence of the gravitation and matter actions λI_G, λI_M on χ for the $N = 0, .., 5$ wormholes. The action has been scaled by $\sinh^{-1}$ to magnify the behaviour at small actions.

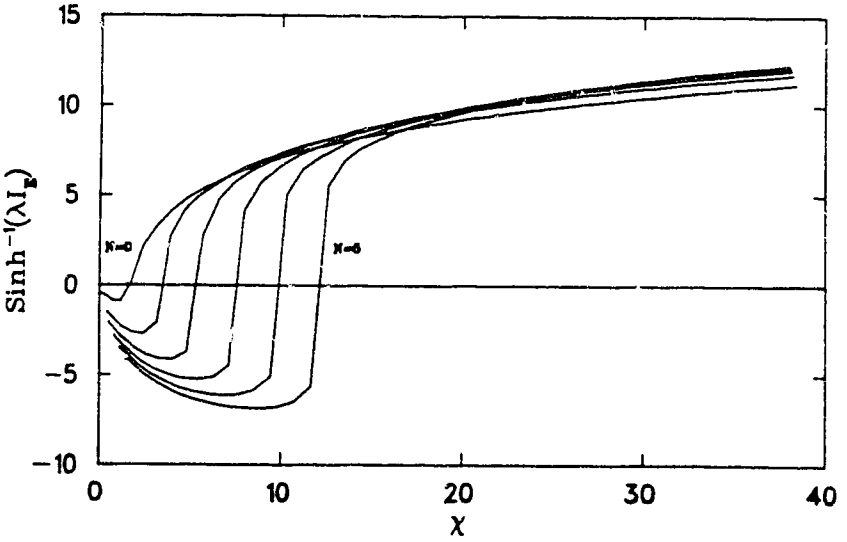

Figure 3.10: Dependence of the total actionλI_E on χ for the $N = 0, .., 5$ wormholes. The action has been scaled by $\sinh^{-1}$ to magnify the behaviour at small actions.

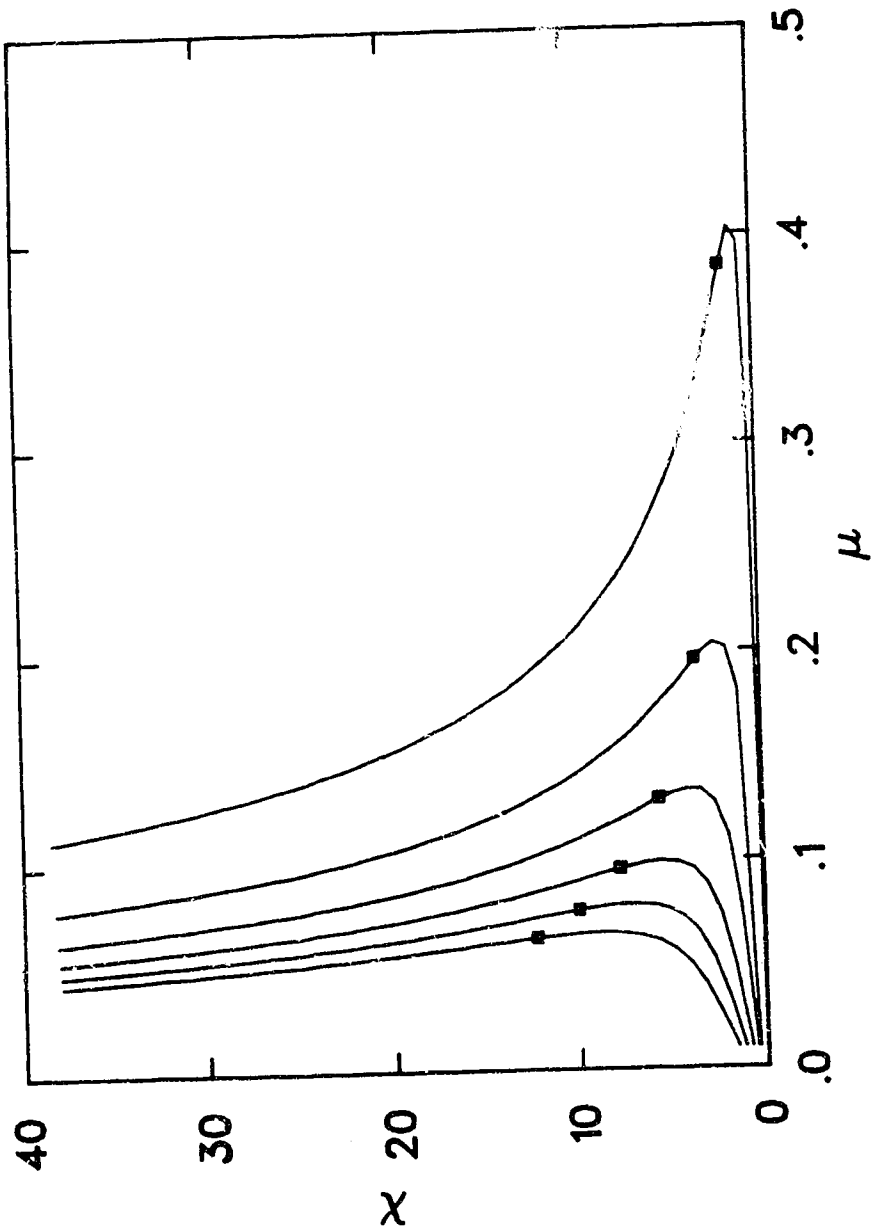

Figure 3.11: Approximate locations of zero action wormholes in the (χ, μ) parameter space.

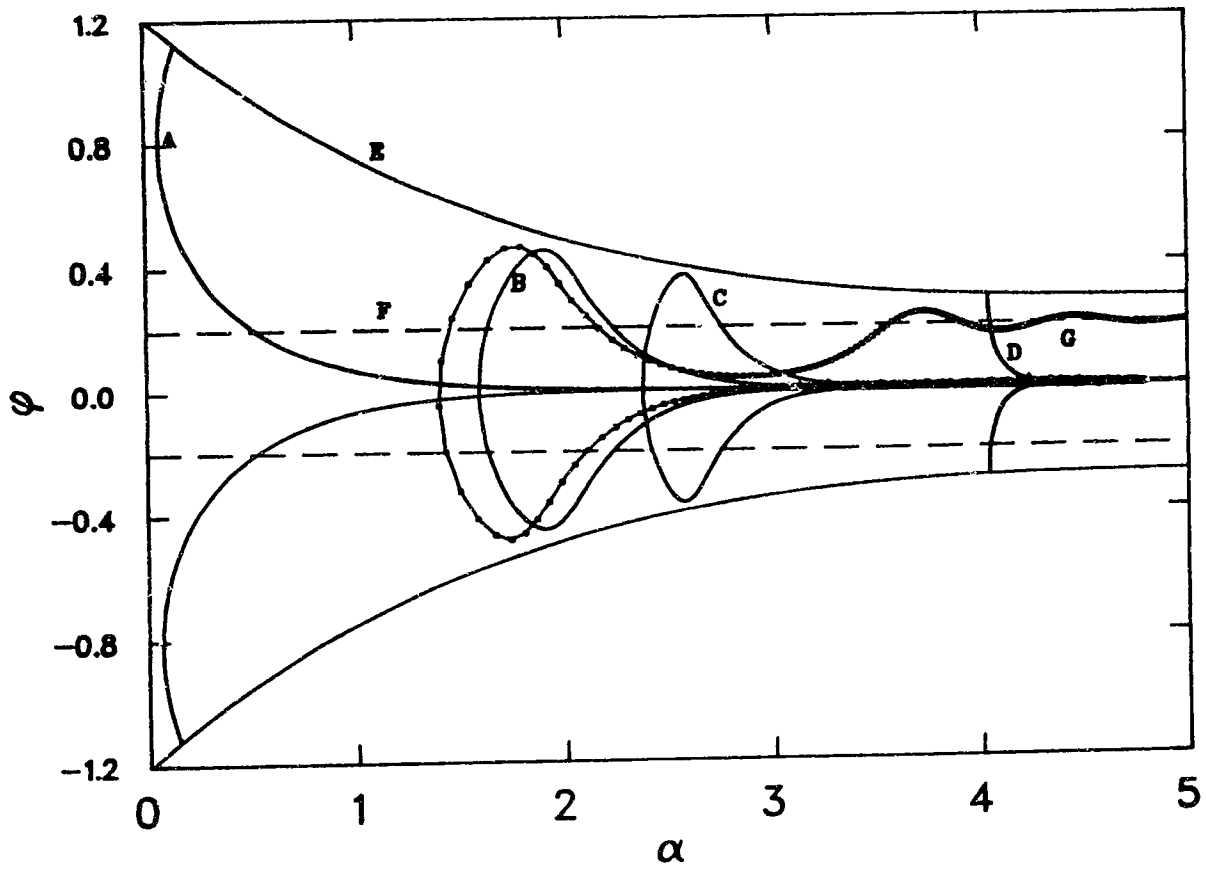

Figure 3.12: Graphical presentation of the four $\mu = 0.2$ wormholes in the (α, φ) auxiliary minisuperspace. The separate curves (A), (B), (C) and (D) are the four wormhole solutions referred to in table (3.1), (E) zero of $F(\alpha, \varphi)$ (3.3.12), (F) minimum of $V(\varphi)$ i.e. the "true vacuum", (G) trajectory of a non-wormhole solution which falls into a true vacuum. Due to the symmetry $\varphi \rightarrow -\varphi$, curves (A), (D), (E) and (F) are mirrored in the $\varphi = 0$ axis.

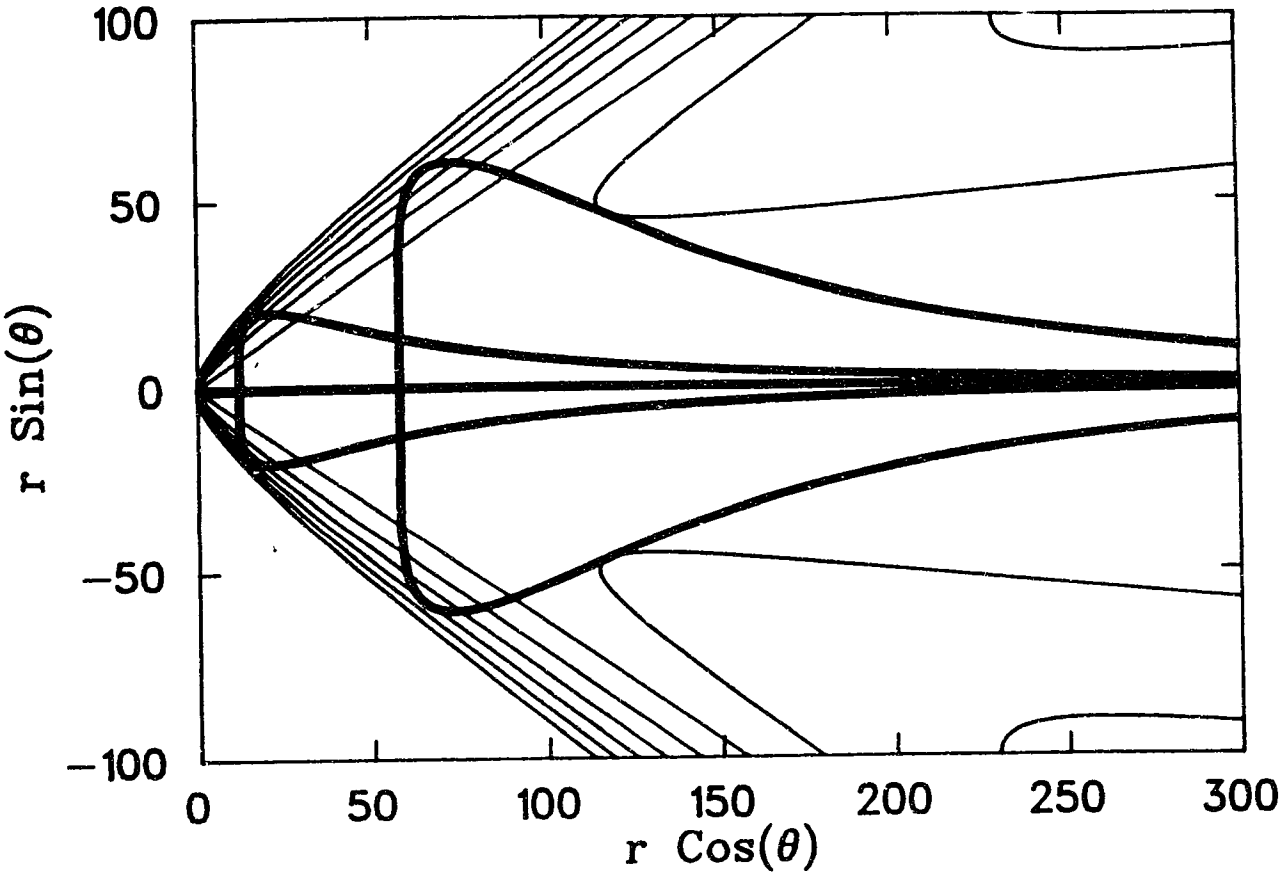

Figure 3.13: Graphical presentation of the four $\mu = 0.2$ wormholes in the (r, θ) auxiliary minisuperspace. Shown are the contours of constant P in $\Delta P = 0.2$ intervals beginning at $P = 0$. Only wormholes (A), (B) and (C) are shown as bold lines (3.1).

3.5 Analytical Approximations

In this section, we briefly outline the key assumptions and calculational steps needed to arrive at an approximate analytical form for the curves displayed in figure (3.3). We also derive an approximate analytical expression for the action. The central premise of the approximation scheme is that $|\frac{\Delta a}{a}| << 1$ and $|\frac{\Delta \dot{a}}{\dot{a}}| << 1$ during a single oscillation in φ, which we may expect to be valid for large N. We are thus able to calculate the adiabatic change in various quantities, and in particular, the change in $\dot{a}$, during a quarter cycle of φ. We can then integrate $\frac{\Delta n}{\Delta|\dot{a}|}$ as if it were $\frac{\partial n}{\partial|\dot{a}|}$, where n is the number of quarter cycles, from $|\dot{a}| = 1$ to $|\dot{a}| = 0$, to obtain an estimate for Σ, the total number of quarter cycles of φ occurring in the evolution of φ as $|\dot{a}|$ ranges from $1 \rightarrow 0$. (A quarter cycle is the evolution between successive zeros of $\varphi\dot{\varphi}$.) The number of zeros of φ throughout the whole evolution of the wormhole is then given by $N = \Sigma - 1$.

We begin by noting that asymptotically $\varphi \rightarrow 0$ as $a \rightarrow \infty$. However, as the evolution proceeds towards the throat, φ will deviate from zero and will roll down into the trough. It will then execute a number of quarter oscillations. The asymptotic expression for φ can be written as

$$\varphi \sim \mu \left(\frac{a}{a_1}\right)^{-3/2} e^{\mu(a_1 - a)} \quad , \tag{3.5.1}$$

or introducing $x = \mu a$, $\chi = m a_1$,

$$\varphi \sim \mu \left(\frac{x}{\chi}\right)^{-3/2} e^{\chi - x} \quad , \tag{3.5.2}$$

where χ is related to c (3.4.17) by

$$\chi + \frac{3}{2} \ln\ \chi = \ln(c\mu^{1/2}) \equiv \delta \quad , \tag{3.5.3}$$

or

$$\chi \approx \delta - \frac{3}{2} \ln \delta \ , \tag{3.5.4}$$

for large χ. φ will cross the trough roughly at $a = a_1$ or $x = \chi$ (but see below for a small correction). For future reference, we now obtain the approximate behaviour of $|\dot{a}|$ for $x \geq \chi$. Introducing the variables

$$z = \dot{a}^{-2}, \quad y = \sqrt{\tfrac{1}{2\mu^2}}\, \varphi \tag{3.5.5}$$

and eliminating time from the equations of motion we can obtain

$$a\frac{d\varphi}{da} = \frac{d\varphi}{d\alpha} = \mp \left(-2a^2 V z + z - 1\right)^{1/2} \ , \tag{3.5.6}$$

$$a\frac{dz}{da} = \frac{dz}{d\alpha} = -4z \left(-3a^2 V z + z - 1\right) \ . \tag{3.5.7}$$

For $x = \mu a \gg 1$, $\varphi \ll \mu$ we have (3.4.16)

$$\varphi \approx \mu \left(\frac{\mu a}{\chi}\right)^{-3/2} e^{\chi - \mu a} \ , \tag{3.5.8}$$

which is obtainable from (3.5.6) in the approximation $-2a^2 V z > z - 1$, i.e. at large a, and ignoring φ^4 in V. With these same approximations, (3.5.7) yields

$$z - 1 \approx 3x\varphi^2 \ . \tag{3.5.9}$$

We now find an approximate solution for φ which is valid up to a point near the end of the second quarter cycle, where φ crosses zero for the first time. Using the variables x, y and z, equations (3.5.6),(3.5.7) and (3.5.9) become

$$x\frac{dy}{dx} = \mp \left[y^2 \left(1 - y^2\right)^2 z + \frac{1}{2\mu^2}(z-1)\right]^{1/2} \ , \tag{3.5.10}$$

$$x\frac{dz}{dx} = -4z \left[3\mu^2 y^2 \left(1 - y^2\right) x^2 z + z - 1\right] \ , \tag{3.5.11}$$

$$z - 1 \approx 6\mu^2 x y^2 \ . \tag{3.5.12}$$

Introducing the quantity $Z \equiv (z-1)/(2\mu^2 x^2 z)$, from (3.5.10) we can express Z as

$$Z = \frac{(dy/dx)^2 - y^2(1-y^2)}{1 + 2\mu^2 x^2 (dy/dx)^2} \quad . \tag{3.5.13}$$

Inserting the asymptotic expansion (3.5.2) for y we see that $y^2(1-y^2) \sim \frac{x}{3} Z$ and thus we can consider Z a constant in (3.5.10) and write

$$\frac{dy}{dx} \approx \mp y \left(1 + \frac{3}{x} - y^2\right)^{1/2} \quad . \tag{3.5.14}$$

Setting $x = \chi$, a constant, in equation (3.5.14), integrate and match to (3.5.8) to get

$$y \approx \beta \,\mathrm{Sech}\left[\beta\left(x - \chi + \frac{3}{2}\ln 2\right)\right], \quad \beta = \sqrt{1 + \frac{3}{\chi}} \quad . \tag{3.5.15}$$

Inserting (3.5.12) into (3.5.11) we get

$$\frac{dz}{dx} \approx -12\mu^2 z^2 y^2 \left[\left(1 - y^2\right) x + \frac{2}{z}\right] \quad , \tag{3.5.16}$$

which, with $\Psi = \beta(x - \chi)$ as the new integration variable and using (3.5.15), becomes

$$-\frac{dz}{z^2} \approx 12\mu^2 d\Psi \left[\frac{\Psi + \beta\chi + \frac{2\beta}{z}}{\cosh^2 \Psi} - \frac{\beta^2 \Psi + \beta^3 \chi}{\cosh^4 \Psi}\right] \quad . \tag{3.5.17}$$

Integrating in from $x = \infty$, (where $\Psi = \infty$, $z = 1$) we get, to leading order in χ,

$$\frac{1}{z} \approx 1 - 4\mu^2 \chi \left[1 \pm \left(1 - y^2\right)^{3/2}\right] \quad . \tag{3.5.18}$$

The upper sign holds during the first quarter cycle, as y increases from 0 to 1 (where $\dot{\varphi} = 0$), and the lower sign holds during the second cycle, when y decreases back to 0. Equation (3.5.15) breaks down near the end of the second quarter cycle, as y actually crosses the ridge at $y = 0$ rather than simply asymptotically approaching it as it would if z stayed at unity. However, (3.5.18) should be valid through most of the second quarter cycle, so long as $|x - \chi| \ll \chi \gg 1$, and so (3.5.15) is valid with $\beta \approx 1$.

We now begin the calculation of the change in various quantities over a quarter cycle of φ. During the analysis we will make several assumptions, some of which will be recursively justified by the results.

We first calculate $\left|\frac{\Delta x}{x}\right|$ over a quarter cycle. We make the assumption the z is approximately constant during a cycle. This will be shown to hold for Σ large. Using (3.5.10) with

$$Z \equiv \frac{(z-1)}{2\mu^2 x^2 z} \ , \tag{3.5.19}$$

we can obtain

$$x = \mp \frac{1}{z^{1/2}\left(y_m^2-1\right)^{1/2}} \int \frac{dt}{\left[(1-t^2)\left(1+\frac{y_m^2 t^2}{y_m^2-1}\right)\right]^{1/2}} \ , \tag{3.5.20}$$

where $y = y_m t$ and $y_m^2\left(y_m^2-1\right) = Z$. Integrating between the limits of $t = 0$ (at which $\varphi = 0$), and $t = 1$, (at which $\dot{\varphi} = 0$), we obtain

$$\left|\frac{\Delta x}{x}\right| \approx \left(2k^2-1\right)^{1/2} \mathrm{K}(k^2)\, x^{-1} z^{-1/2} \ , \tag{3.5.21}$$

where $\mathrm{K}(k^2)$ is the complete elliptic integral of the first kind,

$$k^2 = \frac{1+\sqrt{1+4Z}}{2\sqrt{1+4Z}} \ , \tag{3.5.22}$$

$$\text{and} \quad m_1 \equiv k_c^2 = 1-k^2 = \frac{\sqrt{1+4Z}-1}{2\sqrt{1+4Z}} \ , \tag{3.5.23}$$

$$\text{or} \quad Z = \frac{k^2(1-k^2)}{\left(2k^2-1\right)^2} \ . \tag{3.5.24}$$

To estimate $\left|\frac{\Delta x}{x}\right|$, note from (3.5.18) that φ just crosses the trough at $\varphi^2 = \mu^2$ or $y^2 = 1/2$ for the first time when $x \approx \chi + \ln(\sqrt{2}+1) - \frac{3}{2}\ln 2$, and φ reaches its maximum (the completion of the first quarter cycle) at $x \approx \chi - \frac{3}{2}\ln 2$.

Thus, for $\chi \gg 1$, the first part of the first quarter cycle ($y^2 = 0$ to $y^2 = 1$) has $\left|\frac{\Delta x}{x}\right| \ll 1$. Equation (3.5.15) would give an infinite Δx for the completion of the second quarter cycle (to $y = 0$), but that formula breaks down and should be replaced by (3.5.21), which gives $\left|\frac{\Delta x}{x}\right| \sim \frac{\ln \chi}{2\chi} \ll 1$ for $1 \ll x \sim \chi$, using the expansion $\mathrm{K}(m_1 \ll 1) \approx \frac{1}{2} \ln\left(\frac{16}{m_1}\right)$.

We now calculate $\left|\frac{\Delta z}{z}\right|$ over a quarter oscillation. Equations (3.5.10) and (3.5.11) may be divided to give

$$\frac{dz}{dy} = \pm 12\mu^2 z^{3/2} \frac{\left[y^2(1-y^2) + \frac{2}{3}Z\right]}{\sqrt{[y^2(1-y^2)+Z]}} \ . \tag{3.5.25}$$

Letting $y = y_m(1 - X^2)$ with $Z = y_m^2(y_m^2 - 1)$, we can integrate (3.5.25) from $y = 0$ to $y = y_m$, giving

$$\left|\frac{\Delta z}{z}\right| \approx \frac{2(2k^2-1)^{1/2}}{k^2(1-k^2)} \left[\frac{(z-1)}{x\sqrt{z}}\right] F(k^2) = \frac{4\mu^2 x z^{1/2}}{(2k^2-1)^{3/2}} F(k^2) \ , \tag{3.5.26}$$

where

$$F(k^2) \equiv \left(1-k^2\right)^2 \mathrm{K}(k^2) + \left(2k^2-1\right) \mathrm{E}(k^2) \ , \tag{3.5.27}$$

and where $\mathrm{E}(k^2)$ is the complete elliptic integral of the second kind. Since $k^1 = 1$ for $z = 1$, and $F(1) = 1$, we see that $|\Delta z| \approx 4\mu^2 x$ where $z \approx 1$, which agrees with (3.5.18) where $x \approx \chi$.

From the definitions of k^2 and Z we can also compute

$$\Delta(k^2) \approx -2\left(2k^2-1\right)^{3/2} G(k^2) x^{-1} z^{-1/2} \ , \tag{3.5.28}$$

$$\frac{\Delta Z}{Z} \approx \frac{2(2k^2-1)^{1/2}}{k^2(1-k^2)} G(k^2) \ , \tag{3.5.29}$$

$$\text{where} \quad G(k^2) \equiv (1-k^2)\,\mathrm{K}(k^2) + (2k^2-1)\,\mathrm{E}(k^2) \ . \tag{3.5.30}$$

Since $G(1) = 1$, $|\Delta(k^2)| \ll 1$ and $|\Delta Z| \ll 1$ for $z \approx 1$ and $x \gg 1$, ' ugh $\Delta Z/Z$ is large because Z is small.

Now, for $k^2 \sim 1$, $\left|\frac{\Delta z}{z}\right| \sim 4\mu^2 x$. Thus, our initial assumption that z changed little during an oscillation $\Rightarrow$ $\mu^2 x \ll 1$. We now adopt the new variable $\nu \equiv |\dot{a}| \propto z^{-1/2}$, and find that

$$\Delta\nu \approx -F(k^2)\frac{2\mu^2 x}{(2k^2-1)^{3/2}} \tag{3.5.31}$$

$$\approx -2\mu^2 x \quad \text{when} \quad k^2 \sim 1. \tag{3.5.32}$$

Using $\left|\frac{\Delta x}{x}\right| \ll 1$, $\left|\frac{\Delta\nu}{\nu}\right| \ll 1$ we can write

$$\frac{d\nu}{dn} \approx \frac{2\mu^2 x}{(1-2m_1)^{3/2}}F(m_1) \ , \tag{3.5.33}$$

$$\frac{dZ}{dn} \approx \frac{2G(m_1)\nu}{x\,(1-2m_1)^{3/2}} \ , \tag{3.5.34}$$

$$\frac{dx}{dn} \approx -(1-2m_1)^{1/2}\,K(m_1)\nu \ , \tag{3.5.35}$$

$$\frac{dm_1}{dn} \approx 2(1-2m_1)^{3/2}\,\frac{G(m_1)\nu}{x} \ , \tag{3.5.36}$$

where n is the number of quarter cycles, and (3.5.24) gave $m_1 = 1 - k^2$. We are now assuming Σ is large and taking the continuum approximation for n.

By integrating (3.5.33) we can get an estimate for Σ,

$$\Sigma \approx \int_0^1 \frac{d\nu}{\left[1+2\frac{1-\nu^2}{\mu^2 x^2}\right]^{3/4} x\mu^2 F(k^2)} \ . \tag{3.5.37}$$

To integrate (3.5.37) we must have $x(\nu)$ and $F(\nu)$. To find $x(\nu)$ let us call $u \equiv 1-\nu^2$. We see that

$$\frac{d\ln Z}{d\ln u} = -\frac{u}{2Z\nu}\frac{dZ}{d\nu} = \frac{G(k^2)}{F(k^2)} \tag{3.5.38}$$

and thus,

$$\ln u \approx \int \frac{dZ}{Z}\frac{F}{G} \ . \tag{3.5.39}$$

From (3.5.23) we have

$$Z = \frac{1}{4}\left[\frac{1}{(1-2m_1)^2} - 1\right] \quad , \tag{3.5.40}$$

yielding

$$\frac{dZ}{Z} = \frac{dm_1}{m_1(1-m_1)(1-2m_1)} \quad . \tag{3.5.41}$$

Inserting (3.5.41) into (3.5.39) we have

$$\ln\left(1-\nu^2\right) \equiv \ln u \approx \int \frac{dm_1}{m_1(1-m_1)(1-2m_1)} \left[\frac{m_1^2 \mathrm{K}(m_1) + (1-2m_1)\,\mathrm{E}(m_1)}{m_1 \mathrm{K}(m_1) + (1-2m_1)\mathrm{E}(m_1)}\right] . \tag{3.5.42}$$

Now, to provide a rough estimate of (3.5.42), we make the approximation of the square bracket above, F/G, as

$$\frac{F}{G} \approx 1 - m_1 \quad . \tag{3.5.43}$$

This is not as crude as it may first appear, as

$$\frac{F}{G}\Big|_{m_1=\frac{1}{2}} = \frac{1}{2}, \qquad \frac{F}{G} \approx 1 - \frac{1}{2} m_1 \ln \frac{16}{m_1} \qquad m_1 \ll 1. \tag{3.5.44}$$

Since $Z \leq \frac{1}{2\mu^2 x^2}$ will be small for large $x \sim \chi$, the maximum possible $m_1 \sim Z$ will also be small. A more accurate estimate is $F/G \sim 1 - \frac{2}{3} m_1^{2/5}$. Inserting the approximation (3.5.43) into (3.5.42), integrating, and matching to (3.5.18) at the end of the first quarter cycle, where

$$1 - \nu^2 = 1 - |\dot{a}^2| = 1 - \frac{1}{z} = 4\mu^2(\delta - \frac{3}{2}\ln\delta) = 4\mu^2\chi \quad , \tag{3.5.45}$$

we get

$$m_1 \approx \frac{1}{2}\left[1 + \frac{\mu^2\chi^2}{u}\right]^{-1} \quad . \tag{3.5.46}$$

Inserting (3.5.46) into $1 + 4Z = (1-2m_1)^{-2}$, and using the definition of Z, we finally obtain

$$x \approx \chi\left[1 + \frac{1-\nu^2}{2\mu^2}\chi^2\right]^{-1/2} \quad . \tag{3.5.47}$$

Using the approximation $F \sim 1 - m_1$ together with (3.5.47) and (3.5.46), we can now evaluate the integral (3.5.37),

$$\Sigma \approx \frac{1}{\sqrt{2}}\chi \int_0^1 d\nu \left(1 - \nu^2 + \mu^2\chi^2\right)^{-1/2} \left(1 - \nu^2 + 2\mu^2\chi^2\right)^{-1/2} \quad (3.5.48)$$

$$\approx \frac{1}{\sqrt{2}}\chi \left(1 + 2\mu^2\chi^2\right)^{-1/2} \mathrm{F}\left(\cot^{-1}\mu\chi \,|k^2 = \tfrac{1+\mu^2\chi^2}{1+2\mu^2\chi^2}\right) , \quad (3.5.49)$$

where $\chi \approx \delta - \frac{3}{2}\ln\delta$, $\delta = \ln(c\mu^{1/2})$ and F is the incomplete elliptic integral of the first kind. Letting $\omega \equiv \mu\chi$ we can obtain expressions for N and Σ for $\omega \gg 1$,

$$\Sigma = N + 1 \sim \frac{1}{2\mu\omega} \quad \text{or} \quad \mu\Sigma \sim \frac{1}{2\omega} , \quad (3.5.50)$$

and for $\omega \ll 1$,

$$\Sigma = N + 1 \sim \frac{1}{\sqrt{2}\mu}\left[\omega\left(\ln\frac{4}{\omega}\right)\left(1 - \frac{3}{4}\omega^2\right) - \omega\ln(\sqrt{2}+1)\right] . \quad (3.5.51)$$

We note that

$$\frac{d}{d\omega}(\mu\Sigma)\Big|_{\omega\sim 0.51} = 0 , \quad (3.5.52)$$

giving

$$N_{MAX} = 2\Sigma_{MAX} \sim 0.39\mu^{-1} . \quad (3.5.53)$$

In figure (3.14) we compare $\Sigma(x,\mu)$, as predicted by (3.5.49), with the numerical results. The fit is surprisingly good. Thus, we can alternately label the curves by N, the number of zeros of φ throughout the whole evolution, or by Σ, the number of quarter oscillations of φ on one side of the throat. This again indicates that only two types of wormholes exist, types (i) and (ii) referred to in section a). From figure (3.15), we see that the fit is best when $\mu\omega \ll 1$, that is, when the adiabaticity condition for z is satisfied. However the results for $\mu\omega \leq 1$ are reasonably good.

The estimates (3.5.52) and (3.5.53) also match well with the empirical estimates shown in figures (3.5) and (3.6).

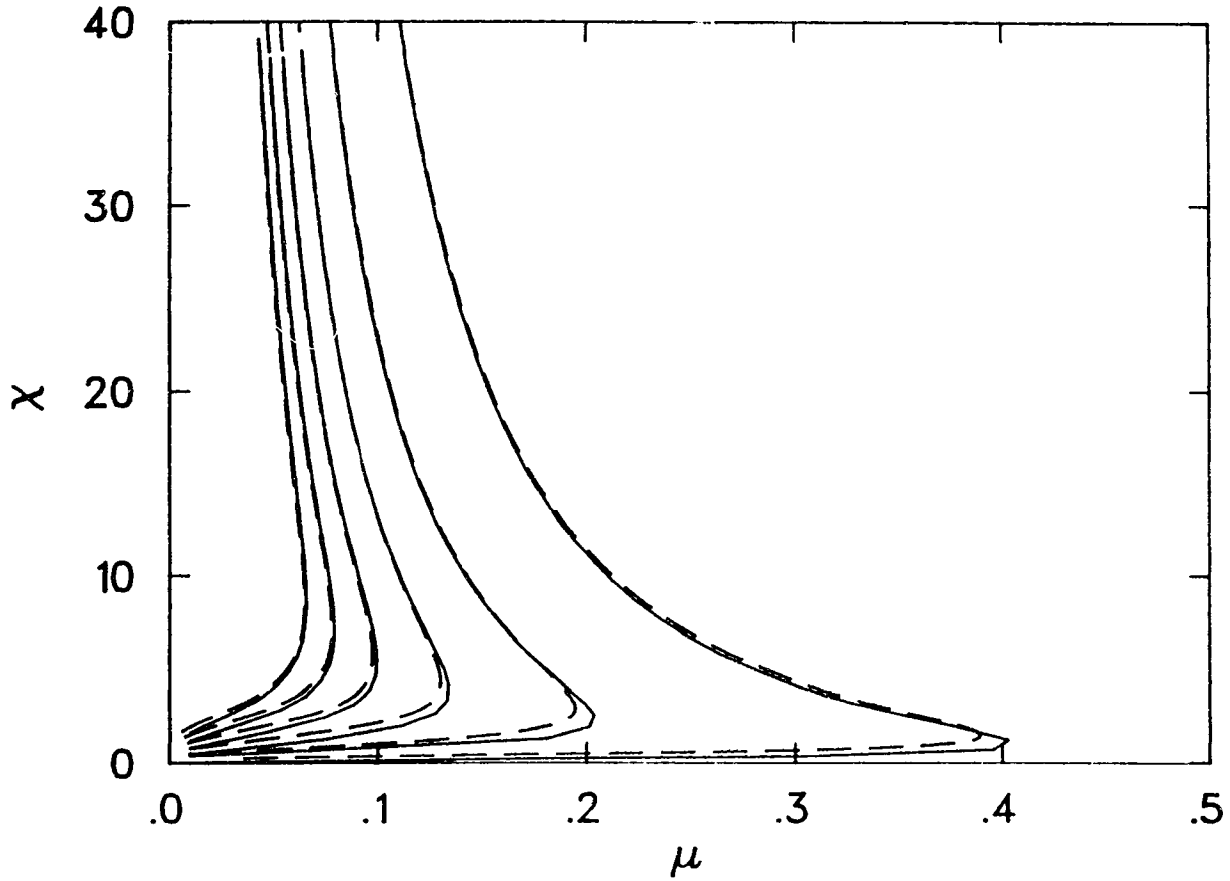

Figure 3.14: Comparison between numerical and analytical results for the loci of valid wormhole solutions in the (χ, μ) parameter space. The solid curves are the numerical results ranging from $N = 0, .., 5$. The dashed lines are the analytical approximation (3.5.49) for $\Sigma = 1, .., 6$.

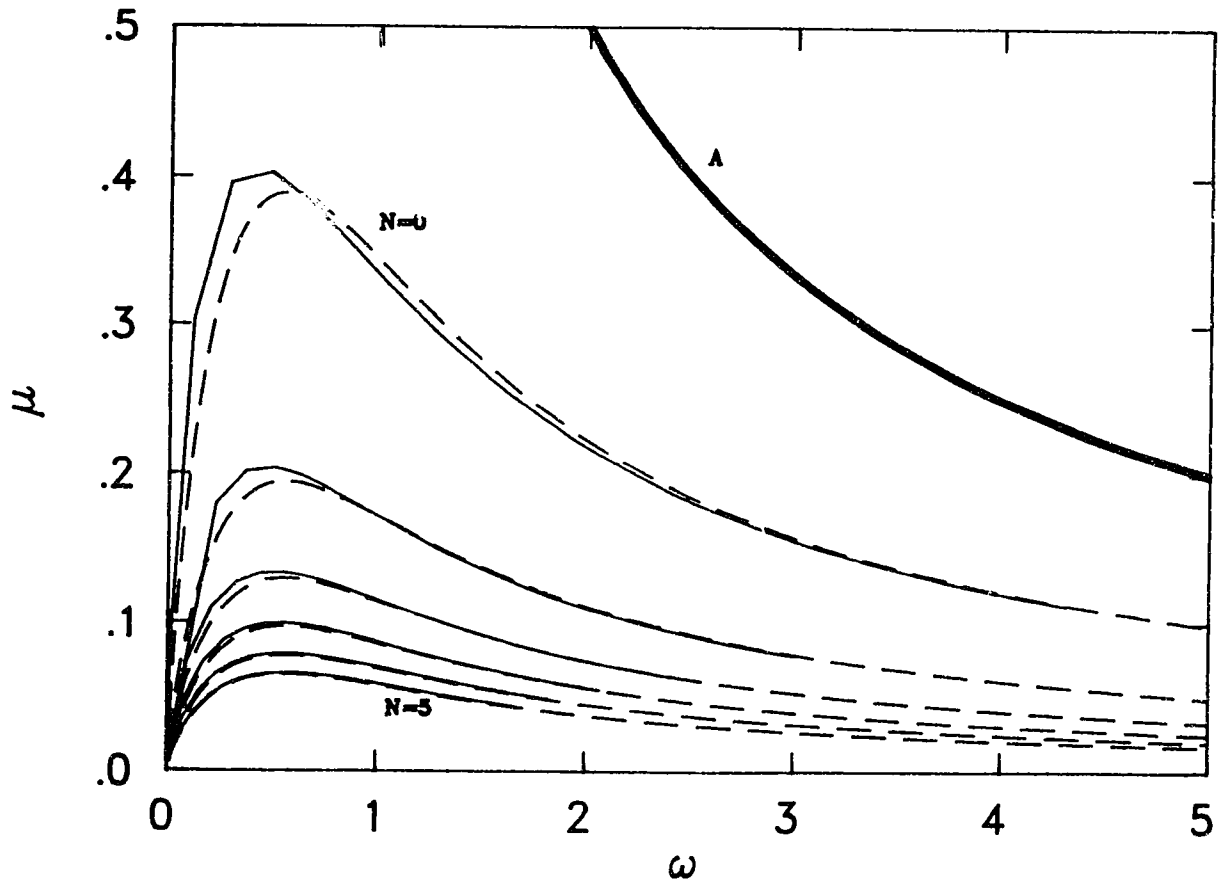

Figure 3.15: Comparison between numerical and analytical results for the loci of valid wormhole solutions in the (μ,ω) parameter space. Graph (A) is the curve $\mu = 1/\omega$. The solid and dashed lines have the same nomenclature as in figure (3.14).

a) Approximation to the action

From section b),

$$I_E = -I_V = -\int a^3 N V dt \ . \tag{3.5.54}$$

Introducing $\nu = \dot{a}$, the action can be written as

$$I_E = -\int a^3 V \frac{da}{\nu} \ , \tag{3.5.55}$$

where the potential $V = -\mu^2\varphi + \varphi^4 = \mu^4 y^2 (y^2 - 1)$. Using the variable $x = \mu a$ and referring to section 3.3, we obtain

$$\lambda I_E = 2J(x_{MIN}) \quad \text{where} \quad J(X) = \int_X^\infty \frac{x^3 dx y^2 (1 - y^2)}{\nu} \ . \tag{3.5.56}$$

Differentiating J with respect to x and using (3.5.10),

$$\frac{dJ}{dy} = \pm \frac{x^3 y^2 (1 - y^2)}{[y^2 (1 - y^2) + Z]^{1/2}} \ . \tag{3.5.57}$$

From (3.5.29) one can show that $\Delta Z \sim 2/x$ for $k^2 \sim 1$ ($Z \ll 1$), and so we may treat Z as a constant in (3.5.57) during a quarter cycle. Letting $y^2 = y_m^2 (1 - X^2)$, integrating (3.5.57) from $X = 0$ to $X = 1$ yields

$$\frac{dJ}{dn} \approx \frac{k^2 x^3}{(2k^2 - 1)^{3/2}} \int_0^1 \frac{[k^2 - 1 + k^2 X^2](1 - X^2)^{1/2}}{(1 - k^2 X^2)^{1/2}} dX \tag{3.5.58}$$

$$\approx \left[\left(1 - k^2\right)\left(1 - 3k^2\right) \mathrm{K}(k^2) + \left(2k^2 - 1\right) \mathrm{E}(k^2)\right] \frac{x^3}{3\,(2k^2 - 1)^{3/2}} \tag{3.5.59}$$

where k^2 is defined in (3.5.22). Referring to (3.5.27) and (3.5.30) we may thus write

$$\frac{dJ}{dn} \approx \frac{(3F - 2G)x^3}{3(1 - 2m_1)^{3/2}} \ , \tag{3.5.60}$$

which, together with (3.5.33), gives

$$\frac{dJ}{d\nu} \approx -\frac{x^2}{6\mu^2} \left[3 - 2\frac{G}{F}\right] \ . \tag{3.5.61}$$

In order to integrate (3.5.61) from $\nu = 1$ to $\nu = 0$, we must have $x(\nu)$ and $G(\nu)/F(\nu)$. Using the approximation (3.5.43) for F/G, (3.5.47) for $x(\nu)$ and letting $\omega \equiv \mu\chi$, we arrive at

$$dJ \approx \frac{\chi^4}{3}\frac{(2\omega^2 - 1 + \nu^2)}{(2\omega^2 + 1 - \nu^2)^2}d\nu \quad , \tag{3.5.62}$$

which, when integrated, finally gives

$$\lambda I_E = 2J(X = X_{MIN}) = \frac{2\chi^4}{3\,(1+2\omega^2)^{3/2}}\left[\left(1+2\omega^2\right)^{1/2} - \sinh^{-1}\frac{1}{\sqrt{2}\omega}\right] \quad . \tag{3.5.63}$$

Limiting form of λI_E are,

$$\omega \ll 1 \quad \lambda I_E \sim -\frac{2\chi^4}{3}\ln\frac{\sqrt{2}}{\omega} \quad , \tag{3.5.64}$$

$$\omega \gg 1 \quad \lambda I_E \sim \frac{\omega^2}{3\mu^4} \quad . \tag{3.5.65}$$

Eliminating ω from (3.5.64) and (3.5.65) through the use of (3.5.50) and (3.5.51) we have

$$\omega \ll 1 \quad \lambda I_E \sim -\frac{8\Sigma^4}{4\ln\epsilon}[\ln\ln\epsilon - \ln\mu\Sigma] \quad , \tag{3.5.66}$$

$$\omega \gg 1 \quad \lambda I_E \sim +\frac{1}{12\mu^6\Sigma^2} \quad , \tag{3.5.67}$$

where $\epsilon = \dfrac{2\sqrt{2}}{\mu\Sigma}$.

In figures (3.16) and (3.17) we compare the behaviour predicted by (3.5.63) with the numerical results. Keeping in mind the exponential compression of the action in this figure, the comparison is again remarkably good. The action (3.5.63) is zero when

$$\sinh^{-1} A = \sqrt{1 + \frac{1}{A^2}} \quad , \tag{3.5.68}$$

where $A = \dfrac{1}{\sqrt{2}\omega}$, which gives $\omega = \omega_0 \approx 0.46865$. In figure (3.18) we again graph the numerical results of figure (3.11) and superimpose the curve $\chi = \omega_0/\mu$. The

comparison of the analytical approximation (3.5.68) with the numerical results is not quite as impressive as in figure (3.14). However, an empirical result for the zeros of the action $\omega_{EMP} \approx 0.75$ shows that the discrepancy is relatively small.

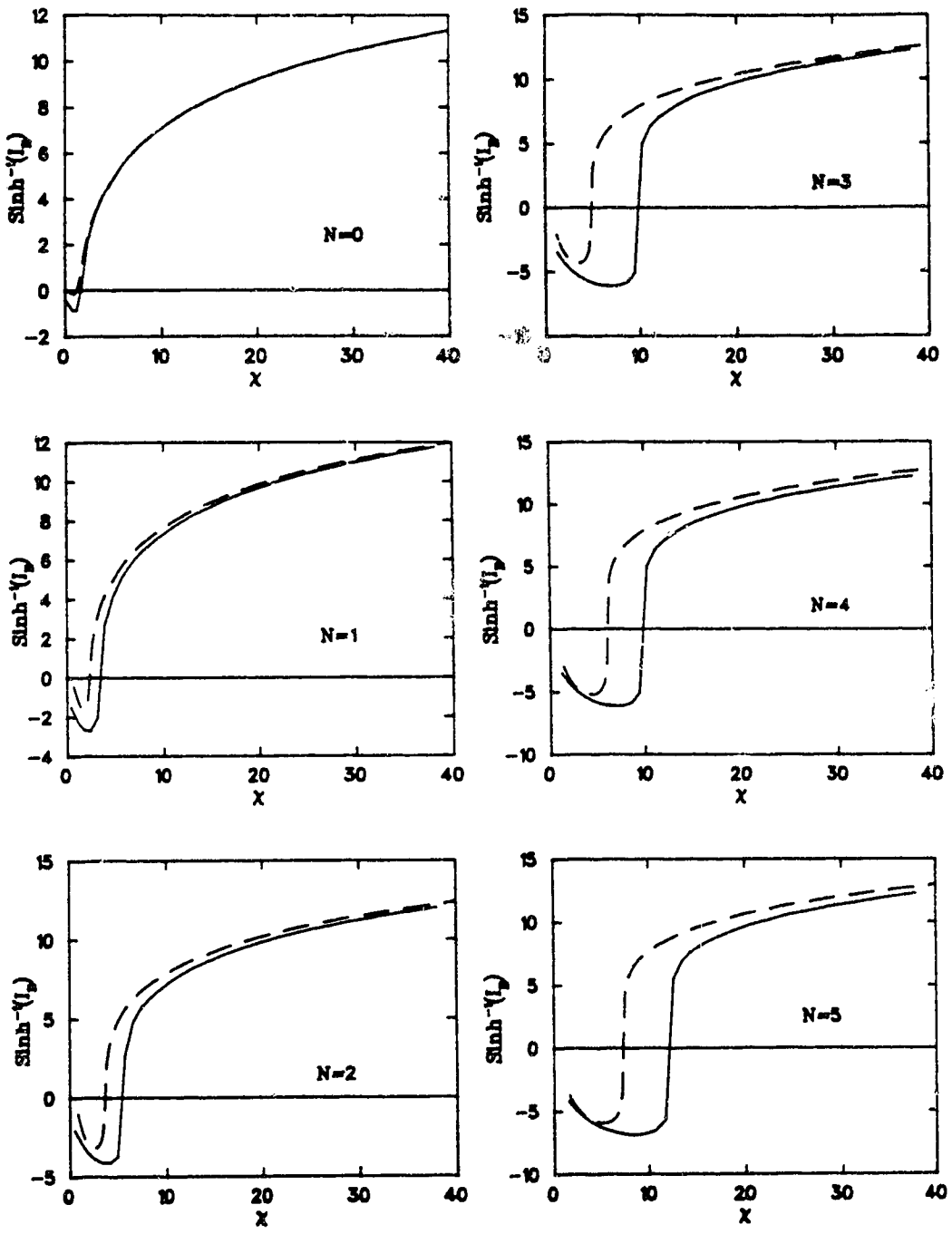

Figure 3.16: Comparison between numerical and analytical results for the action of wormhole solutions with $N = 0,..,5$. The solid curves are the numerical results, while the dashed curves are the analytical approximations.

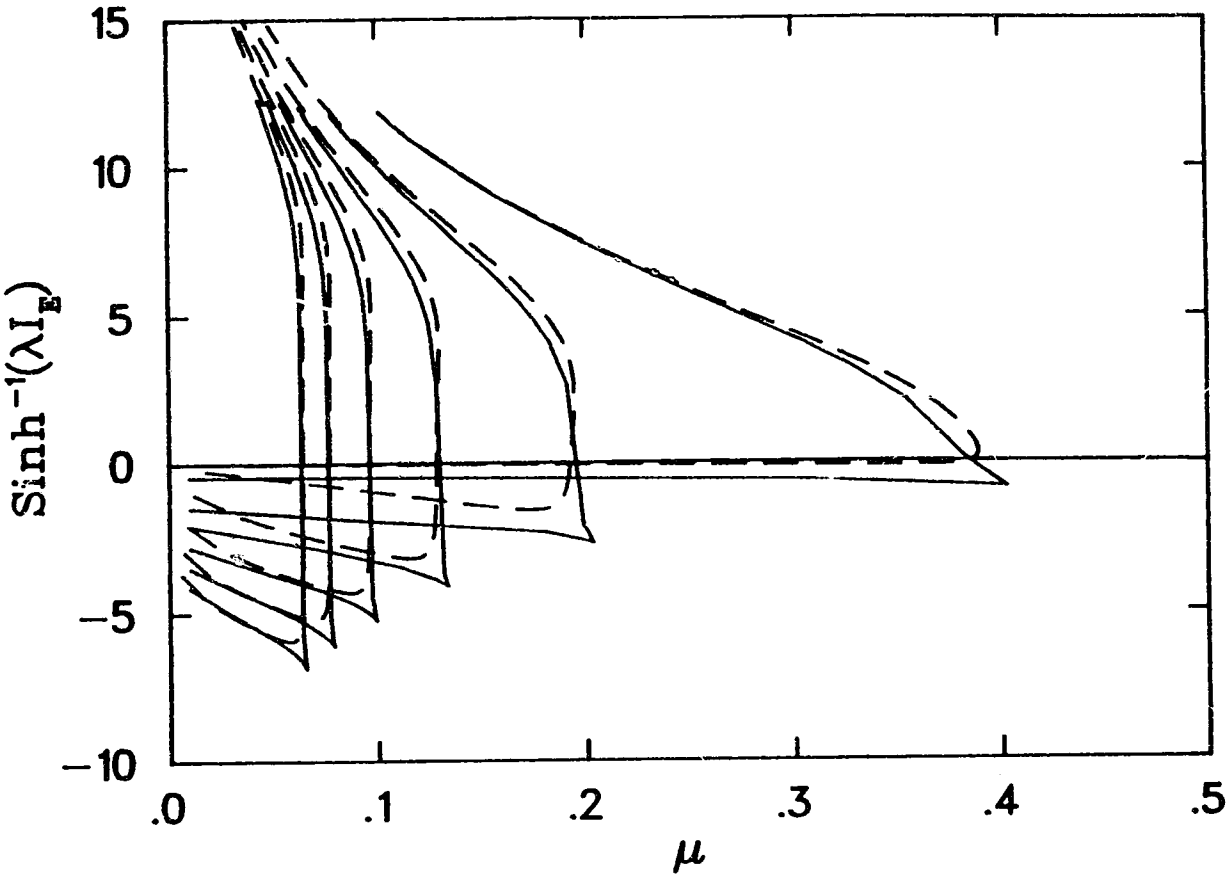

Figure 3.17: Comparison between numerical and analytical results for the action of wormhole solutions with $N = 0,..,5$ plotted against μ. The solid curves are the numerical results, while the dashed curves are the analytical approximations.

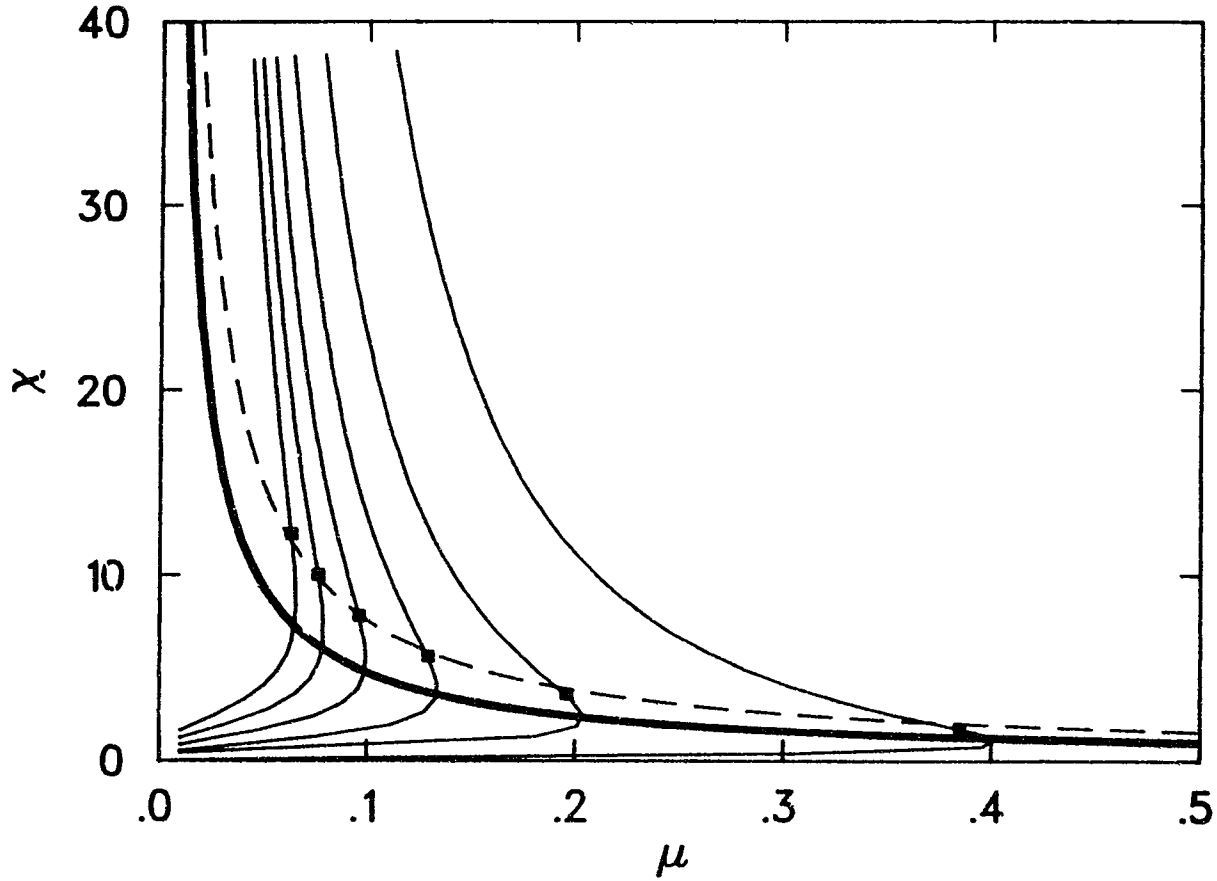

Figure 3.18: Comparison between numerical and analytical results for the zeros of the action of wormhole solutions with $N = 0, .., 5$. Shown are the loci of valid wormhole solutions for $N = 1, .., 5$ together with the numerical estimate of the zero action wormholes (shown as black squares). The bold curve is $\chi = \omega_0/\mu$, while the dashed curve is $\chi = 0.75/\mu$.

BIBLIOGRAPHY

[1] J. Twamley and D. N. Page, "Wormholes without a conserved charge", submitted to Physics Letters B, (1990).

[2] W. Fischler and L. Susskind, *Phys. Lett.* **217**B (1989) 48.

[3] J. Preskill, *Nucl. Phys.* B**323** (1989) 141; J Polchinski, *Nucl. Phys.* B**325** (1989) 619; S Coleman and K. Lee, *Phys. Lett.* **221**B (1989) 242; A Iwazaki, *Phys. Lett.* **229**B (1989) 211; B Grinstein, *Nucl. Phys.* B**321** (1989) 439; S Coleman and K. Lee, *Nucl. Phys.* B**341** (1990) 101.

[4] S. B. Giddings and A. Strominger, *Nucl. Phys.* B**307** (1988) 854; S Coleman, *Nucl. Phys.* B**307** (1988) 867; T Banks, *Nucl. Phys.* B**309** (1988) 493; S Coleman, *Nucl. Phys.* B**310** (1988) 643; S W. Hawking, *Nucl. Phys.* B**335** (1990) 155.

[5] S. Coleman and K. Lee, *Phys. Lett.* **221**B (1989) 242.

[6] S. Giddings and A. Strominger, *Nucl. Phys.* B**306** (1988) 890; K Lee, *Phys. Rev. Lett.* **61** (1988) 263; C P. Burgess and A. Kshirsagar, *Nucl. Phys.* B**324** (1989) 157; J D. Brown, C. P. Burgess, A. Kshirsagar, B. F. Whiting and J. W. York, *Nucl. Phys.* B**328** (1989) 213.

[7] J. B. Hartle, *J. Math. Phys.* **30** (1989) 452; J J. Halliwell and R. Myers, *Phys. Rev.* D**40** (1989) 4011; J J. Halliwell and J. Louko, *Phys. Rev.* D**39** (1989) 2206; J J. Halliwell and J. Louko, *Phys. Rev.* D**40** (1989) 1868; S Chakraborty, *Phys. Rev.* D**42** (1990) 2924; J J. Halliwell and J. Louko, *Phys. Rev.* D**42** (1990) 3997; J Louko and P. Tuckey (in preparation).

[8] G. W. Gibbons, S. W. Hawking, and M. J. Perry, *Nucl. Phys.* **B138** (1978) 141.

[9] K. Schleich, *Phys. Rev.* **D36** (1987) 2342; J B. Hartle, *ibid.* **29** (1984) 2730; J. B. Hartle and K. Schleich, in *Quantum Field Theory and Quantum Statistics: Essays in Honour of the Sixtieth Birthday of E. .S. Fradkin*, edited by I. A. Batalin, G. Vilkovisky, and C. J. Isham (Hilger, Bristol, 1987); H. Arisue, T. Fyjuwara, M. Kato, and K. Ogawa, *Phys. Rev.* **D35** (1987) 2308.

[10] S. W. Hawking, in *Astrophysical Cosmology*, edited by H. A. Brück, G. V. Coyne, and M. S. Longair (Pontifica Academia Scientarium, vatican City, 1982); J. B. Hartle and S. W. Hawking, *Phys. Rev.* **D28** (1983) 2960; S W. Hawking, *Nucl. Phys.* **B239** (1984) 257.

[11] A. Vilenkin, *Phys. Rev.* **D30** (1984) 509; A Vilenkin, *Phys. Rev.* **D33** (1986) 3560; A Vilenkin, *Phys. Rev.* **D37** (1988) 888.

[12] J. J. Halliwell and J. B. Hartle, *Phys. Rev.* **D41** (1990) 1815.

[13] S. Fubini, *Nuovo Cim.* **34A** (1976) 521.

[14] G. V. Lavrelashvili, V. A. Rubakov, M. S. Serebryakov, and P. G. Tinyakov, *Nucl. Phys.* **B329** (1990) 98.

[15] J. W. York, *Phys. Rev. Lett.* **28** (1972) 1082; G W. Gibbons and S. W. Hawking, *Phys. Rev.* **D15** (1977) 2752.

[16] G. W. Gibbons and C. Pope, *Commun. Math. Phys.* **66** (1979) 267.

[17] R. Schoen and S. T. Yau, *Commun. Math. Phys.* **79** (1982) 281.

[18] J. Cheeger and D. Grommol, *J. Diff. Geom.* **4** (1971) 119.

[19] G. Jungman and R. M. Wald, *Phys. Rev.* **D40** (1989) 2615.

[20] H. Berestycki, P. L. Lions and L. A. Peltier, Indiana University Mathematics Journal **30** (1981) 141.

[21] W. H. Press, B. P. Flannery, S. A. Teukolsky and W. T. Vetterling, *Numerical Recipes* (Cambridge University Press , Cambridge, 1990.)

CHAPTER FOUR

LARGE SCALE STRUCTURE IN A HYPERBOLIC SMALL UNIVERSE MODEL

4.1 Introduction and Astrophysical Observations

Until December of 1989 the largest scale astrophysical structure discovered was the "Great Wall" [3]. It measures approximately 170 h_0^{-1}Mpc (where h_0 is the Hubble constant in units of 100km/s) in diameter. However, in February 1990 new results from four deep space pencil beam surveys along the north-south galactic axis were reported in Nature by Broadhurst, Ellis, Koo and Szalay (BEKS) [4]. Their results cover a distance in excess of 2000 h_0^{-1}Mpc. They found a remarkably regular distribution of galaxies along their line of sight with most galaxies lying in narrow bands or walls separated by a characteristic distance of 128 h_0^{-1}Mpc (where $\Omega_0 = 1$ in their original calculations). Since publishing, BEKS have subjected their data to more rigorous statistical tests. In May 1990 Szalay reported [5] that the characteristic distance of 128 h_0^{-1}Mpc had passed all tests even when parts of a survey or even a complete survey is discarded. Furthermore, preliminary results from two other deep space pencil surveys were presented. Similar galaxy distributions were seen although the actual galaxy count was not as high as the north-south survey. As regards the degree of phase coherence of the data (the degree to which the data is approximated by a periodic distribution) BEKS, by examining the higher harmonics in a Fourier decomposition of the galaxy distribution, have found greater phase coherence in the north-south data than in the other two surveys. Furthermore, they found that the phase coherence present was

optimized if one chooses $\Omega_0 < 1$ and quoted the characteristic distances for the north-south survey to be 135 h_0^{-1}Mpc while the other surveys gave 109 h_0^{-1}Mpc and 125 h_0^{-1}Mpc for $\Omega_0 = .1$. Also, as has been pointed out by Davis [6], the statistical significance of the degree of phase coherence present cannot be easily judged since it was found *a posteriori*. BEKS claim that they have found a definitive characteristic distance associated with each survey but do not claim that they have found conclusive evidence for a periodic structure.

Leaving the issue of phase coherence aside, the discovery of significant structure on such a large scale is very surprising. Structure on this scale is totally unexpected and incompatible with most cosmological models to date. The central difficulty lies with the compatibility between the stringent bounds for the isotropy of the cosmic microwave background radiation (cbr for short) and the anisotropies needed to form the large scale structure. Currently COBE (Cosmic Background Explorer) data has constrained $\frac{\delta T}{T}$ to be less than 10^{-5} for the cbr on angular scales exceeding 2° and stronger constraints are expected this year. In this paper we describe a model which can 'naturally' solve this problem and gives similar galaxy distributions to those reported by BEKS. Our model is that of a small universe [7]. A small universe cosmological model is a generic term for any cosmological model which possesses compact, closed spatial sections. Models of this type have appeared in the literature but have been largely discounted, partly due to poor astrophysical data and partly due to apparent 'philosophical prejudices' [8].

For reasons given below, we will only consider models which are locally isotropic and homogenous and in particular, possess constant negative spatial curvature i.e. a three dimensional compact hyperbolic manifold. The predictive power of the model is somewhat curtailed due to insufficient understanding of the

properties of three dimensional hyperbolic manifolds. Indeed the study of such manifolds plays an important part in the current research of topology. However we feel that the predictions made are sufficient at this time to differentiate it from other models [9], and it provides a very simple description of the large scale structure without recourse to CDM, HDM etc. while explaining the observed isotropy of the cbr. We have also not included an inflationary era. One can indeed include inflation; however, we wish to show that it is not necessary from the viewpoint of the large-scale structure and cbr isotropy.

4.2 Description of the small universe model

A small universe model which is locally isotropic and homogenous is locally identical to a Friedmann–Lemaître–Robinson–Walker (FLRW) universe [7]. This restricts one to small universe models possessing three surfaces with constant three curvature. This greatly simplifies the mathematical treatment of the model.

The essential property that we will make use of is the multiple imaging of an object within a small universe. If the size of the universe is small enough, and the object is old enough, light from the object will have travelled around the universe a number of times and consequently multiple images of that object will be seen by the observer.

To obtain a small universe model with a constant curvature three surface, one makes suitable identifications of the FLRW space (universal covering space) under a freely acting discrete isometry group. The closed compact three space is in fact the quotient space of the universal covering space,

$$\text{covering manifold: } \tilde{M}$$

closed compact manifold: $M = \tilde{M}/\Gamma$

where Γ is a freely acting, properly discontinuous isometry group of $\tilde{M}$. However not all Γ result in closed compact three spaces. The problem of finding and classifying all such Γ is known as the Clifford- Klein space-form problem [10,11]. A simple example is the construction of a toroidal topology from $\mathbf{R}^3$ through the identification of opposite sides of a parallelepiped. One can form other topologies with zero three curvature by rotating opposite sides by π, $\frac{\pi}{2}$ etc. before identifying. In fact there are ten distinct topologies possible in the flat case [10,11]. In the case of positive three curvature there are an infinite number of possible topologies, all of which have been classified. In the case of constant negative curvature however, an infinite number of distinct topologies have been found, but not all. It is this case that will be of interest to us.

Compact hyperbolic three spaces with constant negative curvature best represent our Universe. Observational evidence strongly suggests that $\Omega < 1$ so that our Universe has overall negative spatial curvature [12,13]. There is, of course, a prevalent theoretical prejudice that Ω should equal unity as predicted by most inflationary models. However there is as yet no observational evidence to support this belief [12], and it appears that current scenarios for the 'missing mass' (cold dark matter etc.) will be sorely pressed (if not dismissed entirely) through new limits on the cbr isotropy from COBE. Perhaps the strongest evidence that we are living in a low density universe comes from Peeble's galaxy trajectory simulations for the local group [13]. Thus, we will assume $\Omega < 1$ and a small universe with a hyperbolic space section with constant negative curvature.

The metric for the model is the same as that of the corresponding covering

space, i.e. the open FLRW universe

$$ds^2 = a(\eta)^2 \left[-d\eta^2 + d\chi^2 + \sinh^2(d\theta^2 + \sin^2\theta d\phi^2)\right], \tag{4.2.1}$$

where $a(\eta)$ is the scale factor and the proper time is given by

$$t = c^{-1} \int_0^\eta a(\eta) d\eta. \tag{4.2.2}$$

In the radiation-dominated regime

$$\begin{aligned} a(\eta) &= a_* \sinh\eta \ , \\ \Omega(\eta) &= \frac{1}{\cosh^2\eta} \ , \end{aligned} \tag{4.2.3}$$

whereas in the matter-dominated regime we have

$$\begin{aligned} a(\eta) &= a_*\Big(\cosh(\eta) - 1\Big) \ , \\ \Omega(\eta) &= \frac{2}{1 + \cosh(\eta)} \ . \end{aligned} \tag{4.2.4}$$

One can obtain a current estimate for the scale factor to be $a(\eta_0) = \frac{3000}{\sqrt{1-\Omega_0}}\ h_0^{-1}\mathrm{Mpc}$, where $.1 < \Omega_0 < 1$ and $.4 < h_0 < 1$.

A major difficulty with all previous small universe models has been the arbitrariness of the universe size (or fundamental cell size). The 'natural' scale to pick is the Planck scale, but choosing a Planck volume at the Planck time results in a current volume which is at least sixty orders of magnitude to small. In this paper, we shall adopt the position that the boundary conditions governing the evolution of the universe be imposed at the present epoch. We then use these boundary conditions to evolve the model to previous epochs and compare the predictions with observations.

However, for the hyperbolic case, in distinction from both the closed and flat cases, Thurston and Jorgenson [14], have shown that given the curvature, the

three volume cannot be arbitrarily small. More specifically, they were able to show that for a given curvature, the set of all hyperbolic three manifolds can be well ordered by their volume and that this set has a lower bound, i.e., a manifold of least volume. Mateev and Fomenko [15] have also showed that this set is also ordered with respect to the 'topological complexity' of the member manifolds, i.e., low volume manifolds are the least complex.

We shall now suppose that, given the discrete spectrum of the set of all hyperbolic 3-volumes/topological complexity, the Universe is either in or near the ground state of least volume/complexity. We appeal perhaps to some more fundamental theory–a theory of quantum topology–in which topologies are weighted by a topological action and states of minimum volume and/or 'complexity' dominate. Admittedly this supposition remains essentially unjustified. Nonetheless it is as well founded as the assumption normally made that the Universe is spatially infinite or that the Universe is in the ground state as made in the No-boundary proposals to the wavefunction of the Universe [16]. In any case, we take the minimum volume/complexity conjecture as a working hypothesis and aim to calculate typical repetition distances for ghost images and physical consequences for the isotropy of the cbr.

Unfortunately, although one knows that the volumes of the hyperbolic manifolds are bounded from below, the actual manifold (cell) of least volume/complexity remains as yet undiscovered. Recent estimates and bounds are as follows. In 1978, Thurston [14] found a cell with a volume of $.98a^3$. In 1986, R. Meyerhoff [17] showed that the minimum volume must be greater than $.00082a^3$. In 1988 Mateev, Fomenko [15] and independently Weeks [18] found a cell of volume $.94a^3$. In what follows we take the Meyerhoff volume as a lower bound and the Weeks,

Mateev, Fomenko (WMF) volume as an upper bound for the volume of the as yet undiscovered minimal volume manifold.

With respect to the presence of large scale structure in the model, what are the relevant physical quantities one wishes to calculate? What will interest us is a typical spatial repetition distance between ghost images. To be more specific let us take the simple case of a two dimensional toroidal topology. This topology can be represented through the identifications of opposite sides of a rectangle in $\mathbb{R}^2$. Let us take the sides of this rectangle to be equal to L. Now if we imagine placing some observer in the center of such a rectangle, the observer (because of the identifications) will perceive a crystaline network of images of herself (see Fig (4.1) in reference [7]). One can define three relevant distances associated with the distribution of the images. Define $\frac{L1}{2}$ to be the greatest distance from the observer within which no ghost images will be seen. Define $\frac{L2}{2}$ to be the smallest distance from the observer beyond which one will only see ghost images. One can also define a typical repetition distance scale which falls between $L1$ and $L2$ by taking the diameter of a two dimensional ball whose volume equals that of the fundamental cell $\bar{L} = \frac{2L}{\sqrt{\pi}}$. Thus the observer should expect to see, on average, at least one ghost image within a distance $\frac{\bar{L}}{2}$ in a pencil beam survey along any given line of sight.

The case of the hyperbolic manifold is slightly more difficult. All hyperbolic manifolds of constant curvature are globally non-homogenous and thus the distances $L1, L2$ will depend on the position of the observer in the manifold. However $\bar{L}$ will still represent a typical repetition scale for the manifold and in particular will remain an upper bound for $L1$. To obtain $\bar{L}$ we equate the volume of a hyperball to the volume of the fundamental cell and extract the diameter of the

ball,

$$V = \pi a^3(\sinh(2\chi) - 2\chi)$$

where $\bar{L} = 2a\chi$. Thus, along any given line of sight, one should see at least one ghost image within the distance $\frac{\bar{L}}{2}$.

Using Meyerhoff's lower bound and the WMF upper bound one obtains,

$$\frac{\bar{L}_{Meyerhoff}}{2} = \frac{174}{\sqrt{1-\Omega_0}}\, h_0^{-1}\text{Mpc}, \tag{4.2.5}$$

$$\frac{\bar{L}_{WMF}}{2} = \frac{1776}{\sqrt{1-\Omega_0}}\, h_0^{-1}\text{Mpc}. \tag{4.2.6}$$

One can check these predictions against observations. Sokolov and Schvartsmann [19] estimate $\frac{\bar{L}}{2} > 300\ h_0^{-1}$Mpc based on the observation of ever richer Abell clusters out to a redshift of approximately 0.1. Gott [20] estimates $\frac{\bar{L}}{2} > 200\ h_0^{-1}$Mpc based on the absence of ghost images of the Serpens–Virgo cloud in the survey region of the Soniera–Peebles galaxy map [21]. [Note: estimates are adjusted to conform with the convention for h_0 used here.] Both the Meyerhoff and WMF cells are compatible with the above observational constraints for resonable values of Ω_0! We will also point out that the actual feat of identifying two objects in a two dimensional deep sky map as being images of a single object is very difficult, if not impossible, and thus one should take these observational estimates with a grain of salt, so to speak. We again make the distinction between the quantity $\frac{\bar{L}}{2}$, which is the distance from an observer within which at least one ghost image should be seen on average in a pencil beam survey along any given line of sight, and the quantity $\bar{L}$, the typical scale associated with the fundamental cell.

To summarize, we have hypothesized that the universe may be modeled as

a manifold with topology $\mathbb{R}\times H^3/\Gamma$ where H^3 is a three- manifold with constant negative curvature and Γ is a freely acting discrete isometry group of H^3. Furthermore, we conjecture that the Universe is near the 'ground state' of minimum volume and topological complexity and find that our conjecture is in accord with observational constraints.

4.3 Predictions and observational tests

Due to the extremely limited information we have concerning the Universe and our inability to perform true cosmological 'experiments', cosmological models have had much more success at 'post-diction' than prediction. Nonetheless, prediction of observable phenomena remains an essential prerequisite for useful models. While the predictive power of our model is partially curtailed by limitations in the current understanding of compact hyperbolic manifolds, we find that certain general predictions can be made. We outline these below.

We consider first the question of the cosmic microwave isotropy. Let α be the observed angular width of the fundamental cell at decoupling, as seen from the present epoch. The mechanisms which produce cbr isotropy on angular widths less than α are distinct from those which produce isotropy on larger angular widths.

Take the case where the angular scale of observation is less than α, i.e., $\theta < \alpha$. The most obvious mechanism for achieving isotropy would be the complete thermalization of the universe before the surface of last scattering. For this to occur the universe must necessarily become causally connected with itself, i.e., the entire cell must come within the cosmological horizon before the time of last

scattering. The surface of last scattering occurs at a red shift

$$1 + z = \frac{a(\eta_0)}{a(\eta_{sls})} \approx 1500 \ . \tag{4.3.7}$$

Equations (4.2.3), which are appropriate for the radiation dominated phase, yield

$$\eta_{sls} = \chi_{sls} = 0.063\sqrt{\frac{1}{\Omega_0} - 1} \ . \tag{4.3.8}$$

Thus, assuming that the fundamental cell is roughly spherical, so long as it has a volume

$$V < \pi a^3(\sinh 2\chi_{sls} - 2\chi_{sls}) \ , \tag{4.3.9}$$

the entire universe would be causally connected before the surface of last scattering and thermalization could occur.

For the Meyerhoff volume, equation (4.3.9) will be satisfied for $\Omega_0 < .54$. This is compatible with observation and so causal connectivity will occur well before the surface of last scattering. Hence, thermalization before the surface of last scattering is a mechanism which can account for microwave isotropy on angular scales less than α. For the WMF limit, condition (4.3.9) will only be satisfied for $\Omega_0 < 0.011$, which is not compatible with observation and thus, since the WMF cell is so much larger than the Meyerhoff cell, causal connectivity will not be achieved. It should be pointed out that even though causal contact is a necessary condition it is not sufficient for total thermalization before the surface of last scattering. Suitable physical mechanisms for thermalization are also required.

However, a number of other mechanisms can contribute to microwave isotropy at small angular widths. For instance, Kaiser and Silk [22] emphasize that there exists considerable ambiguity in the theoretical treatment of small scale anisotropies due, in part, to an uncertain thermal history of the universe from $30 < z < 1000$.

Factors which contribute to the small scale isotropy are re–ionization and the finite thickness of the surface of last scattering. Also, Gott points out that at small angular separations anisotropies may be randomized through interactions of the microwave radiation with dust [20]. Kaiser and Silk estimate that these factors may well result in microwave isotropy up to angular widths of approximately 2°.

For $\Omega_0 = .1$ the WMF cell has an apparent angular width of 2°. Such a value for Ω_0 is compatible with observational constraints. Hence, even if the volume of the Universe is equal to (or less than) that of the upper limit (WMF cell), microwave isotropy can still be accounted for at angular widths less than α.

On angular scales greater than α, microwave isotropy is enhanced by the multiple imaging. More precisely, two apparently causally disconnected regions of the sky, each of angular width $\delta\theta >> \alpha$, appear to be at the same temperature because each region consists of many identical replicas of the fundamental cell. The larger the regions are the more exactly their temperatures should correspond. Crudely speaking, the degree of isotropy should increase by a factor of $(\frac{\alpha}{\delta\theta})^2$ as one increases the angular width, $\delta\theta$, of the sampled regions. One would also expect anisotropy to be most prominent at angular widths of 2°. Under special conditions (eg. relatively large fundamental cell, no re- ionization, thin surface of last scattering and/or a relatively large value for Ω_0) our proposal can allow for microwave anisotropies at these scales. If indeed some anisotropy were eventually found, ideally the model would predict that the anisotropy would be periodically tiled across the sky. However the scattering of the microwave radiation by the above mentioned mechanisms, would distort and smear the tiling effect thus obscuring the periodic pattern. Since the model can predict isotropy for angular widths less than α, it can predict isotropy at all angular widths.

We shall next deal with the appearance of large scale structure in the model and how this relates to the BEKS data. As we have shown previously, the typical spatial repetition scale for the model is

$$\bar{L}_{Meyerhoff} = \frac{350}{\sqrt{1-\Omega_0}}\, h_0^{-1}\text{Mpc} \tag{4.3.10}$$

$$\bar{L}_{WMF} = \frac{3600}{\sqrt{1-\Omega_0}}\, h_0^{-1}\text{Mpc}. \tag{4.3.11}$$

In what follows we will simulate a pencil beam survey in our model and will find that even though we have exact periodicity of the universe, a typical pencil beam survey will not be able to observe this periodicity in a 'clean' manner. In fact it turns out that it is extremely unlikely that the consecutive groups of galaxies seen in a pencil beam survey are ghost images of each other. This has profound implications as regards the BEKS data as we shall see.

The first point to note is that along a typical pencil beam the repetition lengths between images of a particular object can be quite different from the lattice periodicities. Let us consider two simple examples. Consider again the tessellation of R^2 produced by the torus (see Fig 4.1). We will take the special case when both sides of the fundamental cell are equal in length, $L_{min} = L_{max} = L$. Position the observer at the center of the fundamental cell and position another object, say a galaxy, at some generic position in the cell. The galaxy will produce a crystalline pattern of ghost images as seen by the observer. However for a pencil beam survey the observer will typically not see periodic ghost images of the galaxy with period of order L. For simplicity, consider the case where the object galaxy is the observers own and that the pencil beam and object are infinitesimally thin. There will then only exist four directions where the periodicity of the images seen in the pencil beam equals L. For all other directions the period between repeated images is greater than L. Indeed, if the tangent of the angle between the pencil

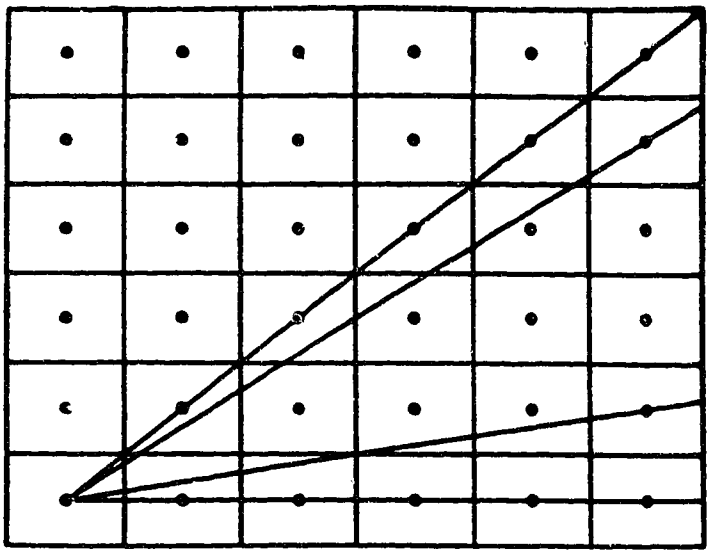

Figure 4.1: A tessellation of $\mathbb{R}^2$ by a torus where the fundamental cell has dimensions $L \times L$. For an observer located at a, infinitesimally thin pencil beam surveys in different directions would demonstrate different periodicities.

beam and the primary axes of the lattice is irrational then the period is infinite. More realistically, if the pencil beam and object are of finite extent but thin then one would again expect generic directions to display periods between ghost images significantly larger than L.

For our second example let us add some simple realistic extended structure into the fundamental cell, for example a great wall. Ghost imaging will create a crystal lattice of great walls separated by great voids (see Fig 4.2). For an observer positioned at the center of the cell, a pencil beam survey along a particular direction will intersect consecutive ghost images of the great wall at different points in the imaged walls. Since the actual Great Wall is not uniform and we are indeed positioned slightly off center one would not expect to see the same number of galaxies in consecutive peaks in the galaxy distribution along the beam. Such

an effect *is seen in the BEKS data.* The galaxies seen in the second, third and some subsequent peaks of the pencil beam data would *not* be ghost images of galaxies in the first peak. Eventually there will come a point where the pencil beam will intersect a repeated ghost image but as we have argued above, this distance will typically be far greater than the scale of the lattice. Thus, the model seems consistent with the experimental data observed.

One will also note that exact phase coherence of the galaxy distribution is only achieved along certain special directions. To be more concrete let us define characteristic lengths L_{int}, and L_{ext}, associated with the interior and exterior of the walls by,

$$L_{int} \approx V_{int}^{\frac{1}{3}}$$

$$L_{ext} \approx (V_{cell} - V_{int})^{\frac{1}{3}}.$$

A pencil beam survey should indicate two separate characteristic scales: that of the great wall, which we will take to be $100 - 200\ h_0^{-1}$Mpc [3], and that of the external voids, which could range from 0 to $3600\ h_0^{-1}$Mpc. Thus the problem of explaining the BEKS data takes a bizarre twist. The difficulty is not to explain a characteristic length scale of $100 - 200\ h_0^{-1}$Mpc, the appearance of such a characteristic length in the data is guaranteed by ghost imaging of the great wall and hence its characteristic length. The problem is to explain the absence of the other characteristic length, that associated with the voids.

One possible, but we feel not probable, resolution to the above dilemma would be that there exists a large disparity between the lengths L_{max} and L_{min}. In this case the characteristic length of the voids may be smeared out making it difficult to detect in a pencil beam survey along a typical line of sight. We feel that effects of this sort are not seen in the BEKS data.

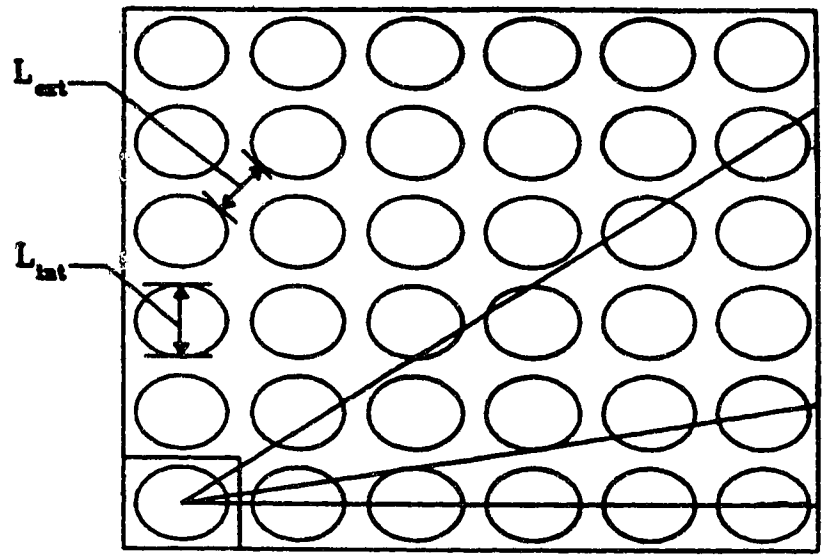

Figure 4.2: A tessellation of $\mathbb{R}^2$ by a torus where the fundamental cell contains a 'great wall' like structure.

However a neater explanation for the absence of the second characteristic length suggests itself. Suppose that structure in the universe appears on a maximal scale within the fundamental cell. Since what constitutes the 'inside' or the 'outside' of the great wall depends entirely on where the observer is located in the fundamental cell we will invoke a type of cosmological principle with respect to the structure and require that $L_{int} \approx L_{ext}$. In this case the two characteristic lengths predicted by our proposal now coincide at somewhere between $100 - 200\ h_0^{-1}$Mpc. For this we require $\bar{L} \approx 200 - 400\ h_0^{-1}$Mpc. This is certainly possible with the Meyerhoff cell and perhaps with also the WMF cell.

This maximal structure hypothesis is particularly interesting because it suggests a gestalt shift in the way we interpret the universe. Since the development of FLRW theory, cosmologists have worked under the edict that the universe gets increasingly isotropic at large scales. For the last decade or so we have been

repeatedly surprised by structure on ever larger scales. Here, we discover that the general structure of the BEKS data might be expected precisely if structure were to appear on the largest possible scale within the Universe.

Needless to say, attempts to explain detailed observations with our proposal at this stage of its development are speculative. None the less, even at this stage it may be possible to devise observational tests for the proposal.

One test would be to look for anisotropy at angular widths (eg. $\sim 2°$). If any is found, it should be regularly 'tiled' across the sky. However, this does not provide an ideal test because the absence of this tiling, due to the smearing effect of dust and the other factors mentioned above [20,22], is entirely compatible with our model.

Another test, which at first glance might seem profitable, would be the identification of multiple ghost images of a particular fundamental structure as they appear in a two dimensional projection of the heavens. However, as has been pointed out by Ellis and Schreiber [7], attempting to identify a periodic structure by studying the spatial distribution of repeated ghost images in the sky may prove very difficult. Ghost images observed in different parts of the sky will present completely different orientations of the fundamental object thus making spatial correlations extremely difficult to discern. Furthermore, ghost images are not expected to be identical to the originals due to evolution effects, obscuration, proper motions (if significant) and selection effects. Evolution effects could be minimized by comparing ghost images of equal redshift.

The strongest test would be to conduct a deep space three dimensional survey. Our proposal predicts periodic three dimensional structure must occur

with periodicity less than 3600 h_0^{-1}Mpc. Again this tessellation will not be perfect for the above mentioned reasons of evolution and proper motion. Again one can compensate to some extent by comparing those images of the great wall at equal redshifts.

Finally, it is important to point out that our proposal has an important advantage over virtually all inflation proposals; its predictions for microwave isotropy do not depend on the properties of unobserved particle fields. It predicts the existence of large scale structure while maintaining microwave isotropy—a goal which may be difficult to meet 'naturally' by any other theory. Central predictions of our proposal emanate from a simple topological constraint. This constraint allows us to conjecture a resolution of the 'scale problem'; that is, the problem of determining an appropriate volume for the Universe. Our conjecture leads directly to the prediction of ghost imaging at scales below 350 to 3600 h_0^{-1}Mpc for $.1 < \Omega < 1$. From this, we suggest that the characteristic scale of between 100 and 200 h_0^{-1}Mpc in BEKS's observations may be due to nothing more than ghost imaging of the great wall.

BIBLIOGRAPHY

[1] J. Twamley, in *Proceedings of the Banff Summer Institute in Gravitation*, eds. R. Mann and P. Wesson, to appear (World Scientific, Singapore, 1991).

[2] G. Hayward and J. Twamley, *Phys. Lett.* **A149**, (1990) 84.

[3] M. J. Geller and J. P. Huchra, *Science* **246**, (1989) 897.

[4] T. J. Broadhurst, R. S. Ellis, D. C. Koo, and A. S. Szalay, Nature, (1990) 726.

[5] A. S. Szalay, presentation at the *Vancouver workshop on Quantum cosmology and Inflation*, May 1990.

[6] M. Davis, *Nature* **343**, (1990) 699.

[7] G. F. R. Ellis, and G. Schreiber, *Phys. Lett.* **A115** , (1986) 97.

[8] G. F. R. Ellis, Major Themes in the relation between Philosophy and Cosmology, *University of Cape Town preprint*, (1990), to be published.

[9] M. Morikawa, Oscillating Universe, *University of British Columbia preprint*, (1990), to be published.

[10] J. A. Wolf, *"Spaces of constant curvature"*, (McGraw–Hill, New York, 1967).

[11] P. Scott, *Bull. London Math. Soc.* **15**, (1983) 401.

[12] G. F. R. Ellis, D. H. Lyth and M. B. Mijić, Inflationary models with $\Omega \neq 1$, *SISSA preprint*, (1990), to be published.

[13] P. J. E. Peebles, *Ap. J.* **344**, (1989) L53 148-B5.

[14] W. Thurston, *"The Geometry and Topology of 3-Manifolds,"* Princeton University preprint (1978).

[15] S. V. Matveev and A. T. Fomenko, *Russian Math. Surveys* **43**, 1, (1988) 3.

[16] J. B. Hartle and S. W. Hawking, *Phys. Rev.* **D23**(1983) 2960.

[17] R. Meyerhoff, *Comment. Math. Helvetici* **61**, (1986) 271.

[18] J. Weeks, *Princeton University Ph. D. thesis*, (1985).

[19] D. D. Sokolov and V. F. Schvartsmann, *Sov. Phys. JETP* **39**, (1974) 196.

[20] J. R. Gott III, *Mon. Not. R. Astr. Soc.* **193**, (1980) 153.

[21] R. Soniera and P. J. E. Peebles, *Astr. J.* **83**, (1978) 845.

[22] N. Kaiser and J. Silk, *Nature* **324**, (1986) 529.

CHAPTER FIVE

CONCLUSIONS

We now conclude with a short review and make some comments concerning future research on the topics covered in this thesis.

In Chapter 1 we presented a brief overview of quantum cosmology and in particular, emphasised the Euclidean path-integral approach, the contour of integration, and the effects of wormholes on the low-energy coupling constants.

In Chapter 2 we used a FRW cosmology minimally coupled to an imaginary scalar field with a quartic self-interaction. Using numerical techniques, two asymptotically flat Euclidean wormhole configurations were found. In both cases the geometry was strictly real while the matter fields were either symmetric, with φ strictly positive or negative, or antisymmetric, with φ crossing zero only once. The action for both wormholes was negative and arose solely from the matter sector.

In Chapter 3 we again used a FRW cosmology minimally coupled to an imaginary scalar field with the potential $V(\phi) = \frac{1}{2}m^2\phi^2 + \frac{1}{4}\lambda\phi^4$. Using analytical and numerical techniques, an elaborate "spectrum" of asymptotically flat wormhole configurations was found. Wormholes only occurred for $\mu < \mu_c \approx 0.402$ ($\mu = m/\sqrt{\lambda}$).For $\mu < \mu_c$, there are $N_{MAX} + 1$ pairs of wormholes, where N_{MAX} is the maximum number of zero crossings of φ. These configurations could be labelled by an asymptotic constant χ. The loci of wormhole solutions in the (χ, μ) parameter space for the first six wormholes were obtained numerically, and approximately by analytical means. The solutions could also be labelled by their

minimal scale factor size a_{MIN}. The action was found to be negative, zero, or positive depending on the values of (χ, μ) for that particular wormhole solution.

In Chapter 4 we considered a small universe cosmological model possessing closed and compact spatial sections of constant negative curvature. We found that the available topologies were well-ordered by volume and complexity. Hypothesising that the universe is in the "ground state" of lowest topological complexity, we obtained a crude estimate of the typical repetition distance between consecutive ghost images of an extended object along a given line of sight. This estimate matched the observational evidence found by Broadhurst, Ellis, Koo, and Szalay in a deep sky pencil beam galaxy survey.

Regarding the discovery of these new non-charge-conserving wormholes; although the large wormhole problem does not occur to the extent that it does in the Giddings-Strominger wormhole (this is because the Giddings-Strominger wormhole is scale invariant and any size solution is possible, whereas these new solutions possess a maximum size), we still expect the double exponential in the α-probability distribution function to cause all the wormhole solutions, with positive action, to be dense in spacetime. However, as has been pointed out by Polchinski and Iwazaki [1], if the wormholes occur on vastly seperate scales (as in the model of Chapter 3 when $\mu \ll \mu_c$), then going beyond the dilute approximation and including the smallest wormholes into the base lagrangian, may very well result in a new field theory which does not admit the large wormhole solutions that existed in the dilute approximation. While the wormhole actions are bounded below, those with negative actions are expected to proliferate exponentially. These configuration would, presumably, not be included in the path-integral.

One is also interested in the stability properties of these wormholes. How-

ever, it is unclear whether the perturbations to test for such stability should be real, imaginary, or generally complex. Further investigation concerning the implications of imaginary fields is also warranted. As was explained in Chapter 1, current research on the contour of integration suggests that one must choose complex contours for the gravitational and matter sectors. However, only one contour analysis including gravity and matter ha been investigated [2]. Further, it appears that imaginary matter fields are generally picked out by the stationary configurations when one imposes momentum boundary conditions in the Euclidean path-integral [3]. One is thus interested in discovering the physical implications of imposing such momentum boundary conditions within the framework of the Euclidean path-integral.

Regarding the small universe model, we presented a mechanism wherein, perhaps, microwave isotropy on all angular scales could be predicted without recourse to inflation. However, the situation may possibly be greatly improved. It is well known that the geodesic flow on compact manifolds of no-where positive curvature is ergodic and is a classic example of chaos [4]. Thus the mixing of the cmwbr may be, in part, ergodic. Further research and computer simulation is needed to judge these effects.

BIBLIOGRAPHY

[1] J. Polchinski, *Nucl. Phys.* **B325** (1989) 619; A Iwazaki, *Phys. Lett.* **229B** (1989) 211.

[2] L. J. Garay, J. J. Halliwell, and G. A. Marugán, *Path-Integral Quantum Cosmology: A class of exactly soluble scalar field minisuperspace models with exponential potentials*, MIT/CTP preprint #1923, (1990).

[3] W. G. Unruh, *Class. Quantum Grav.* **7** (1990) 2331.

[4] M. C. Gutzwiller, *Chaos in Classical and Quantum Mechanics*, (Springer-Verlag, New-York, 1990).

APPENDIX A

PROGRAMS RELEVANT TO CHAPTER 2

1.1 Symbolic code to calculate asymptotic expansion

In this appendix we give the Macsyma (©Symbolics) code which derives the large time asymptotic expansion of the solution for which φ decays to zero. This was also computed to the same accuracy by hand. This code is only exact in $\varphi(a)$ to order $1/a^{10}$. However, by increasing the number of unknown coefficients b[i], c[i], it is a trivial matter to obtain a greater accuracy. This was implemented on Macsyma version 309.3 running on a VAX11/70.

```
/* We will obtain an asymptotic expansion for phi(a) for the Friedmann */
/* Robertson Walker model with a minimally coupled scalar field with a */
/* quartic self-interaction term */
/* Jason Twamley Jan 9th 1991 */
/* */
/* We first define an expansion for the scale factor and phi in terms of t */
/* for large t behaviour */
a:t+sum(b[i]*t^(-2*i-1),i,1,5);
p:sum(c[i]*t^(-2*i),i,1,5);
/* We next construct the Hamiltonian constraint where the lapse N=1 and we */
/* represent lambda by l */
ham:diff(a,t)^2+a^2*diff(p,t)^2-1+.5*l*a^2*p^4;
/* We then taylor expand this in inverse powers of t */
ham1:taylor(ham,[t,0,12,asymp]);
/* We then isolate the coefficients of the powers of t and label them as */
/* eq1,eq2,eqi etc. To be solved as a system eq1=0,eq2=0 later */
eq1:coeff(ham1,t,4);
eq2:coeff(ham1,t,6);
eq3:coeff(ham1,t,8);
eq4:coeff(ham1,t,10);
eq5:coeff(ham1,t,12);
/* We now construct the phi dynamical equation */
peq:diff(p,t,2)+3*diff(a,t)*diff(p,t)/a+l*p^3;
/* We again taylor expand in t */
peq1:taylor(peq,[t,0,12,asymp]);
/* We again isolate the respective coefficients and label then eqj to be */
/* solved eqj=0 later */
eq6:coeff(peq1,t,6);
eq7:coeff(peq1,t,8);
eq8:coeff(peq1,t,10);
eq9:coeff(peq1,t,12);
```

```
/* We now have a set of 9 equations for 10 unknowns b[i],c[i] i=1..5 */
/* We now solve these */
root:expand(solve([eq1,eq2,eq3,eq4,eq5,eq6,eq7,eq8,eq9],
[b[1],b[2],b[3],b[4],b[5],c[2],c[3],c[4],c[5]]));
/* Save this is a file */
save([root],root);
/* To speed up execution we can comment out the solve function above and */
/* just load the results from the file "root". */
/* loadfile("root");
/
/* We have expanded the solution to get the a   r in separate fractions */
/* We have also chosen that the arbitrary const  be c[1] */
/* We now evaluate a and phi for these coefficients */
ais:ev(a,root);
phiis:ev(p,root);
/* We now invert the a relation to get a first approximation to t */
tlong:-ais+t+am;
/* Where am is the symbol for the scale factor */
/* We now re-insert t again into this definition to get a better estimate */
/* for t(am). Note: doing this a second time gives an even better estimate */
/* but get much too complicated */
tmedium:coeff(tlong,t,0)+coeff(tlong,t,-3)*t^(-3)+coeff(tlong,t,-5)*t^(-5);
tshort:coeff(tlong,t,0)+coeff(tlong,t,-3)*t^(-3);
tveryshort:am;
tinv:ev(tlong,t=tmedium);
tinv:ev(tinv,t=tshort);
tinv:ev(tinv,t=tveryshort);
/* Now Taylor expand in am */
tinv:taylor(tinv,[am,0,9,asymp]);
/* Substitute t(am) into phi(am) */
phireallyis:ev(phiis,t=tinv);
/* taylor expand in am */
phireallyis:taylor(phireallyis,[am,0,10,asymp]);
expand(%);
```

1.2 Fortran code to generate evolution of geometry and matter for $V = \frac{\lambda}{4}\phi^4$

We now list the Fortran code used to generate the relevant data concerning the Euclidean time evolution of the scale factor a and imaginary matter field $\phi = i\varphi$ with a self-interaction potential $V = \frac{\lambda}{4}\phi^4 = \frac{\lambda}{4}\varphi^4$. This code was adapted from reference [1]. The other main portion of code used in chapter 2 was Brent's root finding algorithim which was also adapted from reference [1].

```
cccccccccccccccccccccccccccccccccccccccccccccccccccccccccccccccccccccc
```

```
c       Program Phi_fourth_model   Jason Twamley (Last Rev: Jan 30 1991)
C
c       Description:
C
c       This program evolves the geometry and matter fields of a FRW type
c       minisuperspace model minimally coupled to an imaginary scalar
c       field with a self-interaction term lambda*phi^4. The behaviour of
c       the relevant quantities are output to two files for further use.
c       Initial conditions are specified in the subroutine setup(). Three
c       main initial conditions are used:
c        a) asymptotically flat perturbation from the Giddings-Strominger
c           solution (see Chapter 2 page 13),
c        b) starting from the center of the throat with both da/dt=0 and
c            dphi/dt=0$,
c        c) starting from the center of the throat with da/dt=0 and
c           phi=0.
c
c        Necessary inputs for the program are:
C|Type |Variable: Description (Type D=double precision, C=double complex)
C-------------------------------------------------------------------------
C|D     |  XDXSAV: the seperation in parameter time t between saved data points.
C|D     |      H1: the initial step size for the Runge-Kutta integrator.
C|D     |     EPS: the degree of fractional accuracy desired.
C|D     |    HMIN: the lower limit on step size.
C|D     |      X2: the final parameter time t.
C|Char  |FILENAME: the base name of the filename to save the data.
C|      |          the data is stored in two files - FILENAME.DAT and
C|      |          FILENAME1.DAT
C|c     |     eta: asymptotic time to evaluate the asymptotic solution -
C|      |          value of 5 - 10 fine.
C|c     |      a0: can either be the 1 parameter specifying the asymptotic
C|      |          solution or the throat size in b) or c) above.
C|D     | xlambda: the value of lambda.
C|c     |       N: the lapse.
C|D     |    xtop: the ceiling of the scale factor below which one saves data
C|      |          points in xdxsav intervals of parameter time.
C
c       Also present are calls to low level graphics library routines in
c       SYS$USEFUL:lib.olb which are capable of producing an interactive
c       graph of several relevant quantities.
C
CCCCCCCCCCCCCCCCCCCCCCCCCCCCCCCCCCCCCCCCCCCCCCCCCCCCCCCCCCCCCCCCCCCCCCCCCCCC
        PROGRAM Phi_fourth_model

        IMPLICIT DOUBLE COMPLEX (A-H,P-W,Y-Z)
        IMPLICIT REAL*8 (X)
        double complex          lap
        REAL*8          EPS,    H1,     HMIN,     const
        REAL*8          X1,     X2
        real*4          ar(1000), xx(1000)
        CHARACTER*20    FILENAME1, FILENAME2
        COMMON /PATH/ KMAX,     KOUNT,    XDXSAV,     XP(20000),  YP(10,20000)
        COMMON /lapse/          lap,      xlambda
        DIMENSION YSTART(10)
C
c       Variables:      Eps,H1,Hmin,X2,Filename1,Filename2,Xdxsav -- as above
c                       lap         : complex lapse
c                       const       : constraint
c                       X1          : initial parameter time
c                       ar          : y abscissa for graphics
c                       xx          : x abscissa for graphics
```

```
c                   Kmax        : max number of data points that can be saved
c                   Kount       : actual number of data points saved
c                   XP          : array of saved parameter times
c                   YP          : array of saved variables
c                   xlambda     : lambda


      NVAR=6
      WRITE(6,*) '*********************************************************'
      WRITE(6,*)
      WRITE(6,*) 'Pathways of the Universe ---- V=lambda*Phi**4'
      WRITE(6,*)
      WRITE(6,*) '*********************************************************'
      WRITE(6,110)
110   FORMAT(' ','Enter the time step between recorded points       :',$)
      READ(5,*) XDXSAV
      WRITE(6,120)
120   FORMAT(' ','Enter the required accuracy                       :',$)
      READ(5,*) EPS
      IF(EPS.EQ.0.0) EPS=1.0E-15
      WRITE(6,130)
130   FORMAT(' ','Enter the initial step size                       :',$)
      READ(5,*) H1
      IF(H1.EQ.0.0) H1=1.E-11
      WRITE(6,135)
135   FORMAT(' ','Enter in minimum step size                       :',$)
      READ(5,*) HMIN
      IF(HMIN.EQ.0.) THEN HMIN=1.E-30
      WRITE(6,140)
140   FORMAT(' ','Enter the final time to integrate to (begin at t=0):',$)
C
c     Remember..if you are using method a) above we integrate inwards so
c     X2=-1 whereas for b) and c) we set X2=+1.
C
      READ(5,*) X2
      X1=0.0
      WRITE(6,150)
150   FORMAT(' ','Type in Data Filename                        :',$)
      READ(5,22) FILENAME1
      IJ=INDEX(FILENAME1,'.')-1
      IE=INDEX(FILENAME1,' ')+1
      FILENAME2=FILENAME1(1:IJ)//'2'//FILENAME1(IJ+1:IE)
22    FORMAT(A10)

555   KMAX=20000
C
c     Set up the initial conditions for the variables and their derivatives
c     and the lapse and lambda. The contents of the various ystart(1:6) are
c       ystart(1): phi(t)
c       ystart(2): dphi(t)/dt
c       ystart(3): dalpha(t)/dt
c       ystart(4): alpha(t)
c       ystart(5): matter action
c       ystart(6): gravitational action without boundary corrections
c     where t is the parameter time (multiply by the lapse to get the proper
c     time) and alpha=log(scale factor)
c
      call setup(ystart)

c     Initial values for the actions
      ystart(5)=dcmplx(0.0d0,0.0d0)
```

```
      ystart(6)=dcmplx(0.0d0,0.0d0)

c     Initialize the Hamiltonian constraint to zero.
      CONST=0.0d0

      write(6,301)
301   format(' Do you wish to save the trajectory(y=1):',$)
      read(5,*) iy

c     Save the initial scale factor for the gravitational action boundary
c     correction
      ai=cdexp(ystart(4))

c     Do the integration...
      CALL ODEINT(YSTART,NVAR,X1,X2,EPS,H1,HMIN,NOK,NBAD,CONST)

      WRITE(6,220) const
220   FORMAT(' During this run the maximum abs value of the constraint:',
     *       e16.6)

c     Low Level graphics routines to graph certain variables
      write(6,1256)
      read(5,*) ig
556   do i=1,kount
       xx(i)=xp(i)
       a=cdexp(yp(4,i))
       dphi=yp(2,i)/lap
       phi=yp(1,i)
       cons=dphi*a**3
       if(ig.eq.1) then
         ar(i)=dreal(a)
       else if(ig.eq.2) then
         ar(i)=dreal(phi)
       else if(ig.eq.3) then
         ar(i)=dreal(cons)
       else if (ig.eq.4) then
         ca=cdexp(yp(4,i))
         cp=yp(1,i)
         cda=yp(3,i)*ca
         cdp=yp(2,i)
         cz=ca*cp
         if(i.eq.1) then
             dpdalpha=(cp**2-xm**2)/cp/(cp**2/2.0d0-xm**2)
         else
            dpdalpha=ca*(cdp+1.d-14)/(cda+1.d-14)
         end if
         cdz=ca*cp+ca*dpdalpha
            ckonst=.5d0*cdz**2-.5d0*cz**2+.25d0*cz**4
         ar(i)=dreal(ckonst)
        end if
      end do

c     Graphing calls
c     call clear_plot
c     call cltrans
c     call setnam('YAUTO',2.)
c     call setnam('XAUTO',2.)
c     call gplot(xx,ar,kount,1)
c     call transparent_mode(0)
      if(ig.eq.4) write(6,*) 'Final E:',ar(kount)
```

```
      write(6,1256)
1256  format(' 1 View a',/,' 2 View Phi',/,' 3 View Cons',/,' 4 E',
     *       /,' 5 Exit',
     *       /,' Choice:',$)
      read(5,*) ig
      if(ig.ne.5) goto 556
       if(iy.ne.1) goto 555


c     Opening files to save data points
      OPEN(20,FILE=FILENAME1,STATUS='NEW',recl=255)
      OPEN(21,FILE=FILENAME2,STATUS='NEW',recl=255)

c     Save final scale factor for boundary correction to action
      ae=cdexp(yp(4,kount))

      do i=1,kount
       a=cdexp(yp(4,i))
       phi=yp(1,i)

c      Rescale by 1/lap to get proper time derivatives
       da=yp(3,i)*a/lap
       dphi=yp(2,i)/lap

c      cons=the conserved quantity a^{3}dphi/dt in the Giddings-
c      Strominger wormhole
       cons=dphi*a**3

c Action have reversed signature because we are integrating in -t
c                   direction.
c      Matter action
       ActionMatter=-yp(5,i)

c      Gravitational action with boundary correction
       ActionGrav=-yp(6,i)+.5d0*(ai**2+ae**2)

c      Hamiltonian constraint
       CTEMP=-Yp(2,i)**2-Yp(3,i)**2+lap*lap*(-xlambda*yp(1,i)**4/2.0d0
     *   +CDEXP(-2.0*Yp(4,i)))

c      Defining z and dz to calculate the asymptotic constant
c      $E=\f{1}{2}\f{dz}{d\alpha}^{2}-\f{1}{2}z^{2}+\f{1}{4}z^4$
       z=a*phi
       dz=a*phi+a*a*(dphi+1.d-8)/(da+1.d-8)
        ckonst=.5d0*dz**2-.5d0*z**2+.25d0*z**4

       write(20,1010) xp(i),dreal(a),dreal(phi),dreal(da),dreal(dphi),
     *       dreal(cons)
       write(21,1020) xp(i),dreal(actionmatter),dreal(actiongrav),
     *       dreal(ctemp)
      end do
1010  format(6(e16.10,2x))
1020  format(4(e16.10,2x))
      CLOSE(20)
      close(21)


      WRITE(6,*) 'We have written ',KOUNT,' entries to file'
      WRITE(6,*)'Thats all Mate....Gday'
      END
```

```
ccccccccccccccccccccccccccccccccccccccccccccccccccccccccccccccccccccccccccccc
c
c       Subroutine to calculate the derivatives of the four first order ODEs
c       which describe the dynamics. Also the Matter and Gravitational actions
c       are integrated.
c
ccccccccccccccccccccccccccccccccccccccccccccccccccccccccccccccccccccccccccccc
        SUBROUTINE DERIVS(X,Y,DYDX)
        DOUBLE COMPLEX Y,DYDX,n
        DOUBLE PRECISION X,xlambda
        DIMENSION Y(4),DYDX(4)
        common /lapse/ n,xlambda,xtop

c       Dynamical first order ODEs
        DYDX(1)=Y(2)
        DYDX(2)=-xlambda*Y(1)**3*n*n-3.0*Y(3)*Y(2)
        DYDX(3)=-xlambda/2.0d0*Y(1)**4*n*n-Y(3)**2+2.0*Y(2)**2
        DYDX(4)=Y(3)

c       Matter action
        dydx(5)=-0.5d0*(cdexp(3.0d0*y(4))*y(2)**2/n
     *        -xlambda*y(1)**4/2.0d0*n*cdexp(3.0d0*y(4)) )
c       Grav action
        dydx(6)=-0.5d0*( cdexp(3.0d0*y(4))*y(3)**2/n+n*cdexp(y(4)) )

        RETURN
        END


ccccccccccccccccccccccccccccccccccccccccccccccccccccccccccccccccccccccccccccc
c
c       Subroutine which actually does the fourth order Runge-Kutta integration
c       with adaptive step size. This is based on similar routines in
c       NUMERICAL RECIPES by  W. H. Press, B. P. Flannery, S. A. Teukolsky
c       and W. T. Vetterling.
c
ccccccccccccccccccccccccccccccccccccccccccccccccccccccccccccccccccccccccccccc
        SUBROUTINE ODEINT(YSTART,NVAR,X1,X2,EPS,H1,HMIN,NOK,NBAD,CONST)
        IMPLICIT DOUBLE COMPLEX (A-H,P-W,Y-Z)
        IMPLICIT REAL*8 (X)
        double complex lap
        REAL*8 X,X1,X2,EPS,H1,HMIN,XSAV,H,HDID,HNEXT,CONST,CMAX
        PARAMETER( MAXSTP=5000000, NMAX=10, XTWO=2., XZERO=0., XTINY=1.E-30)
        COMMON /PATH/ KMAX,KOUNT,XDXSAV,XP(20000),YP(10,20000)
        COMMON /lapse/ lap,xlambda,xtop
        DIMENSION YSTART(NVAR),YSCAL(NMAX),Y(NMAX),DYDX(NMAX),xdeltaa(4,2)

        X=X1
        H=DSIGN(H1,X2-X1)
        NOK=0
        NBAD=0
        KOUNT=0
        CONST=0.0d0

c       We set the maximum allowable size to which the hamiltonian constraint
c       may grow before we signal an error.

        CMAX=1.E-2
        DO 11 I=1,NVAR
           Y(I)=YSTART(I)
11      CONTINUE
        XSAV=X-XDXSAV*XTWO
        DO 16 NSTP=1,MAXSTP
```

```
          CALL DERIVS(X,Y,DYDX)
          DO 12 I=1,NVAR
              YSCAL(I)=cdabs(Y(I))+H*cdabs(DYDX(I))+XTINY
12        CONTINUE
          IF(KMAX.GT.0) THEN

c       Modify to save only those data points which have a scale factor smaller
c       than xtop

              IF(DABS(X-XSAV).GT.DABS(XDXSAV).and.
     *                          dexp(dreal(y(4))) .lt.xtop) THEN
                    IF(KOUNT.LT.KMAX-1) THEN
                       KOUNT=KOUNT+1
                       XP(KOUNT)=X
                       DO 13 I=1,NVAR
                           YP(I,KOUNT)=Y(I)
13                     CONTINUE
                       XSAV=X
                    ENDIF
              ENDIF
          ENDIF
          IF((X+H-X2)*(X+H-X1).GT.XZERO) H=X2-X
          CALL RKQC(Y,DYDX,NVAR,X,H,EPS,YSCAL,HDID,HNEXT,IFLAG)
          IF(IFLAG.EQ.1) THEN
              WRITE(6,*) 'Hit a boundary in RKQC'
              RETURN
          ENDIF
          IF(HDID.EQ.H) THEN
              NOK=NOK+1
          ELSE
              NBAD=NBAD+1
          ENDIF
          IF((X-X2)*(X-X1).GE.XZERO) THEN
              DO 14 I=1,NVAR
                 YSTART(I)=Y(I)
14            CONTINUE
              IF(KMAX.NE.0) THEN
                 KOUNT=KOUNT+1
                 XP(KOUNT)=X
                 DO 15 I=1,NVAR
                     YP(I,KOUNT)=Y(I)
15               CONTINUE
              ENDIF
              RETURN
          ENDIF
          IF(DABS(HNEXT).LT.HMIN) THEN
              WRITE(6,*) 'Hit a boundary in ODEINT'
              RETURN
          ENDIF

c       We evaluate the abs(constraint)
           CTEMP=-Y(2)**2-Y(3)**2+lap*lap*(-xlambda*y(1)**4/2.0d0
     *                                    +CDEXP(-2.0*Y(4)))
          CONST=DMAX1(CONST,cdabs(CTEMP))
c         We stop the traj if this becomes too high..
          IF(CONST.GT.CMAX) THEN
            WRITE(6,*) 'Constraint becoming appreciable'
            WRITE(6,*) 'Halting progress'
            RETURN
          ENDIF

             H=HNEXT
16        CONTINUE
```

```
      PAUSE 'Too many steps.'
      RETURN
      END


      SUBROUTINE RK4(Y,DYDX,N,X,H,YOUT)
      IMPLICIT DOUBLE COMPLEX (A-H,P-W,Y-Z)
      IMPLICIT REAL*8 (X)
      REAL*8 H,X,HH,XH,H6
      PARAMETER( NMAX=10 )
      DIMENSION Y(N),DYDX(N),YOUT(N),YT(NMAX),DYT(NMAX),DYM(NMAX)

      HH=H*0.5
      H6=H/6.
      XH=X+HH
      DO 11 I=1,N
        YT(I)=Y(I)+HH*DYDX(I)
11    CONTINUE
      CALL DERIVS(XH,YT,DYT)
      DO 12 I=1,N
        YT(I)=Y(I)+HH*DYT(I)
12    CONTINUE
      CALL DERIVS(XH,YT,DYM)
      DO 13 I=1,N
         YT(I)=Y(I)+H*DYM(I)
         DYM(I)=DYT(I)+DYM(I)
13    CONTINUE
      CALL DERIVS(X+H,YT,DYT)
      DO 14 I=1,N
         YOUT(I)=Y(I)+H6*(DYDX(I)+DYT(I)+2.*DYM(I))
14    CONTINUE
      RETURN
      END

      SUBROUTINE RKQC(Y,DYDX,N,X,HTRY,EPS,YSCAL,HDID,HNEXT,IFLAG)
      IMPLICIT DOUBLE COMPLEX (A-H,P-W,Y-Z)
      IMPLICIT REAL*8 (X)
      REAL*8 X,EPS,HDID,HNEXT,XSAV,HTRY,H,HH,ERRMAX
      PARAMETER( NMAX=10, XPGROW=-0.20, XPSHRINK=-0.25, XFCOR=1./15.,
     *                  XONE=1., XSAFTEY=0.9, XERRORCON=6.E-4)
      DIMENSION Y(N),DYDX(N),YSCAL(N),YTEMP(NMAX),YSAV(NMAX),DYSAV(NMAX)

      IFLAG=0
      XSAV=X
      DO 11 I=1,N
         YSAV(I)=Y(I)
         DYSAV(I)=DYDX(I)
11    CONTINUE


      H=HTRY
1     HH=0.5*H
      CALL RK4(YSAV,DYSAV,N,XSAV,HH,YTEMP)
      X=XSAV+HH
      CALL DERIVS(X,YTEMP,DYDX)
      CALL RK4(YTEMP,DYDX,N,X,HH,Y)
      X=XSAV+H
      IF(X.EQ.XSAV) THEN
             WRITE(6,*) 'Stepsize not Significant in RKQC'
             IFLAG=1
             RETURN
      ENDIF
      CALL RK4(YSAV,DYSAV,N,XSAV,H,YTEMP)
      ERRMAX=0.
```

```
      DO 12  I=1,N
         YTEMP(I)=Y(I)-YTEMP(I)
         ERRMAX=DMAX1(ERRMAX, cdabs(YTEMP(I)/YSCAL(I)) )
12    CONTINUE
      ERRMAX=ERRMAX/EPS
      IF(ERRMAX.GT.XONE) THEN
         H=XSAFTEY*H*(ERRMAX**XPSHRINK)
         GOTO 1
      ELSE
         HDID=H
         IF(ERRMAX.GT.XERRORCON) THEN
             HNEXT=XSAFTEY*H*(ERRMAX**XPGROW)
         ELSE
             HNEXT=4.*H
         ENDIF
      ENDIF
      DO 13  I=1,N
         Y(I)=Y(I)+YTEMP(I)*XFCOR
13    CONTINUE
      RETURN
      END


ccccccccccccccccccccccccccccccccccccccccccccccccccccccccccccccccccccccccccccccc
c
c     Subroutine to setup the initial values of the dynamical variables
c     and set the lapse and ceiling of recorded points. Three alternative
c     codes are present with the unnecessary portions commented out.
c
ccccccccccccccccccccccccccccccccccccccccccccccccccccccccccccccccccccccccccccccc
      subroutine setup(y)
      implicit double complex (a-h,o-w,y-z)
      implicit real*8 (x)
      double complex n
      dimension y(10)
      COMMON /lapse/ n,xlambda,xtop


c     We first enter the conformal time eta to obtain an asymptotic soln.
c     Eta approx 5-10 are good.
      write(6,101)
101   format(' Enter the asymptotic time (complex)',t45,':',$)
      read(5,*) xr,xi
      t=dcmplx(xr,xi)

c     We next enter the a coefficient. This is either the parameter that
c     labels the asym. flat solutions at infinity in a) above or specifies
c     the throat size in b) or c).
      write(6,111)
111   format(' Enter the a coefficient (complex)',t45,':',$)
      read(5,*) xr,xi
      a0=dcmplx(xr,xi)
      write(6,121)
121   format(' Enter the coupling coeff (real)',t45,':',$)
      read(5,*) xlambda

c     This section of code calculates the initial data for the asymptotic
c     solution.
      t=2.0d0*t
      a=a0*cdsqrt((cdexp(t)+cdexp(-t))/2.0d0)
      f1=-3.0d0*xlambda*a0**2/(48.0d0)*cdexp(-3.0d0*t)
      a=a*cdexp(f1)
```

```
      alpha=cdlog(a)
      phi=cdexp(-t)
      f2=-a0**2*xlambda*cdexp(-2.0d0*t)/16.d0
      phi=phi+f2

c     After calculating a we display the value and decide how far we wish to
c     integrate. Unnecessary for method b) and c).
      write(6,131) dreal(a),dreal(phi)
131   format(' Scale Factor a',t30,':',e16.10,
     *       /,' Matter Field phi',t30,':',e16.10)
      write(6,141)
141   format(' Enter the complex lapse',t30,':',$)
      read(5,*) xr,xi
      n=dcmplx(xr,xi)
      write(6,151)
151   format(' Enter xtop',t30,':',$)
      read(5,*) xtop

c     This section of code continues that of the evaluation of the
c     asymptotic solution and calculated the derivatives with the given lapse
      dphi=(-2.0d0*cdexp(-t)+a0**2*xlambda/4.0d0*cdexp(-2.0d0*t))
      dphi=dphi/a*n
      da=(cdexp(t)-cdexp(-t))/(cdexp(t)+cdexp(-t))
      da=da+3.0d0*xlambda*a0**2*cdexp(-3.0d0*t)/8.0d0
      da=da*n
      dalpha=cdsqrt(-dphi**2+n*n*(-xlambda/2.0d0*phi**4+1.0d0/a**2))

c     This section of code is used to start the evolution at the throat
c     a=a0
c     alpha=cdlog(a)
c     dalpha=dcmplx(0.0d0,0.0d0)

c     With dphi/dt=0 at the throat
c     phi=cdsqrt(cdsqrt(2.0d0/xlambda/a/a))
c     dphi=dcmplx(0.0d0,0.0d0)

c     or with phi=0
c     phi=dcmplx(0.0d0,0.0d0)
c     dphi=n/a

      y(1)=phi
      y(2)=dphi
      y(3)=dalpha
      y(4)=alpha

      write(6,40) cdexp(y(4)),y(1),y(3)*cdexp(y(4))/n,y(2)/n
40    format(' a=',2(e16.10,2x),/,
     *       ' phi=',2(e16.10,2x),/,
     *       ' d=',2(e16.10,2x),/,
     *       ' dphi=',2(e16.10,2x))

c     Evaluate the hamiltonian constraint and see how well we have managed
c     to preserve the constraint. If it is above 10**(-10) we are borderline
c     and we usually want to begin with the constraint near 10**(-14)
      CTEMP=-Y(2)**2-Y(3)**2+n*n*(-xlambda*y(1)**4/2.0d0+CDEXP(-2.0*Y(4)))
      write(6,161) cdabs(ctemp)
161   format(' Hamiltonian Constraint       :',e16.10)
      return
      end
```

BIBLIOGRAPHY

[1] W. H. Press, B. P. Flannery, S. A. Teukolsky and W. T. Vetterling, *Numerical Recipes* (Cambridge University Press , Cambridge, 1990.)

APPENDIX B

PROGRAMS RELEVANT TO CHAPTER 3

2.1 Symbolic code to calculate asymptotic expansion

In this section we give the Macsyma (©Symbolics) code which derives the large time asymptotic expansion of the solution of the Euclidean field equations for a Friedman-Robertson-Walker cosmology coupled to an imaginary massive scalar field, for which φ decays to zero as $t \to \infty$. Only the lowest order solution was computed by hand. In this code we solve for $a(t)$ and $\varphi(t)$. To obtain the asymptotic expansions quoted in Chapter # 3 (3.4.14), (3.4.15) we proceed in two steps. The first is to assume the trial solutions

$$a(t) \approx t + e^{-2\tau} t^{-2} \sum_{n=0}^{6} b_n \tau^{-n} \quad , \tag{B.1}$$

$$\varphi(t) \approx e^{-\tau} t^{-3/2} \sum_{n=0}^{6} c_n \tau^{-n} \quad , \tag{B.2}$$

where $\tau = mt$. We then solve for b_n, c_n. The next program assumes the trial expansions

$$a \approx t + e^{-2\tau} t^{-2} \sum_{n=0}^{6} b_n \tau^{-n} + e^{-4\tau} t^{-5} \sum_{n=0}^{4} d_n \tau^{-n} \quad , \tag{B.3}$$

$$\varphi \approx e^{-\tau} t^{-3/2} \sum_{n=0}^{6} c_n \tau^{-n} + e^{-3\tau} t^{-9/2} \sum_{n=0}^{4} e_n \tau^{-n} \quad . \tag{B.4}$$

and assumes the lower order results we had calculated previously for b_n, c_n. These trial expansions are inserted into the Hamiltonian constraint and the φ dynamical equation. However, to increase speed, only the relevant orders in the exponentials are calculated. The coefficients of the next highier order exponentials are isolated and the determining equations for d_n and e_n are solved. This was implemented on Macsyma version 309.3 running on a VAX11/70. The following is the symbolic computer code. Comments are enclosed by /* comment */.

```
/* This symbolic computer code generates the trial expansions solutions
for the scale factor and the matter field and inserts them into the
Einstein field equations for an Euclidean Freidman-Robertson-Walker
geometry coupled to an imaginary massive scalar field. There are 14
unknowns. 13 equations are obtained relating the coefficients and
these 13 equations are solved for all the coefficients b_n and c_n in terms
of the coefficient c_0 - the single arbitrary parameter

Jason Twamley, Feb 1991
```

```
We first construct the asymptotic trial expansion*/
a:t+exp(-2*m*t)*t^(-2)*sum(b[i]*t^(-i),i,0,6);
p:exp(-m*t)/t^(3/2)*sum(c[i]*t^(-i),i,0,6);

/* We now construct the Hamiltonian constraint equation and the phi
dynamical equation, suitably expanded to isolate all the coefficients of
exp(-k*m*t) where k is an integer */
ham:diff(a,t)^2-1+a^2*(diff(p,t)^2-m^2*p^2)$
ham:expand(%)$
phieq:diff(p,t,2)*a+3*diff(p,t)*diff(a,t)-m^2*a*p$
phieq:expand(%)$

/* We isolate the coefficient of the lowest power exponential term in the
Hamiltonian and extract the non-zero coefficients of inverse powers of
t */
eqa:coeff(ham,exp(-2*m*t));
eq1:coeff(eqa,t,-2);
eq2:coeff(eqa,t,-3);
eq3:coeff(eqa,t,-4);
eq4:coeff(eqa,t,-5);
eq5:coeff(eqa,t,-6);
eq6:coeff(eqa,t,-7);
eq7:coeff(eqa,t,-8);

/* We isolate the coefficient of the lowest power exponential term in the
phi dynamical equation and extract the non-zero coefficients of inverse
powers of t */
eqb:expand(coeff(phieq,exp(-m*t))*t^(5/2));
eq8:coeff(eqb,t,0);
eq9:coeff(eqb,t,-1);
eq10:coeff(eqb,t,-2);
eq11:coeff(eqb,t,-3);
eq12:coeff(eqb,t,-4);
eq13:coeff(eqb,t,-5);

/* We now save these equations (for safety's sake) to a file temp. */
save(temp,eq1,eq2,eq3,eq4,eq5,eq6,eq7,eq8,eq9,eq10,eq11,eq12,eq13);

/* We solve all 13 equations for the 13 unknowns and save the resulting
solution to another file temp1, for future reference. */
solve([eq1,eq2,eq3,eq4,eq5,eq6,eq7,eq8,eq9,eq10,eq11,eq12,eq13],[
b[0],b[1],b[2],b[3],b[4],b[5],b[6],c[1],c[2],c[3],c[4],c[5],c[6]]);
roots:%$
save(temp1,roots);
```

We now present the second code which calculates the asmptotic expansions (3.4.14) and (3.4.15) quoted in chapter 3.

```
/* In this code we calculate the coefficients d_n and e_n occurring in
the enlarged expansions for a(t), varphi(t).
We assume the following trials expansions for the scale factor and the
```

```
matter field.
Jason Twamley, Feb 1991 */

a:t+exp(-2*m*t)/t^2*sum(b[i]*t^(-i),i,0,6)
+exp(-4*m*t)*sum(d[i]*t^(-i),i,0,4)/t^5;
p:exp(-m*t)/t^(3/2)*c[0]*

sum(gamma(1+k+1/2)/(k!*gamma(1-k+1/2)*(2*t*m)^k),k,0,6)
+exp(-3*m*t)/t^(9/2)*sum(e[i]*t^(-i),i,0,4);
/* We have inserted the lowest order terms in p. These were obtained from the
previous code but are, in fact, the terms arrising in the large time
expansion of K_1(-m*t), that is the modified Bessel's function of
first order. We now read in the results for the coefficients b_n obtained
by the previous program and substitute these coefficients into the
expression for a(t).*/
loadfile(temp1);
a:ev(a,roots);

/* We now define some terms that will be useful in isolating certain
expression and begin collecting those terms of lowest order. */
ex1:exp(-m*t)$
ex2:exp(-2*m*t)$
ex3:exp(-3*m*t)$
ex4:exp(-4*m*t)$

aa:t$
ab:coeff(a,ex2)*ex2$
ac:coeff(a,ex4)*ex4$
pa:coeff(p,ex1)*ex1$
pb:coeff(p,ex3)*ex3$
da:expand(diff(a,t))$
dp:expand(diff(p,t))$
daa:1$
dab:coeff(da,ex2)*ex2$
dpa:coeff(dp,ex1)*ex1$
dpb:coeff(dp,ex3)*ex3$
a2:expand(a^2)$
p2:expand(p^2)$
da2:expand(diff(a,t)^2)$
dp2:expand(diff(p,t)^2)$
da2a:1$
da2b:coeff(da2,ex2)*ex2$
da2c:coeff(da2,ex4)*ex4$
dp2a:coeff(dp2,ex2)*ex2$
dp2b:coeff(dp2,ex4)*ex4$
a2a:t^2$
a2b:coeff(a2,ex2)*ex2$
a2c:coeff(a2,ex4)*ex4$
p2a:coeff(p2,ex2)*ex2$
p2b:coeff(p2,ex4)*ex4$
ddp:expand(diff(p,t,2))$
```

```
/* We now evaluate the Hamiltonian constraint equation to the two lowest terms
in the exponentials. Macsyma cannot handle the evaluation of the Hamiltonian
with the full expressions for the relavent quantities, so we must perform
some preliminary pruning of the expressions so as to finally obtain the
lowest terms in the Hamiltonian */
h1:da2-1
+a2a*dp2a+a2a*dp2b+a2b*dp2a
-m^2*a2a*p2a-m^2*a2a*p2b-m^2*a2b*p2a$
ham:expand(h1)$

/* We isolate the coefficients of the two lowest exponentials */
eqa:coeff(ham,ex2);
eqb:coeff(ham,ex4);

/* We examine the highest power of t to occur in the coefficient of
exp(-2*m*t) and find that the coefficient is zero as expected. */
hit:hipow(eqa,t);

/* We obtain the highest power of t to occur in the next highier term and
obtain 5 determining equations for the 10 unknowns d_n, e_n. */
hit:hipow(eqb,t);
eq1:coeff(eqb,t,hit-1);
eq2:coeff(eqb,t,hit-2);
eq3:coeff(eqb,t,hit-3);
eq4:coeff(eqb,t,hit-4);
eq5:coeff(eqb,t,hit-5);

/* We calculate the varphi dynamical equation and repeat the above
analysis. */
phieq:expand( (aa+ab)*ddp+3*(daa*(dpa+dpb)+dab*dpa)-m^2*p*(aa+ab))$
eqc:coeff(phieq,ex1);
eqd:coeff(phieq,ex3);
hit:hipow(eqc,t); /* This is again zero as expected. */
hit:hipow(eqd,t);
eq6:coeff(eqd,t,hit);
eq7:coeff(eqd,t,hit-1);
eq8:coeff(eqd,t,hit-2);
eq9:coeff(eqd,t,hit-3);
eq10:coeff(eqd,t,hit-4);

/* We now solve the 10 determining equations for the 10 unknowns
d_n, e_n and save the results to the file temp2. */
solve([eq1,eq2,eq3,eq4,eq5,eq6,eq7,eq8,eq9,eq10],[
d[0],d[1],d[2],d[3],d[4],e[0],e[1],e[2],e[3],e[4]]);
big_roots:%$
save(temp2,big_roots);
```

2.2 Integration Routine

The basic integration routine differs only slightly from the program described in Appendix 2. The central differences are in the subroutines setup() and derivs(). In setup() we specify the arbitray constant c_0, as defined in the above section, and the large time for which (3.4.14) and (3.4.15) are to be evaluated. The relation between c_0 and χ is given by equation (3.4.17) where $c = c_0$. The time t is chosen large enough so that the accumulated numerical error in the total integration is smaller than 1%. The subroutine derivs() now reads

```
ccccccccccccccccccccccccccccccccccccccccccccccccccccccccccccccccccccccccccccc
c
c       Subroutine to calculate the derivatives of the four first order ODEs
c       which describe the dynamics. Also the Matter, Gravitational, Kinetic
c       and Potential actions are integrated.
c
ccccccccccccccccccccccccccccccccccccccccccccccccccccccccccccccccccccccccccccc
        subroutine derivs(x,y,dydx)
        double complex y,dydx,n
        double precision x,xmu
        dimension y(10),dydx(10)
        common /lapse/ n,xmu

c       Euclidean trajectories
        dydx(1)=y(2)
        dydx(2)=-y(1)**3*n*n-3.0*y(3)*y(2)+xmu**2*y(1)*n*n
        dydx(3)=-2.0d0/2.0d0*y(1)**4*n*n-y(3)**2+2.0*y(2)**2+
     *       xmu**2*y(1)**2*n*n
        dydx(4)=y(3)

c All actions pick up a minus sign as we are integrating in the -t
c       direction.
c       Matter action
        dydx(5)=-(-0.5d0*(cdexp(3.0d0*y(4))*y(2)**2/n
     *  -(y(1)**4/2.0d0-xmu**2*y(1)**2)*n*cdexp(3.0d0*y(4)) )  )

c       Grav action
        dydx(6)=-(-0.5d0*( cdexp(3.0d0*y(4))*y(3)**2/n+n*cdexp(y(4)) )  )

c       Kinetic part of matter action
        dydx(7)=-(-0.5d0*(cdexp(3.0d0*y(4))*y(2)**2/n)  )

c       Potential part of matter action
        dydx(8)=-(-0.5d0*(-(y(1)**4/2.0d0-xmu**2*y(1)**2)*n*
     *  cdexp(3.0d0*y(4)) )   )

        return
        end
```

2.3 Program Description

In this section we briefy describe the program used to find, and trace out, the loci of valid wormhole solutions in the two dimensional parameter space (χ, μ). The general behaviour

of these curves were obtained though initial numerical experiments and it was suspected that a curve of a particular N-type wormhole was single valued in χ. Using the above described integration routine and computing the test function (3.4.26) as $t \to -\infty$, the first $K/2$, with lower χ, of a total number of K possible wormholes for a fixed $\mu = 0.01$ were found. To find the zeros of the test function $\mathcal{F}(\chi, \mu = 0.01)$, Brent's algorithim was used in the χ direction [1]. Each of the $K/2$ roots, (χ_f, μ_f), of $\mathcal{F}$, (now known as "base roots") has a different value of N. These base roots are then given to a program that evaluates the zeros of $\mathcal{F}(\chi = \chi_f, \mu)$ associated with a given value of N. That is, it searches in the $\pm\mu$ direction until it brackets a zero of $\mathcal{F}$ that corresponds to a N-type wormhole. It then utilizes Brent's algorithm again in the μ direction to find the root to the required precision. Then, χ is increased by a fixed amount, $\chi \to \chi + \Delta\chi$, and the process of finding the appropriate root of $\mathcal{F}$ corresponding to a wormhole with the same N is repeated. To increase the speed of execution and to ensure that the subsequent roots found belong to the same continuous curve in the (χ, μ) parameter space, the previous position of the root is remembered and the search for a root for the incremented value of χ along the $\pm\mu$ direction begins at the remembered value of μ. The positions (χ, μ) of all roots corresponding to the particular base value of N are saved to a file. The program begins anew with the next base root of $\mathcal{F}$ found at $\mu = 0.01$ and creeps up the χ axis, tracing out the continuous contour of $\mathcal{F} = 0$ in the (χ, μ) plane corresponding to the new value of N found at the base root. Also gathered during the final numerical integration, when Brent's alorithim has found the root to the required precision, is information concerning the minimum scale factor a_{MIN}, the gravitational and potential actions for the wormhole. These quantities are also saved to the file. On a more technical point, Brent's algorithim can only pin-point the zero of $\mathcal{F}$ to a certain accuracy (machine accuracy $\approx 10^{-14}$). Consequently, for χ large, it is unable to adjust the (χ, μ) parameters so that φ remains near zero for a long time. The wormhole is then taken to extend from the starting point, with t positive and large, through the wormhole, and into the region where t is negative. We stop the evaluation of the actions at the point in the negative t domain where $|\dot{a}| - 1$ is minimum.

BIBLIOGRAPHY

[1] W. H. Press, B. P. Flannery, S. A. Teukolsky and W. T. Vetterling, *Numerical Recipes* (Cambridge University Press , Cambridge, 1990.)